NAL PROPOSAL No. 9

Correspondent: M. L. Stevenson
Experimental Physics
Lawrence Radiation Lab
Berkeley, Calif. 94720

FTS/Commercial 415-843-6301

Proposal for a High-Energy Neutrino Experiment

In The NAL 30 m^3 H_2, D_2 Bubble Chamber

R. Cence, F. Harris, M. Peters, V. Peterson, D. Yount
University of Hawaii

S. Meyer
Northwestern University

M. Alston-Garnjost, R. Birge, G. Goldhaber
J. Kadyk, S. Parker, M. L. Stevenson, G. Trilling
Lawrence Radiation Laboratory

June, 1970

PROPOSAL FOR A HIGH-ENERGY NEUTRINO EXPERIMENT IN THE NAL 30 m^3 H_2, D_2 BUBBLE CHAMBER

University of Hawaii (R. Cence, F. Harris, M. Peters, V. Peterson, D. Yount)

Northwestern University (S. Meyer)

University of California, Lawrence Radiation Laboratory (M. Alston-Garnjost, R. Birge, G. Goldhaber, J. Kadyk, S. Parker, M.L. Stevenson, G. Trilling)

ABSTRACT

We propose to study high-energy neutrino interactions in the NAL 30 m^3 bubble chamber. A slight alteration of the chamber design will allow a large-solid-angle quantameter to be placed just outside the thin (1/2 inch steel) wall of the bubble chamber. A detector, designed to identify the muon of the interaction is placed outside the vacuum tank. With this hybrid system we can reconstruct the neutrino's energy, the lepton momentum transfer squared, Q^2, the lepton energy transfer ($\nu = E-E'$), and measure many features of the final hadron state. This sytem detects with high efficiency over the entire range of variables and is well suited to making a detailed general survey of neutrino interactions in the neutrino energy range 15 to 80 GeV. A million-picture exposure would yield tens of thousands of neutrino interactions with circulating protons at 200 GeV. A similar number of events should be obtained with protons at 500 GeV. Table I summarizes the preliminary cost estimates.

PROPOSAL FOR A HIGH-ENERGY NEUTRINO EXPERIMENT IN THE NAL 30 m^3 H_2, D_2 BUBBLE CHAMBER

University of Hawaii, Northwestern University,
Lawrence Radiation Laboratory

I. INTRODUCTION

We propose an experimental program for studying the interactions of neutrinos on hydrogen and deuterium for neutrino energies above 15 GeV. This program includes measurements of:

a. the total cross section to see if it saturates or remains linear in neutrino energy,

b. distributions in the deep-inelastic region to test scale invariance and various models such as Pomeron exchange and the parton hypothesis,

c. the elastic differential cross section to learn more about nucleon form factors,

d. interactions involving W mesons, if they exist.

A detector similar to the 14-foot BNL bubble chamber, suitably altered to detect π^{o}'s neutrons, and muons electronically, seems ideal for neutrino energies up to 80 GeV.

The proposal parallels experiments on elastic and "deep-inelastic" electron scattering: the neutrino provides an independent probe of nuclear structure with, we believe, comparable sensitivity to the electron, while the bubble-chamber technique makes possible a detailed analysis of the final-state hadrons.

In the case of neutrinos, only the direction of the incident lepton is known, and it is necessary to determine its energy E. This can be done by measuring the energies of all final π^{o}'s, charged hadrons, neutrons, and leptons (muons). Provided we identify which of the final particles is the outgoing lepton (energy E'), we can make the same analysis as in deep-inelastic electron scattering. The total and the "elastic scattering" cross sections will also be measured.

Bubble-chamber detection of neutrino events provides precise information on the location of the interaction vertex as well as the momenta of all charged outgoing particles. Photons from π^o's are detected with essentially 100 $^o/_o$ efficiency by a proportional quantameter (lead plates with wire coordinate planes in the gas gaps), and spatial information as well as the total electromagnetic energy is obtained. A proportional hadrometer (copper or concrete plates with wire coordinate planes in the gas gaps) determines the energy in nuclear cascades and traces individual hadron tracks. Neutrons are also detected in the hadrometer, while muons are identified when they penetrate this hadron absorber. Backgrounds are suppressed by the time resolution of the trigger logic, by the energy discrimination of the quantameter and hadrometer, and by detailed track analysis in the bubble chamber, quantameter, and hadrometer.

There are several major advantages of the hybrid system consisting of the bubble chamber and electronic detectors. First, the bubble chamber permits an accurate (to $\pm$ 3 $^o/_o$) determination of the charged-hadron and lepton energies through track curvature, while the quantameter determines the total electromagnetic energy to about the same precision. The energy appearing in the form of neutrons is detected with the hadrometer to somewhat less accuracy, but this component is normally a small fraction of the total. Detailed vertex information is a second advantage, as already mentioned. Third, the angular acceptance is large, and a wide range of lepton-momentum and lepton-energy transfers is sampled with good efficiency. Finally, since the muon energy is determined in the bubble chamber, the thickness of the muon detector

is much less than the muon range.

In Section II we discuss some of the measurements that might be made in the neutrino energy range from 15 to 80 GeV. We use these considerations as the basis for designing detectors. Section II also contains specifications required for the neutrino beam and a summary of the components of the neutrino facility that participants in this proposal could help to develop. Technical design considerations are discussed in Section III. Finally, in Section IV we suggest a possible schedule for obtaining one million events during both 200-GeV and 500-GeV phases of the accelerator operation.

II. HIGH-ENERGY NEUTRINO INTERACTIONS

A. Kinematics of $\nu + N \rightarrow$ lepton + hadrons

We adopt the notation of Bjorken and Paschos.[1] Fig. 1 then summarizes much of the kinematics where Q^2 is the square of the momentum transfer to the leptons, and ν is the difference in initial and final lepton energies. The solid parallel lines are the loci of equal invariant hadron mass W, given in terms of the nucleon mass M by the following equations:

$$Q^2 = 2M\nu + M^2 - W^2, \tag{1}$$

$$= E - E', \tag{2}$$

$$\gamma_W = (E_H = M + \nu)/W, \tag{3}$$

$$\sin^2 \frac{\theta}{2} = \frac{Q^2}{4EE'}, \tag{4}$$

$$\sin^2 \theta_H = \left[\frac{E'}{E} \frac{\cos^2 \frac{\theta}{2}}{1 + \frac{2\nu}{Q^2}}\right]^{\frac{1}{2}}, \tag{5}$$

where θ and θ_H are the laboratory angles of the final lepton and hadron systems, E is the neutrino energy and E' the final lepton energy.

The loci of equal values of γ_W, the Lorentz-contraction factor, are indicated by the dashed parabolic curves in Fig. 1. The straight lines radiating from the point ($Q^2=0, \nu = 50$ GeV) are loci of equal lepton angles for E=50 GeV. Fig. 2 is the corresponding graph for E=20 GeV.

If all the final hadrons are in thermal equilibrium, we can estimate the pion multiplicity $\langle n\pi \rangle$, which depends only on W. The opening angle for the hadron jet is of order γ_W^{-1}. The rising parallel lines in Figs. 1 and 2 correspond to different values of $\langle n\pi \rangle$. We believe this model provides an upper limit to the multiplicity and serves to emphasize the scope of the experimental task in detecting neutral pions.

B. Dynamics

1. Differential Cross Section

The differential cross section for the interaction of neutrinos on hadrons can be written in terms of the quantities just defined as

$$\frac{d^2\sigma}{dQ^2 d\nu} = \frac{G^2}{2\pi}\frac{E'}{E}\beta\left\{1 - \frac{Q^2}{4EE'} + \frac{\nu^2+Q^2}{2EE'}\left[(R)+(L)\right] + \frac{E+E'}{2EE'}\sqrt{\nu^2+Q^2}\left[(L)-(R)\right]\right\} \tag{6}$$

where

$$\beta = W_2 = \frac{1}{2\pi}\frac{Q^2}{\nu}\left(\frac{1}{1+\frac{Q^2}{\nu^2}}\right)\left(1-\frac{Q^2}{2M\nu}\right)(2\sigma_S + \sigma_R + \sigma_L) \tag{7}$$

$$(R) \equiv \frac{\sigma_R}{2\sigma_S + \sigma_R + \sigma_L}, \qquad (L) \equiv \frac{\sigma_L}{2\sigma_S + \sigma_R + \sigma_L} \tag{8}$$

where σ_R, σ_L and σ_S are cross sections for the appropriate helicity states.

For $Q^2 << \nu^2$, Eq. (6) becomes

$$\frac{d^2\sigma}{dQ^2\, d\nu} = \frac{G^2}{2\pi} \frac{E'}{E} \beta \left[1 + \frac{\nu}{E'} (L) - \frac{\nu}{E} (R) \right] \qquad (9)$$

or

$$\frac{d^2\sigma}{dx\, dy} = \frac{G^2 M E}{\pi} \nu \beta \left[(1-y) + \frac{y^2}{2} ((R)+(L)) + y \left(1-\frac{Y}{2}\right) \{(L)-(R)\} \right] \qquad (10)$$

where

$$\beta = \frac{Q^2}{2\pi} (1-x) (2\sigma_S + \sigma_R + \sigma_L) \qquad (11)$$

and

$$x \equiv \frac{Q^2}{2M\nu}, \quad y \equiv \frac{\nu}{E}, \qquad (12)$$

$$0 \leq x \leq 1, \; 0 \leq y \leq 1.$$

Some motivation for the use of the variable χ can be seen if one supposes that the neutrino might scatter off only a fraction, χ, of the nucleon. The kinematics of quasi-elastic scattering is obtained by replacing M by χM. It would be represented in Fig. 1 by a radial line from the origin with a slope χ times that of the one for $Q^2 = 2M\nu$. Bjorken has shown that at high incident energies if the parts are point-like the σ_R, σ_L, and σ_S are functions of χ only (scale invariance). Consequently, when one integrates equation (10) over χ and y one obtains σ = (constant) E, a relation that we can test experimentally provided we detect all final states.

2. "Spin-$\frac{1}{2}$-Parton" Model

To obtain a feeling for where events would lie in the Q^2 – vs – ν plane for the "spin-$\frac{1}{2}$-parton" model, we have set $\nu\beta$ = (constant)$\cdot$ $(1-\chi)$ and $\sigma_R = \sigma_S = 0$. Fig. 3 shows how 1000 50-GeV neutrino interactions would be distributed under these assumptions. The important point is that all sectors contain statistically significant populations.

3. Pomeranchukon-Exchange Model

Predictions for the Pomeranchukon-exchange model can be obtained by setting $\nu\beta$ = (constant) (1-X) and $\sigma_L = \sigma_R$, $\sigma_S = 0$. The distribution of 1000 events at 50 GeV for these assumptions are shown in Fig. 4.

We propose to make our detection efficiency high in all sectors of the Q^2 -vs-ν plot and consequently, to be able to measure the total cross section.

4. Fireball Model

We introduce the notion of the hadron system being in thermal equilibrium to obtain a crude idea as to what the pion multiplicity might be and how this fireball will emit its products in the lab system. It can be shown that half of the products will be emitted into a cone of half angle,

$$\theta_{cone} \approx \gamma_W^{-1} \approx \sqrt{\left(\frac{2M}{E}\right)\frac{(1-x)}{y}} \quad . \tag{13}$$

The laboratory angle for the final lepton is

$$\theta_\mu \approx \sqrt{\left(\frac{2M}{E}\right)\frac{xy}{(1-y)}} \tag{14}$$

and for the laboratory direction of the hadron system is,

$$\theta_H \sqrt{\left(\frac{2M}{E}\right)\frac{x}{y}\ (1-y)} \quad . \tag{15}$$

In order to summarize the production and decay processes, we distort the triangular sectors of Fig. 5 ab into rectangular ones. Within the rectangular sectors we draw pictures of how the events might look. The kinematics of the outgoing hadron system and final lepton are shown for some of the sectors. Most hadrons will be obtained within the shaded cones; the vector is the outgoing lepton momentum. Fig. 5b summarizes the corresponding information at E=20 GeV. The hadron

cones are constructed with pessimistic (it predicts too many π^0's with cone angles too large) assumptions, namely, those of a fireball model for the hadron system. The Pomeranchukon-exchange model would predict cones with smaller opening angles and smaller meson multiplicity.

Bjorken and Paschos[1] point out that the difference, $\sigma_\nu - \sigma_{\bar{\nu}}$, is very model dependent. We wish to expose the chamber to both ν and $\bar{\nu}$.

C. Event Rate

In estimating the event rate, we assume the radial distribution for the neutrino beam at the detector obtained from the spectra of D. Carey, et al.[2], (reproduced here as Fig. 6c). We then integrate Eq. (10) over χ and y, assuming σ_R, σ_L, and σ_S are functions only of χ. The resulting total cross section is proportional to the neutrino energy E. The event rates are calculated for two assumptions: a.) the linear relation, $\sigma = 0.8$ E GeV x 10^{-38} cm^2, holds for all energies; and b.) the cross section saturates at E = 10 GeV and remains constant at 8×10^{-38} cm^2, for higher energies.

The lower set of curves in Fig. 6a indicates the number of neutrino interactions per GeV per 10^6 beam pulses (at 2×10^{13} protons/pulse) per 10^{-38} cm^2. The upper set of curves in Fig. 6a is for assumption a, $\sigma = 0.8$ E (GeV) x 10^{-38} cm^2, while curves for assumption b with a saturated cross section at 8×10^{-38} cm^2 are shown in Fig. 6b. Also shown in Figs. 6a, b are histograms for the number of interactions per 10^6 pulses that lie within 1 meter of the beam axis. Because there is so much uncertainty about K^- yields and hence $\bar{\nu}$

flux, we show no corresponding curves for antineutrinos.

D. Measurement of $\frac{d N\nu,\bar{\nu}}{d E\nu,\bar{\nu}}$

1. Neutrino Energy Spectrum

In determining cross sections, one must first find the energy spectrum of the incident neutrinos. This spectrum, normalized with the data obtained from the neutrino flux monitor, gives the number of neutrinos incident in each energy interval during the course of the experiment. Neutrino events occurring in the bubble chamber can then be assigned to the appropriate intervals once the total energy of the final-state particles has been measured.

2. Measurement of Meson Production by Protons

As part of an initial beam survey, measurements should be made of meson production by protons of 200 GeV from targets of H_2, D_2, Li, Be, and Al. Data are needed for pion momenta above 20 GeV/c and laboratory angles between zero and 20 milliradians. Similar studies should be carried out at 500 GeV as soon as protons of this energy become available.

We feel that our understanding of the production mechanism would be significantly enhanced if a bubble chamber of modest size were exposed to primary protons at 200 and 500 GeV. Attention would be focused on low-energy charged kaons and pions corresponding to the backward jet in the center-of-mass system. We therefore endorse, and some of us would like to participate in, the bubble-chamber survey proposed by G. Snow.[3] We suggest that NAL investigate the possibility of making the bending magnets of area 2 capable of bending 500 GeV protons. Exposure of only 10 to 20 protons per pulse are needed.

The quadrupoles could remain at their 200 GeV values.

3. Meson-Focusing System

The meson-focusing device should maximize the neutrino flux at 35 GeV with incident protons of 200 GeV. To reduce systematic errors in the cross sections resulting from uncertainties in the neutrino energy and thus the neutrino flux, the meson-focusing device should simultaneously minimize the logarithmic derivative, $\left| \mathrm{d}\ \ell n \frac{\mathrm{d}\, N_\nu}{\mathrm{d}\, E_\nu} / \mathrm{d}\ \ell n\ E_\nu \right|$. This can be accomplished by eliminating those mesons that produce low-energy neutrinos ($E < 16$ GeV) and by focusing those mesons that produce neutrinos near 35 GeV. The low-power, high-band-pass devices proposed by Frisch and Kang[4] and by Palmer[5] appear to be well suited to the neutrino energy selection required. For our hybrid system a one-millisecond beam spill would be ideal, that is, short enough for the bubble chamber and long enough for the electronic devices. (We anticipate of order 1 neutrino interaction per pulse in the quantameter and of order 100 per pulse in the hadrometer. The "deadtime" of these instruments is less than 1 μ sec.)

4. Neutrino Flux Monitor

Wachsmuth[6] has described a monitoring system for the neutrino flux which measures essentially the longitudinal and radial distributions of muons within the muon shield in front of the bubble chamber. We believe such a system is necessary for reliable operation of the neutrino beam, as well as for the flux determinations required in obtaining cross sections.

D. Measurement of the Neutrino Energy

1. Curvature and Total Energy of Charged Hadrons

The neutrino energy, E or E_ν, $\bar{\nu}$, is determined for each event

by measuring the energies of all outgoing particles. The energy of the charged-hadron component is given most precisely by track curvature in the 30-KG field of the bubble chamber, while a less-precise check is obtained from the hadron calorimeter associated with muon identification. The hadrometer is limited primarily by the statistics of hadron cascades in which, unlike electromagnetic cascades, a significant and variable fraction of the energy is lost to secondary neutrinos, slow neutrons, and nuclear binding energy.[7] Fluctuations in these losses are characteristic of all hadron calorimeters, and they point up one of the major advantages of the bubble chamber as a tool for doing neutrino physics. Curvature should give the charged-hadron energy to $\pm 3\ ^{o}/_{o}$, while the hadrometer resolution and precision for single events may be about $\pm 10^{o}/_{o}$ at 35 GeV.[7]

2. Total Energy of π^{o}'s via Proportional Calorimeter

Considerable thought has been given to ways in which neutrals could be detected in the large H_2, D_2 bubble chambers.[8] For chambers of volume exceeding 100 m^3, it is possible to place track-sensitive inserts of H_2 or D_2 into mixtures of H_2-N_e and obtain effective volumes* of order 30 m^3 for neutrino physics. NAL has proposed a chamber smaller than 100 m^3, namely 30 m^3, similar to the proposed BNL 14-foot chamber. The effective volume of inserts into this 12-foot-diameter sphere are less than 3 m^3, a volume that would yield too few events in the high-energy region.

*"Effective volume" is the volume of the insert multiplied by the efficiency for detecting all of the photons from neutral pions in the H_2-N_e mixture.

To permit the necessary determination of the neutral pion energy, we propose to take advantage of a special feature of the NAL 15-foot (30 m^3) bubble chamber design -- namely the thin exit wall of 1/2" steel, less than one radiation length. The thin wall implies that protons from π^o decay can be detected efficiently and the total shower energy measured precisely by a cylindrical π^o quantameter[9] at the downstream end of the chamber. A possible arrangement is shown schematically in Figs. 7 and 8. The quantameter itself is described in more detail in Section III. The total-energy resolution should be better than $\pm 3\ ^o/_o$ for events in which the total energy into neutral pions is above a few GeV. Precise calibration would then permit an obsolute determination of the π^o component in a single event to about the resolution limit.

We propose to install the quantameter in a special reentrant well constructed in the vacuum tank downstream of the hydrogen volume. This location, shown in Fig. 8 requires that the coil diameter be extended about 1/2 meter. These modifications, in addition to permitting a quantameter of 15 to 20 radiation lengths thickness, would preserve the entire useful volume of the bubble chamber. The volume assumed in calculating the yield histograms of Figs. 6a, b is a cylinder of 1-m radius, intercepting a sphere 3.6 m in diameter, and yielding a fiducial volume of 10 m^3. The volume outside this cylinder could be used as a blanket of H-N_e mixture to detect wide-angle photons.

3. Total Energy of Hadrons via Proportional Calorimeter

The total energy of the hadrons (charged hadrons and neutrons)

can be obtained from a hadrometer. This device is analogous to the quantameter except that the plates would be made of copper, non-magnetic steel, or concrete instead of lead (for operation near the bubble chamber), and the plate thicknesses would total 10-15 collision lengths rather than 15-20 radiation lengths. Thus the hadrometer serves three purposes: it stops hadrons permitting muon identification, it measures hadron energy, including the energy of any neutrons emitted from the neutrino vertex, and it follows tracks spatially.

The hadrometer would be located just outside the bubble-chamber magnet as close to the magnet as practical. It's configuration might approximate a vertical half-cylinder, similar to the quantameter, although rectangular modules, such as those shown in Fig. 8, appear to be more practical. As in the case of the quantameter, a portional-calorimeter design with wire readout will be used. This is discussed in more detail in Section III.

4. Lepton Total Energy

The momentum of the final lepton is measured by curvature. Like the curvature measurements of the charged-hadron energy, this possibility is a major advantage of the bubble-chamber approach: peripheral equipment is required only to identify escaping muons, not to stop them or otherwise determine their energy. Final electrons are identified in the quantameter. Thus the hadrometer or absorber used with the bubble chamber is much thinner than the full muon range. This, in turn, permits much larger solid-angle detection for muons at an acceptable cost -- a feature well matched to intrinsically large solid angle of the bubble chamber.

Any particle penetrating 10-15 collision lengths of hadrometer is almost certainly a muon. Proportional (Charpak) chambers[10] or wire chambers can be used to locate the muon path with high spatial resolution. The muon may be identified by projecting each track from the vertex through the quantameter and hadrometer and testing whether its location at the final muon detector is consistent with location at the observed track. We propose to build into the quantameter and hadrometer a number of coordinate-sensitive planes to follow each track in detail, tracing each detected muon backwards into the bubble chamber.

F. Measurement of Structure of Hadronic State

The bubble chamber is ideally suited to studies of the final hadronic system. Hadrons, like muons, trapped in the magnetic field can usually be identified by their interactions in the hydrogen of the chamber. A much larger class of events can be studied in detail by tracing individual tracks through the quantameter and into the hadrometer where energetic nucleons in the final state may possibly be identified.[11]

Similarly, detailed information on individual π^o's and η^o's can be obtained from a knowledge of the vertex location and the origins of correlated γ showers. In many cases, for example, the π^o energy can be determined from the photon opening angle, and in some cases a separation of π^o and η^o decays should be possible.

A procedure of the type just discussed requires extensive use of coordinate-sensitive planes. The proportional-calorimeter design described in Section III permits several planes per gap or per

plate without interfering in any way with the determinations of neutral pion or hadron energy. This option is a major advantage of the proportional (Charpak) chamber.[10]

G. Possible Hadronic Decay Modes of the Intermediate Vector Boson (IVB)

If the mass of the IVB is large many decay modes are possible.[8] Again the high measurement accuracy of the bubble chamber makes it an ideal instrument for detecting these modes. Provided the mass of the IVB is not too large, its width is likely to be much smaller than the experimental resolution function of the bubble chamber. Thus the signal/noise will be improved with increased measurement accuracy.

We list below in diagramatic form some examples of the possible hadronic decay modes of the IVB.

Baryon-Antibaryon

$$W^{\pm} \rightarrow \bar{H}_8\left(\tfrac{1}{2}^+\right) + H_8\left(\tfrac{1}{2}^+\right)$$
$$\rightarrow \bar{H}_8\left(\tfrac{1}{2}^+\right) + H_{10}\left(\tfrac{3}{2}^+\right)$$

Boson-Antiboson

$$W^{\pm} \rightarrow \bar{H}_8\left(0^-\right) + H_8\left(1^-\right)$$

The symbol $\bar{H}_8\left(\frac{1}{2}^+\right)$ represents an antibaryon of the $\frac{1}{2}^+$ octet, etc.

Only those pairs of final particle-antiparticle states that are nearest neighbors in the Y –vs– T plot of Fig. 9 are allowed under the $\Delta S=0$ and $\Delta S=\Delta Q$ rules. For neutral IVB's (if neutral lepton currents exist) the nearest neighbors joined by the dashed lines would be possible decay products.

For low-momentum-transfer production the IVB would receive most of the energy of the incident neutrino. Consequently, the decay fragments would be thrown into a forward cone of half angle $MW/2E$.

The quantameter would easily detect the π^o's that might be among the decay products.

III. EXPERIMENTAL EQUIPMENT

A. Neutrino Beam

1. Targets

The enhancement of the high-energy portion of the neutrino spectrum requires thin targets consisting of light nuclei. Fig. 10 (Fig. 4a of TM 218)[12] summarizes how the number of neutrinos above a certain energy depends upon the target thickness. Our requirement is for $q > 2$, thus the optimum target thickness is about 1 mfp. The detrimental effects on the high-energy neutrino spectrum of multiple interactions of the incident nucleon within a complex nucleus provide strong motivation for developing targets of very light nuclei. Experimentation and design studies for the neutrino target should begin as soon as possible.

2. Meson-Focusing System

We wish to participate in the design and testing of a meson-focusing device[4,5] to produce those special qualities in the neutrino beam alluded in Section II D.3.

3. Neutrino Flux Monitor

The CERN neutrino spectrum was measured by placing emulsions and ionization chambers at various depths and radial positrons in the muon shield to determine the muon flux at these points. Wachsmuth[6] asserts that if the pion and kaon spectra are known and the shield measurements taken, $\frac{d\,N_\nu}{d\,E_\nu}$ at the bubble chamber can be determined to about 5 $^o/_o$. The importance of determining $\frac{d\,N_\nu}{d\,E_\nu}$ is

so great for this experiment that some of us would like to participate in these measurements.

While the equipment relating to the neutrino beam would be part of the NAL facility, members of this proposal are prepared to participate in the design and development of this apparatus.

B. Hybrid Detector System

1. 30 m^3 H_2, D_2 Bubble Chamber

The detector has already been discussed briefly in Section II, dealing with the type of measurements one might make. The hybrid system shown in Fig. 8 is built around the NAL bubble chamber and offers these advantages:

a. precision on $E_\nu = E_\pi o + E_H + E_\mu$ to $\pm 3\ ^o/_o$,

b. vertex information of the bubble chamber,

c. absorber (hadrometer) thickness much less, than the muon range

d. large solid angle,

e. simplicity.

Of these, the first four follow immediately from the use of the bubble chamber itself, particularly its ability to measure E_H and E_μ, once the muon has been identified. Supplementary information on E_H, including identification of baryons, is provided by the hadrometer, while $E_\pi o$ is given solely by the quantameter. The advantage of simplicity follows partly from relatively thin absorber required (since the bubble chamber measures E_μ) and partly from the use of porportional calorimeters to be described.

The reentrant cylindrical tank housing the quantameter is an

important change in the preliminary bubble-chamber design and necessitates an increase in the coil diameter of about 1/2 meter; this change will greatly increase the effectiveness of the bubble chamber for both strong and weak interaction physics, particularly in reactions involving final π^o's.

2. Ionization and Proportional Calorimeters

Parallel-plate ionization calorimeters, such as the quantameters[9] widely used in monitoring photon beams, have several intrinsic properties that are essential in determining E_{π^o} and E_H accurately. First, the response depends only upon the relative ionization in the gas gaps as compared to the ionization in the plates; tolerances of a few percent in these parameters are easily met and insure a uniform response to the same level. Second, since the ratio of gap to plate is independent of track angle in a parallel plate chamber, such a device is intrinsically isotropic. Third, the output of an ionization calorimeter is linear in the energy absorbed over a wide range. Fourth, an ion chamber is operated as a one-parameter device; there is one high-voltage setting and one output signal proportional to the total energy deposited in the chamber as sampled periodically via the ionization in the gas gaps. This last feature greatly simplifies the operation of the calorimeter and results in a high reproducible instrument.

In the case of electromagnetic showers (E_{π^o}), virtually all of the energy appears ultimately in the form of ions, which are sampled directly in the ionization calorimeter thereby avoiding such questions as the response of scintillation or Cerenkov counters.

In the case of hadronic cascades, a certain portion of the energy is lost to neutrinos, slow neutrons, and nuclear binding, as mentioned previously.[7] A typical loss might be 20-30 $^{o}/_{o}$ at 35 GeV, although for some events the loss may be catastrophically large. Within the statistical uncertainties of this process, the response is similar for all hadrons, including high-energy neutrons, providing the absorber thickness is sufficient to contain the cascade. The actual gain can be determined by calibration with hadrons of various energy.

The only serious limitation of ionization calorimeters, as far as the present application is concerned, is their relatively low gain, typically[9] 4×10^3 ions per GeV absorbed with 1-atm of A-CO_2. This small signal appears across the relatively large capacity of the parallel plate structure and is not easily detected.

A much higher gain is possible by using the high electric fields surrounding small-diameter (20-100μ) wires to induce proportional avalanche multiplication. Proportional calorimeters[10] retain the uniformity, isotropy, and linearity of ion chambers, and if the signals from the high-voltage plates are added, there is one high-voltage setting and one output signal. The gain of a proportional chamber, unlike an ion chamber, varies exponentially with the high voltage, but good reproducibility can be obtained.

Proportional, chambers cease to be linear when the space charge in single avlanches appreciably distorts the electric field near the wires. This occurs typically at 5×10^6 ions, and the high voltage is normally set low enough so that this condition is not

exceeded.

A crucial point in our application is that the primary ionization of the shower, consisting of some 4000 ions/GeV, in the gas, is distributed over several hundred tracks in perhaps 10 gaps. As many as 10^3 avalanches may be thus involved so that an output of 5×10^9 ions or more can be obtained without exceeding the linear response region. This largely compensates for the greater capacity of a pair of plates or of an entire chamber, as compared with the capacity of a single wire, and it yields an output voltage within one or two orders of magnitude of that normally obtained on a single wire of a multiwire proportional chamber. Such a net signal can easily be measured, and if necessary, one can afford sensitive amplifiers since only a small number of total-energy outputs are involved. (The situation is quite different when one must read 10^3 to 10^4 separate wires.)

3. Proportional Quantameter

We presently envision the proportional quantameter to consist of 10 lead plates and a similar number of gas gaps totaling 20 radiation lengths of lead, about 11.6 cm. A sector $90^\circ \times 90^\circ$ measured from the center of the bubble chamber would be about 4 meters high with a 3-m arc and would weigh about 16 tons. Each double gap would consist of a single wire plane centered between two lead plates and defining a total gap of 2x.5 cm = 1.0cm. Ten of these gaps would add an additional 10 cm to the quantameter thickness. Allowing an additional 5 cm for flanges and windows, we obtain a total quantameter thickness of about 30 cm. A 35-cm-wide reentrant tank would

allow, in addition, the installation of a couple of scintillation counters or possibly a two-gap spark chamber. Some reduction in quantameter thickness could be obtained by using tungsten plates, fewer gaps, or somewhat less than 20 radiation lengths of material. Note that the steel walls of the bubble chamber and the reentrant wall will amount to 1-2 radiation lengths and may be considered as the first plate of the quantameter, while the quantameter at 1 collision length may be considered the first plate of the hadrometer. The quantameter itself might then begin with a sensitive gap followed by the first lead plate.

The wires of the proportional quantameter will be read out to provide spatial resolution. A wire diameter of 50μ and a spacing of 2mm is probably convenient[10] although 1mm seems feasible if one is willing to try hard enough. Vertical wires are straight forward in the cylindrical configurations, but horizontal wires may force a modular quantameter design with flat parallel plates.

4. Proportional Hadrometer

The hadrometer consists of perhaps 15 plates of copper each 10 cm thick and separated by gaps of 1.2 cm. A less-expensive plate material may be practical, giving the same thickness in collision lengths. The 12-cm lead of the quantameter is equivalent to about 1 collision length for hadrons while the 150 cm of copper adds an additional 13 collision lengths. The copper coils of the bubble chamber magnet amount to several collision lengths but do not seriously limit the accuracy of the hadron-energy determination for most event types.

We presently envision a proportional hadrometer design, with copper plates and wire readout, subtending vertical and horizontal angles of about 90° by 90° as measured at the center of the bubble chamber. The volume of copper would then be 8mx8xm1.5m and the weight about 800 tons.

As indicated in Table I, the cost of such a hadrometer is more than half the total for the experiment. Further, whereas the quantameter is essential to the experiment in providing a unique determination of E_{π^0}, the measurement of E_H is best done by the bubble chamber itself. If one abandons the measurements of E_H in the hadrometer and reduces the track following requirements, a number of cost-saving options are then possible including: reducing the hadrometer acceptance to 45° x 45°, using optical spark chambers instead of proportional chambers, reducing the number of plates, and using cheaper plate materials, for example a single wall of concrete shielding blocks. These options would not optimize the physics but might help to ensure that the essential physics is done.

5. Range Detector for Muons Leaving the Bubble Chamber

Highly peripheral events produce muons at large angles and at sufficiently low momenta that the muons can be trapped in the bubble-chamber magnetic field. Muons of a few GeV and more pass through the 14 collision lengths of photon and hadron absorber and can be identified in that way. A single plane of scintillators downstream of the hadrometer might suffice, while the last several gaps of the hadrometer could provide the spatial resolution necessary to permit muon tracks to be traced back to the bubble chamber. Events withmuons in an intermediate energy range, for example the range from 1 to

3 GeV, may frequently remain ambiguous, as far as muon identification is concerned unless the hadrometer subtends a very large solid angle and unless individual tracks are followed through each plane of the hadrometer until they stop.

6. Triggering Options

Signals should be available from the quantameter and hadrometer

within 100 ns of the occurence of an event and with a time jitter of less than 50 ns.[10]. These signals, in coincidence with scintillator planes, could be used to develop a trigger requiring an interaction having total energy above, for example, 10 GeV. Four scintillator planes might suffice: an anticounter in front of the bubble chamber, a yes-counter in front of the quantameter and another in front of the hadrometer, and finally the muon counter plane already mentioned. The trigger could be used to flash the bubble chamber illumination or fire peripheral spark chambers, or it could simply be recorded for use in analyzing the bubble-chamber film. We presently favor the last option, at least during the early stages of the experiment.

IV. SCHEDULES AND PARTICIPATION

A. Design and Development of Equipment

We shall explore ways in which the participating groups, and particularly LRL as a service to other users, can participate in the design and development of the neutrino beam, quantameter, hadrometer, counters and modifications of the bubble chamber. Arrangements for sharing the cost could be negotiated between our groups and NAL.

B. LRL Development

Work should begin immediately on some of the special items just mentioned. Among these is the design of the reentrant tank for the quantameter, which could be carried out by LRL mechanical engineers skilled in cryogenic equipment. The design could proceed at Berkeley in close collaboration with W. Fowler and his group at

NAL. In addition, the shop and experimental facilities of LRL could be made available to the University of Hawaii group and others involved in developing the quantameter and hadrometer.

C. Participation of Our Personnel at NAL.

The development of the neutrino beam equipment would best be done at NAL. We would hope to make the experience of graduate students stationed at NAL as broad as possible. Thus, while a major fraction of their time would be devoted to development of the neutrino facility and bubble chamber, their direct participation in construction and other activities of the accelerator should be encouraged.

D. Beam Survey Experiment

The meson production measurements should start as soon as the survey beam (10^{10} proton/pulse) is available in Area 2. Here, we could provide experienced personnel and some equipment to aid groups that have made specific survey proposals involving major hardware commitments.

A survey bubble chamber of the type suggested by Snow[3] should be available at the turn-on date of Area 2. The present film and data-analysis equipment at our participating institutions is adequate to handle exposure of several hundred thousand pictures on both hydrogen and deuterium. The information from the yield measurements could be used to up-date the operating parameters of the meson-focusing device. Early exposures to 500-GeV protons would be very useful in designing the focusing for the 500-GeV phase. Since only ten or twenty protons per pulse are required, one might consider

designing the bending magnets of Area 2 (super conducting?) to bend 500-GeV protons, allowing the quadrupoles to remain set at their 200-GeV design values. At the low intensities required, no radiation damage would result to the beam transport equipment, and no additional shielding would be required. Reliable, fail-safe intensity-control equipment would, however, be necessary.

E. Million-Picture Exposure at 200 GeV

The experimental program of preparing the neutrino beam for this application could easily occupy the first year or more after beam turn-on. The accelerator operation in its second and third years is likely to be more reliable, and the bubble chamber will be better understood. We therefore propose that a one-million picture exposure to hydrogen of both neutrinos and anti-neutrinos of high energy be made in the second or third year of operation at NAL. Similar exposures to deuterium would come later.

F. Million-Picture Exposure at 500 GeV

Our reason for requesting an exposure at higher accelerator energy is to allow the energy at which we have a low value of $\left| d \ln \frac{d N_\nu}{d E_\nu} / d \ln E_\nu \right|$ to be increased significantly. This, in turn, would raise the central neutrino energy from 35 GeV to 70 GeV for an acceptable uncertainty in the number of neutrinos incident. The 500-GeV exposure would accur at a much later date.

V. PRELIMINARY COST ESTIMATE

A preliminary cost estimate is given in Table I. The principal assumptions are:

A. Geometry shown in Fig. 8,

B. $1.00/pound for copper plates (container negligible),

C. $.50/pound for lead plates (container 18K),

D. all wires readout, 2-mm wire spacing, 10 planes/chamber, $5/wire to readout, $1.50/wire to fabricate the quantameter, $2.50/wire to fabricate the hadrometer.

As already mentioned, the cost is clearly dominated by the copper plates of the hadrometer,[13] $1600K out of $2600K total. If one reduces the hadrometer to an angular acceptance of 45°x45° (4mx4m), keeping other parameters fixed, the hadrometer cost is reduced from $1900K to $550K and the experiment from $2600K to $1250K, about a factor of two. Other savings could be made by using optical spark chambers or hadrometer plates of concrete shielding blocks. The quantameter and necessary modifications of the bubble chamber seem to us essential if one is to carry out a neutrino program of the type proposed here.

TABLE I

Preliminary Cost Estimates (All Wires Read Out)

			Cost K$	Cost K$
1.	Modifications of Bubble Chamber Coils and Vacuum Tank		300	300
2.	Quantameter:	Lead Plates and Container	50	
		10 Wire Planes	30	
		10x4m/2mm=20,000 Readouts x $5/wire	100	180
3.	Hadrometer:	Copper Plates and Container	1600	
		10 Wire Planes	100	
		10x8m/2mm=40,000 Readouts x $5/wire	200	1900
4.	Counter Planes:	4mx4m Anti (8scintillators 16 PMS)	20	
		4mx4m Yes at Quantameter In	20	
		8xm8x Yes at Hadrometer In (16 scintillators, 32 PMS)	40	
		8mx8m Yest at Hadrometer Out	40	120
5.	Computer Interfacing		50	50
6.	Fast Logic, Slow Logic, etc.		50	50

TOTAL = $2600K ($90^{\circ}x90^{\circ}$ Hadrometer)

If the plate area of the hadrometer is reduced from 8mx8m to 4mx4m, the estimated cost of the experiment is

TOTAL = $1250K ($45^{\circ}x45^{\circ}$ Hadrometer)

REFERENCES

1. J.D. Bjorken and E.A. Paschos, SIAC-PUB-678, December, 1969 (Lectures by Bjorken at 1969 Summer Study).

2. D. Carey, Y.W. Kang, F.A. Nezrick, and R. Stefanski, TM-222 "A Note on the 200-GeV Neutrino Design."

3. G.A. Snow (correspondent) "Preliminary Proposal to Study Multiparticle p-p and π-p Interactions from 75 to 200 GeV/c (and higher momenta as soon as they become available), April 23, 1970. University of Maryland High Energy Physics Group.

4. D. Frisch and Y.W. Kang, "D.C. Horn for Very-High-Energy Spark-Chamber Neutrino Experiments," 1969 NAL Summer Study 1, 389.

5. R.B. Palmer, "The Design of Long-Pulse Monopole Focusing Elements," 1969 NAL Summer Study 1, 383.

6. H. Wachsmuth, "Neutrino Spectrum Determination from Muon Flux Measurements," 1969 NAL Summer Study 1, 367.

7. V.S. Murzin, Progress in Elementary-Particle and Cosmic-Ray and Cosmic-Ray Physics, (North-Holland Publishing Company, Amsterdam, The Netherlands, 1967), Vol. IX, p. 245.

8. See for example M.L. Stevenson, "High-Energy Neutrino Physics $< E_\nu >$ 20 GeV and the Constraints Placed on Detectors," 1969, NAL Summer Study 2, 121.

9. R.R. Wilson, Nucl. Instr. 1, 101 (1957). A high-energy (multi-GeV) quantameter is described by D. Yount, Nucl. Instr. Methods 52, 1 (1957).

10. G. Charpak, D. Rahm, and H. Steiner, "Some Developments in the Operation of Multiwire Proportional Chambers," CERN Preprint.

11. A. Pais, "Weak Interactions at High Energies," Presented at the Conference on "Expections for Particle Reactions at the New Accelerators," University of Wisconsin, 1970; S.D. Drell and Tung-Mow Yan, "Final Particle Correlations in Deep Inelastic Lepton Processes," Phys. Rev. Letters 24, 855 (1970).

12. M.L. Stevenson, "Targets for the Neutrino Beam: Concepts," NAL Report TM 218.

13. D.D. Jovanovic, R. Palmer, and B. Roe, "Muon Detectors after the 25-foot Chamber" Aspen 1969 Summer Study, 2, 207.

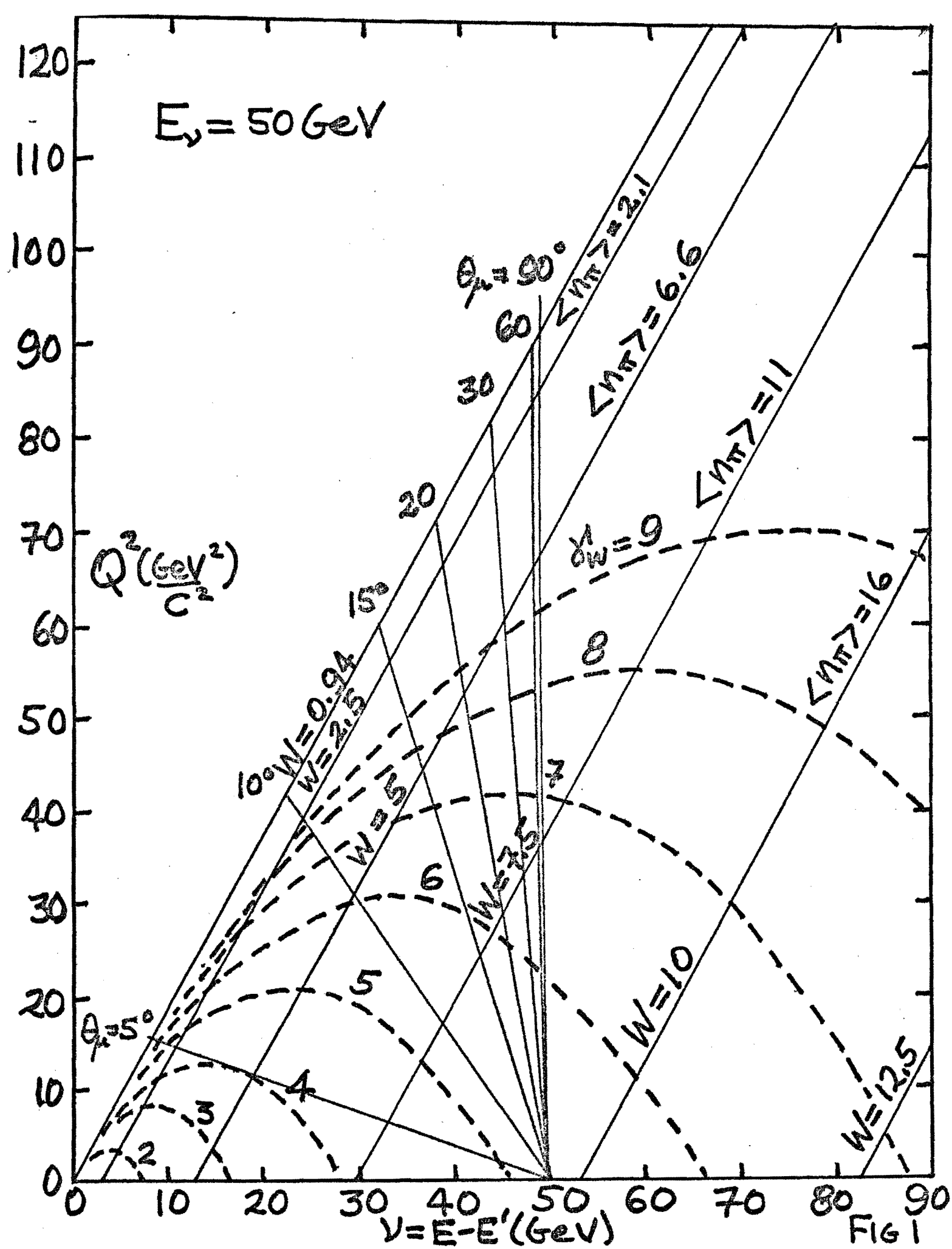
$E_\nu = 50\,GeV$
$Q^2\left(\frac{GeV^2}{c^2}\right)$
$\nu = E - E'(GeV)$
$\theta_\mu = 90°$
60
30
20
15°
10°
$\theta_\mu = 5°$
$\langle n_{\pi^+} \rangle = 2.1$
$\langle n_{\pi^+} \rangle = 6.6$
$\langle n_{\pi^+} \rangle = 11$
$\langle n_{\pi^+} \rangle = 16$
$W = 0.94$
$W = 2.5$
$W = 5$
$W = 7.5$
$W = 10$
$W = 12.5$
$\gamma_W = 9$
8
7
6
5
4
3
2
0
10
20
30
40
50
60
70
80
90
100
110
120

Fig 1

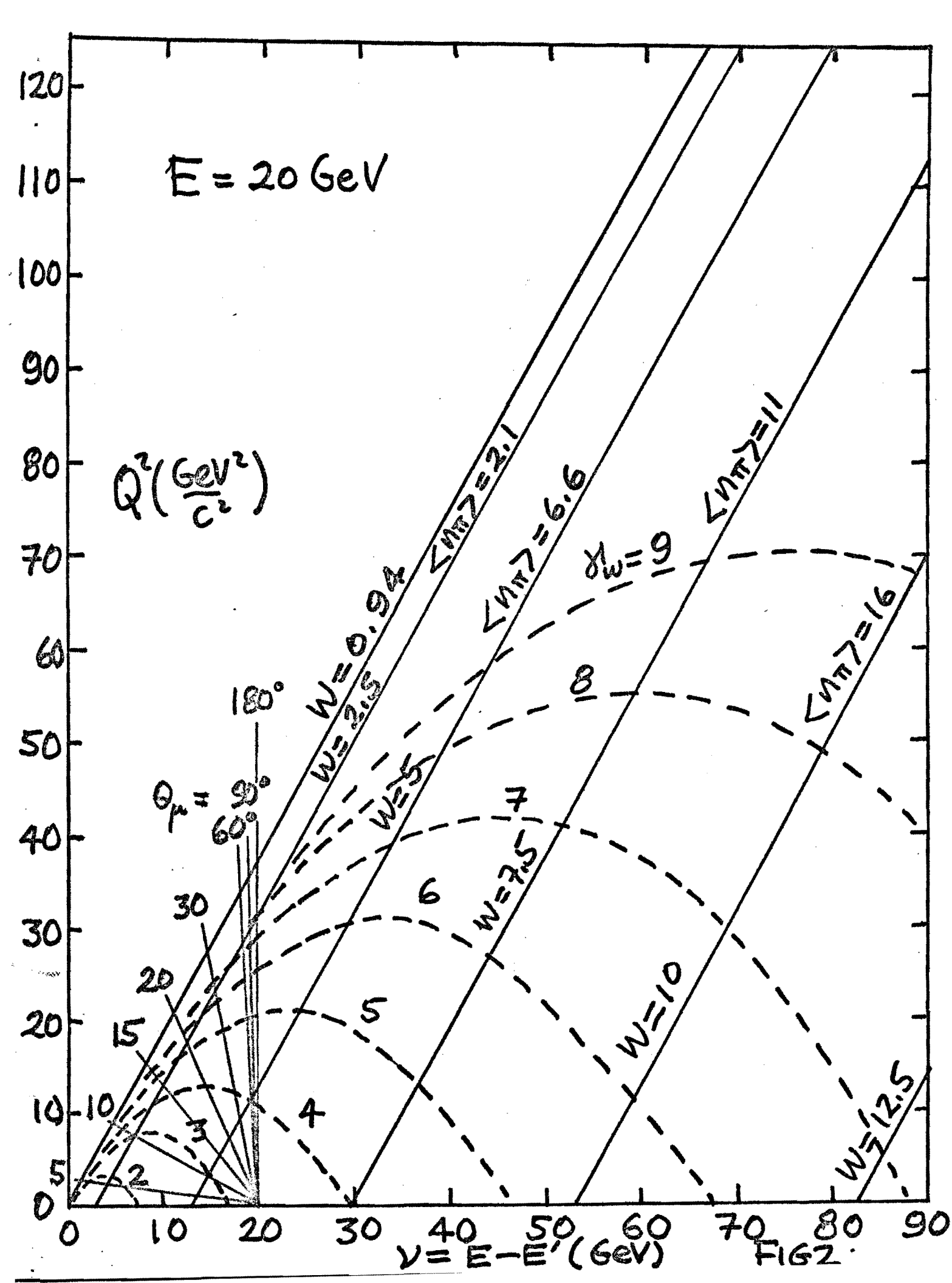
E = 20 GeV
$Q^2\left(\frac{GeV^2}{c^2}\right)$
W = 0.94
W = 2.5
W = 5
W = 7.5
W = 10
W = 12.5
$\langle n_{\pi^+} \rangle = 2.1$
$\langle n_{\pi^+} \rangle = 6.6$
$\langle n_{\pi^+} \rangle = 11$
$\langle n_{\pi^+} \rangle = 16$
$\gamma_W = 9$
8
7
6
5
4
3
2
$\theta_\mu = 180°$
90°
60°
30
20
15
10
5
0
10
20
30
40
50
60
70
80
90
$\nu = E - E'$ (GeV)

FIG 2.

Distribution of 1000 Events

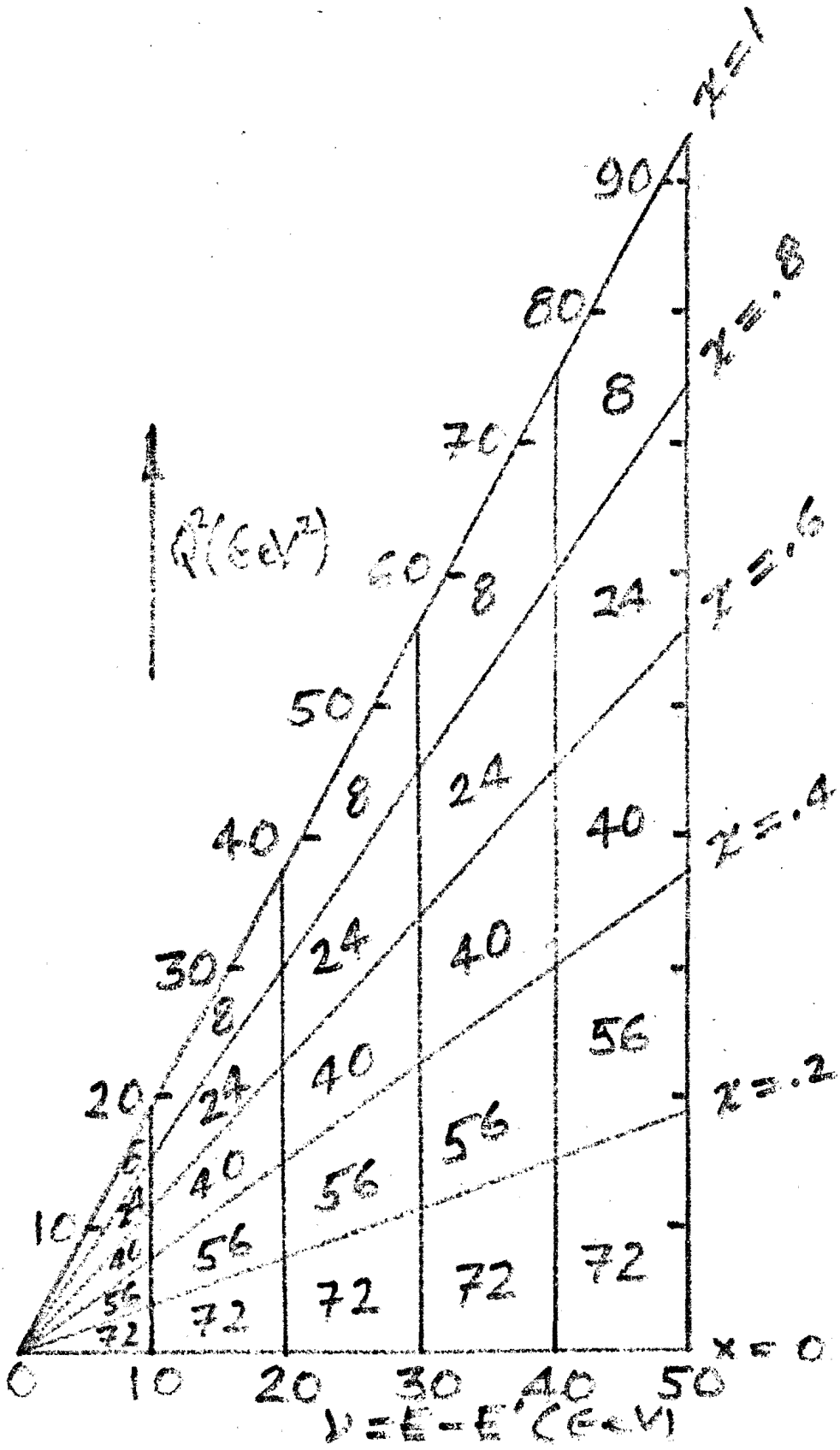

$E_\nu = 50$ GeV

for $\nu_2 = K(1-x)$

$C_R = C_3 = 0$

SPIN $\frac{1}{2}$ PARTONS

$M_W = \infty$

FIG 3

Distribution of 1000 Events

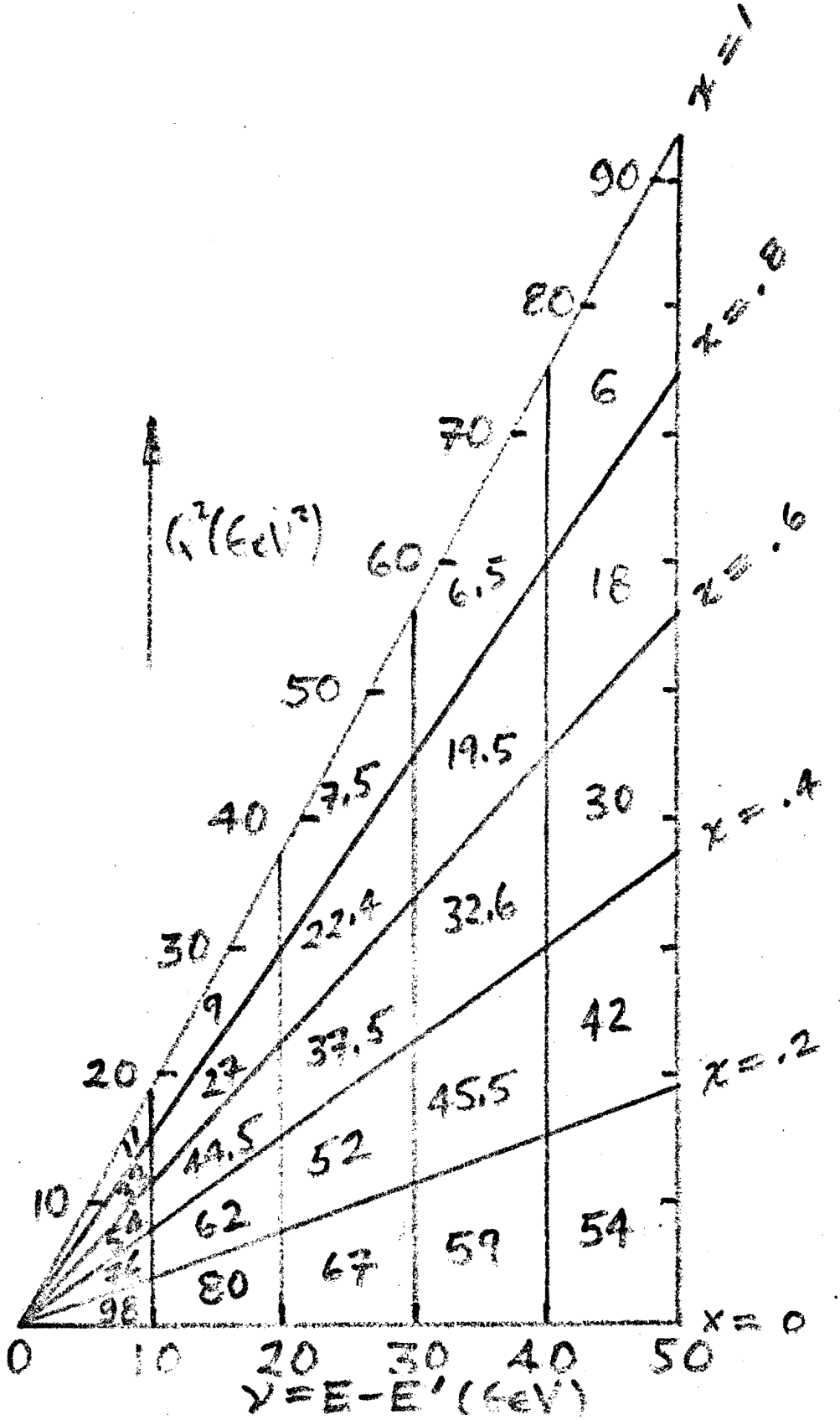

$E_\nu = 50$ GeV

for $\nu_3 = k(1-x)$

and $\sigma_L = \sigma_R$

(Pom. Exch)

$M_W = \infty$

FIG 4

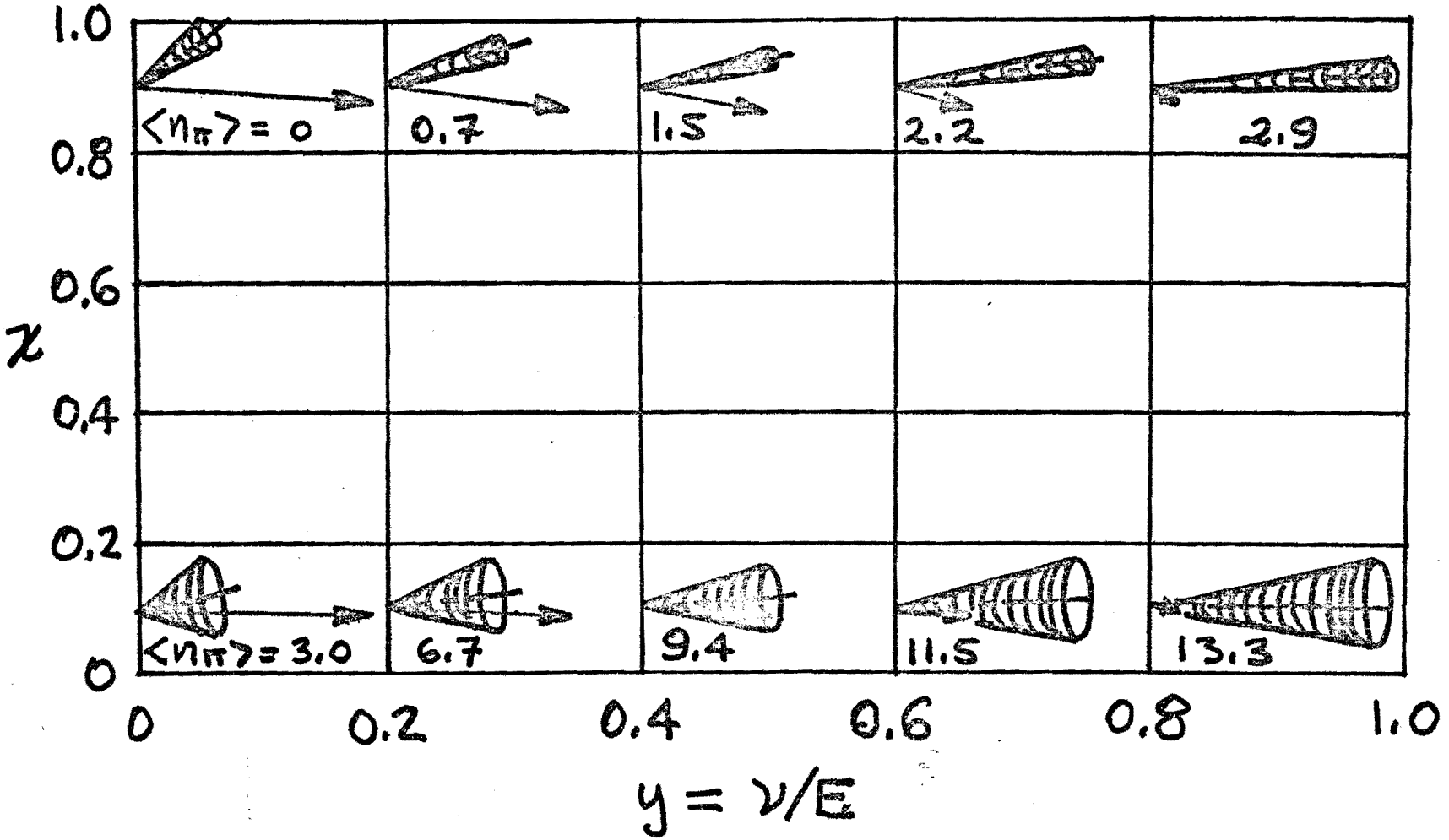
E = 50 GeV
1.0
0.8
0.6
0.4
0.2
0
x
<nπ> = 0
0.7
1.5
2.2
2.9
<nπ> = 3.0
6.7
9.4
11.5
13.3
0
0.2
0.4
0.6
0.8
1.0
y = ν/E

FIG 5a

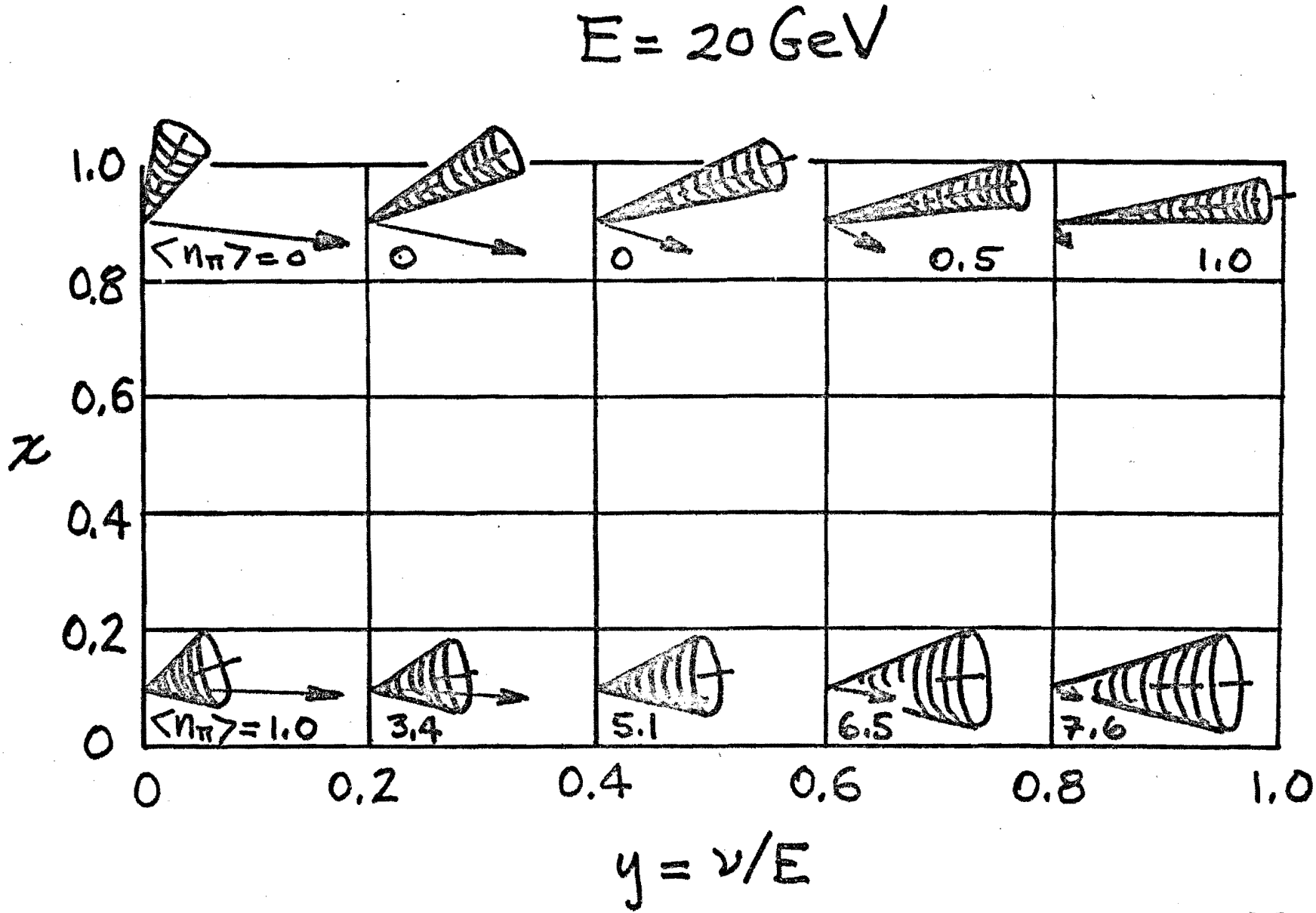
E = 20 GeV
1.0
0.8
0.6
0.4
0.2
0
x
<nπ> = 0
0
0
0.5
1.0
<nπ> = 1.0
3.4
5.1
6.5
7.6
0
0.2
0.4
0.6
0.8
1.0
y = ν/E

Fig. 5b

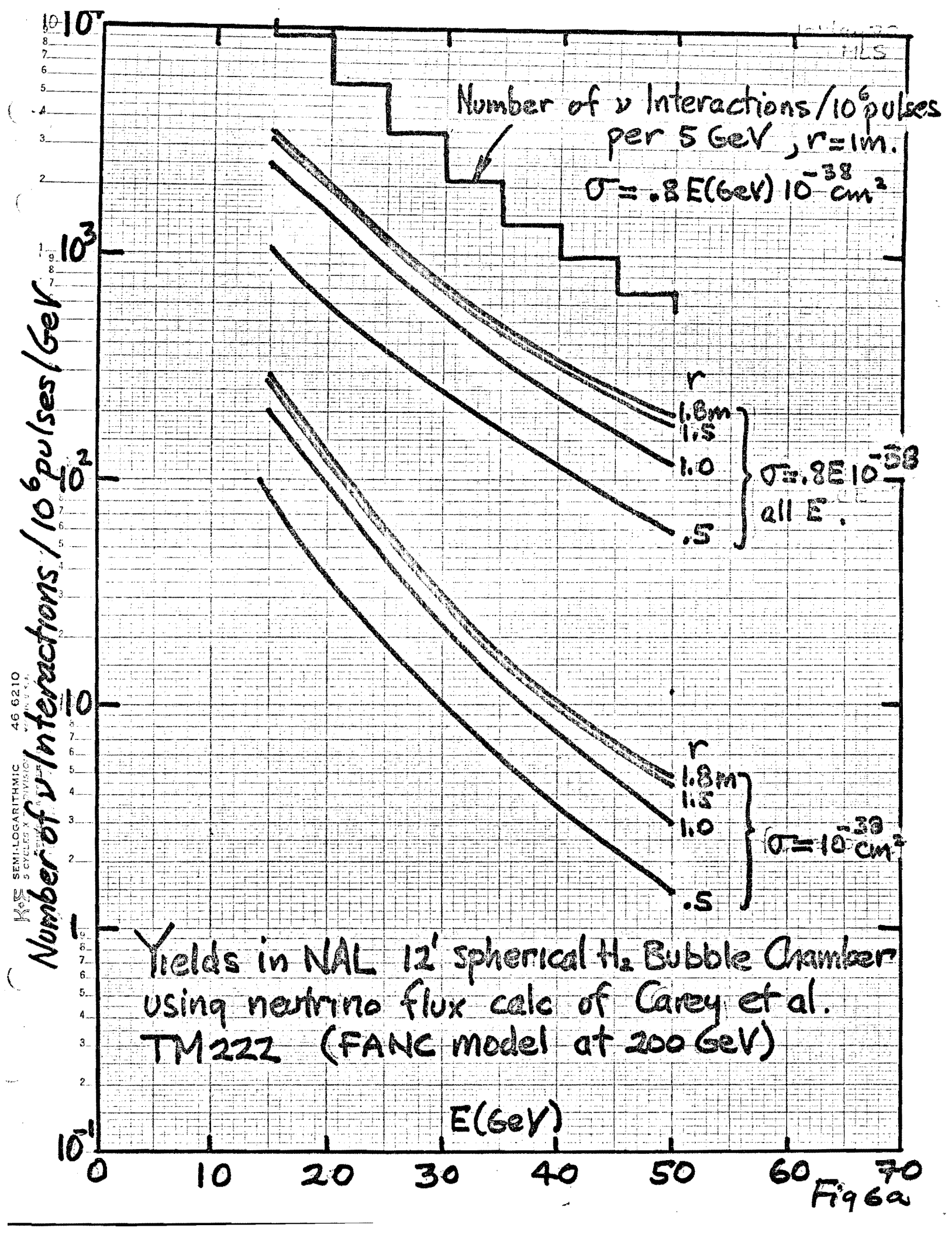
Number of ν Interactions/10⁶ pulses per 5 GeV, r=1m.
σ = .8 E(GeV) 10⁻³⁸ cm²
r
1.8m
1.5
1.0
.5
σ = .8E 10⁻³⁸ all E.
r
1.8m
1.5
1.0
.5
σ = 10⁻³⁸ cm²
Number of ν-Interactions / 10⁶ pulses / GeV
E(GeV)
Yields in NAL 12' spherical H₂ Bubble Chamber using neutrino flux calc of Carey et al. TM222 (FANC model at 200 GeV)
SEMI-LOGARITHMIC 46 6210
5 CYCLES X

Fig 6a

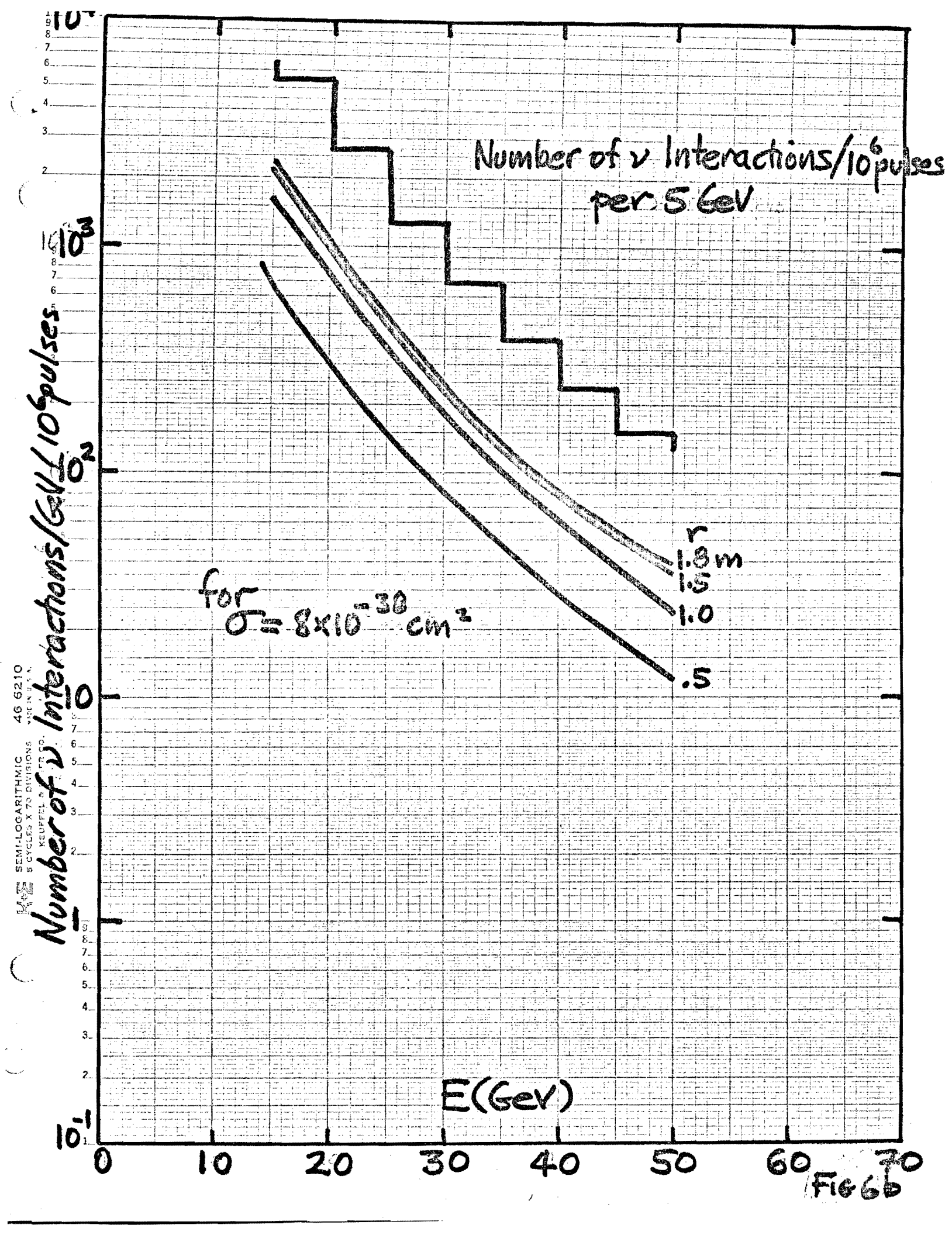
Number of ν Interactions/10^6 pulses per 5 GeV
Number of ν Interactions/GeV/10^6 pulses
for σ = 8×10^-38 cm^2
r
1.8 m
1.5
1.0
.5
E(GeV)
0
10
20
30
40
50
60
70
SEMI-LOGARITHMIC
5 CYCLES X 70 DIVISIONS
46 6210

Fig 6b

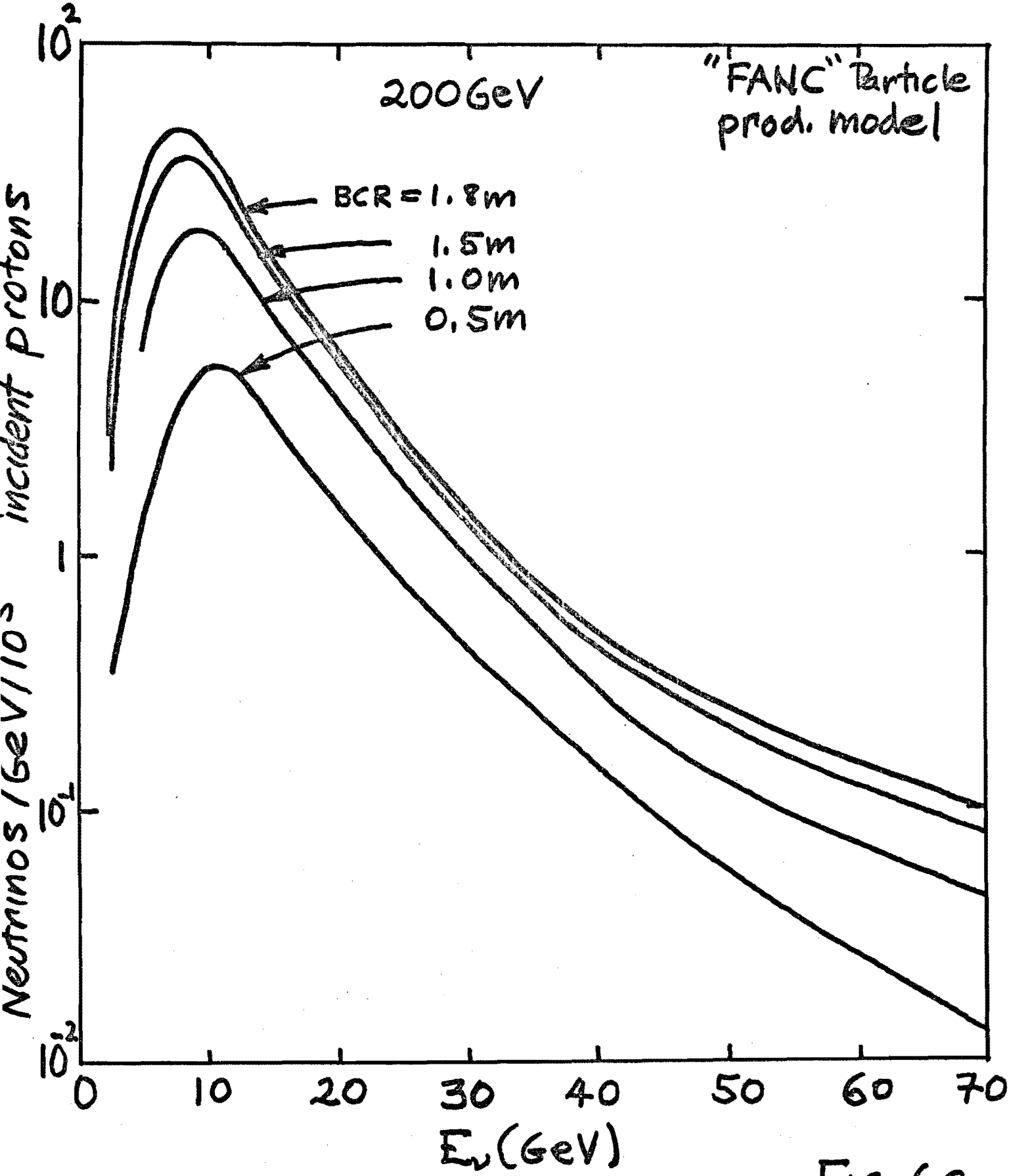
200GeV
"FANC" Particle prod. model
BCR = 1.8m
1.5m
1.0m
0.5m
Neutrinos/GeV/10³ incident protons
10^2
10
1
10^{-1}
10^{-2}
0
10
20
30
40
50
60
70
E_ν (GeV)

FIG 6C

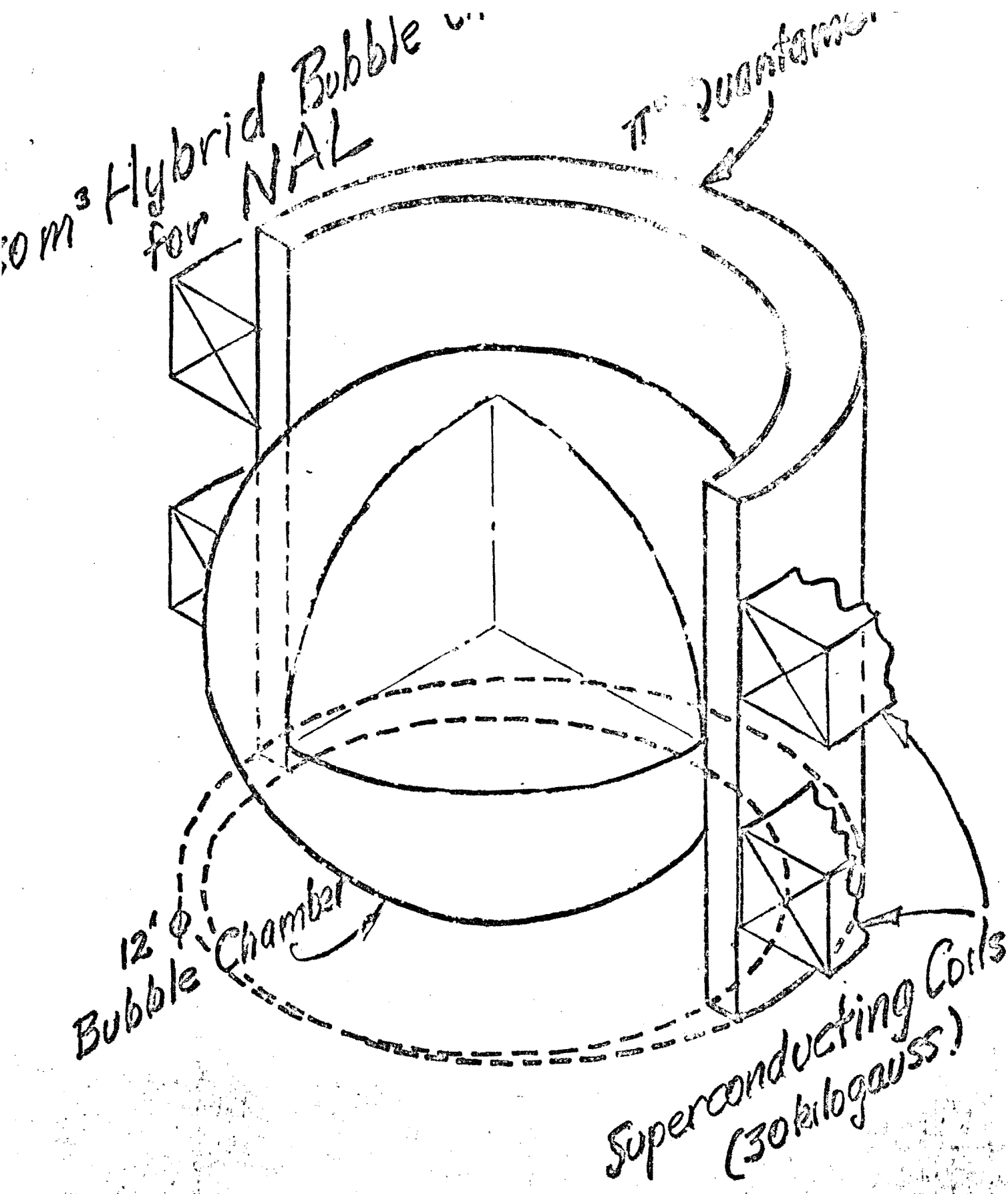
30 m³ Hybrid Bubble
for NAL
12' ϕ
Bubble Chamber
Superconducting Coils
(30 kilogauss)

FIG #7

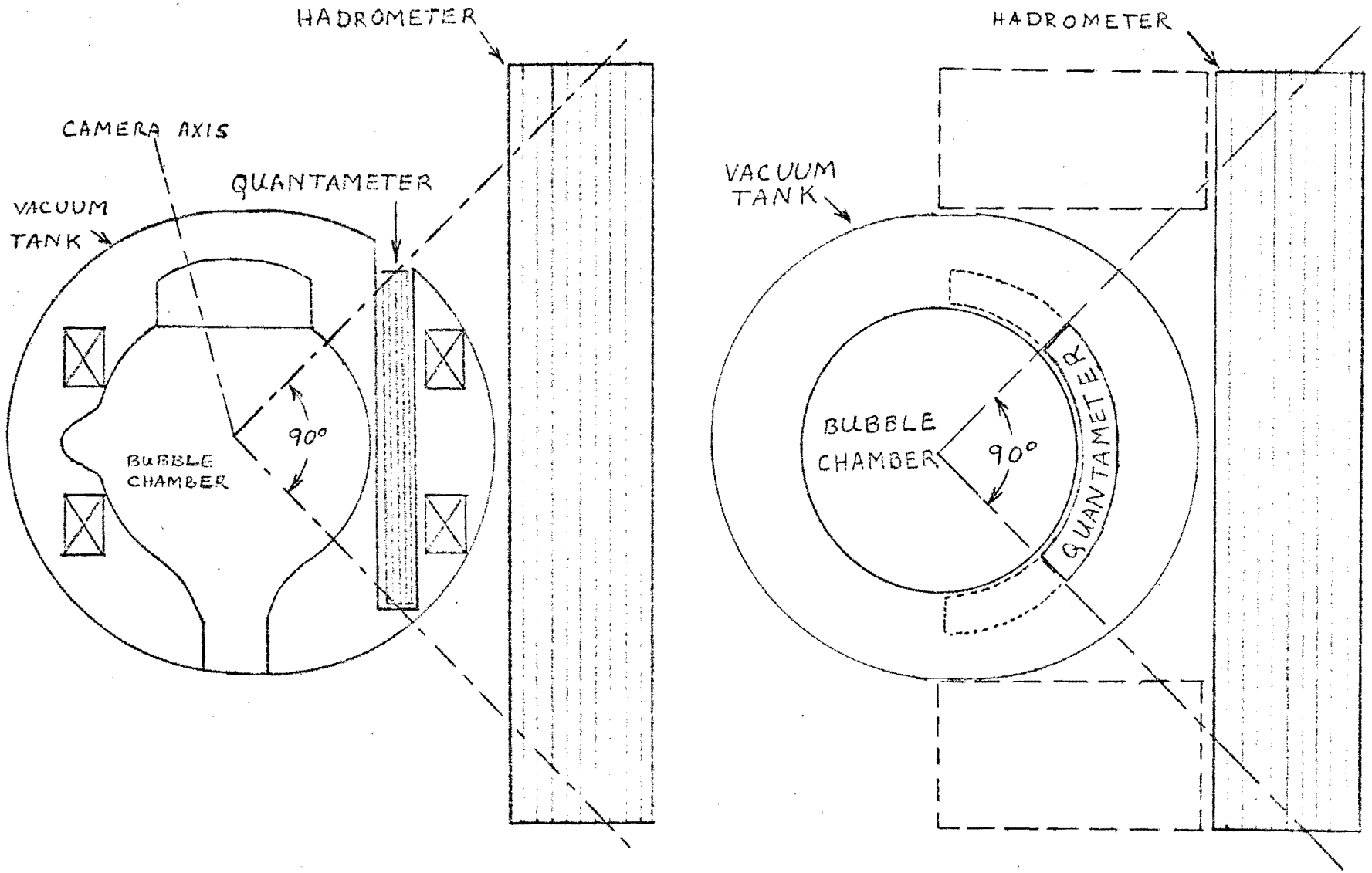
HADROMETER
CAMERA AXIS
QUANTAMETER
VACUUM TANK
BUBBLE CHAMBER
90°
SIDE VIEW
HADROMETER
VACUUM TANK
BUBBLE CHAMBER
90°
QUANTAMETER
TOP VIEW

FIG. 8

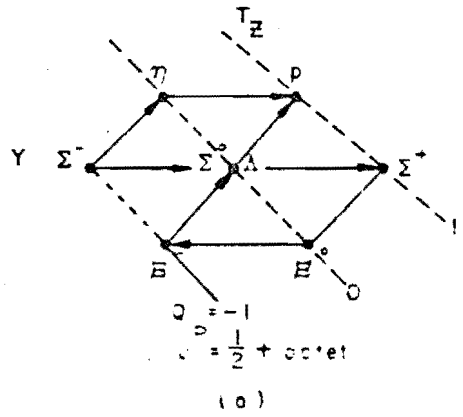

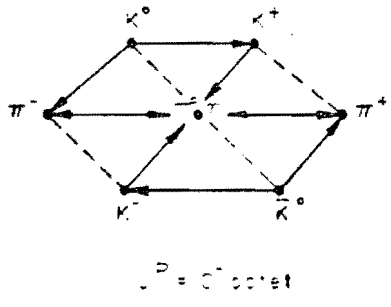

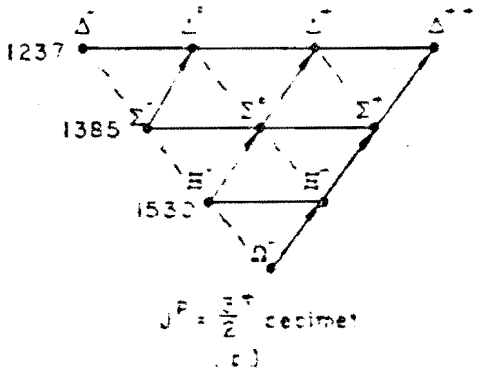

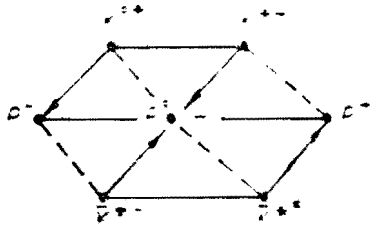

Fig. 9 (a) The hadronic currents allowed under the Cabibbo theory are indicated by arrows. (b) Allowed currents in the strangeness-zero octet. (c) Currents in the $J^P = \frac{3}{2}^+$ decimet and currents in the nucleon octet.

9
FIG 10

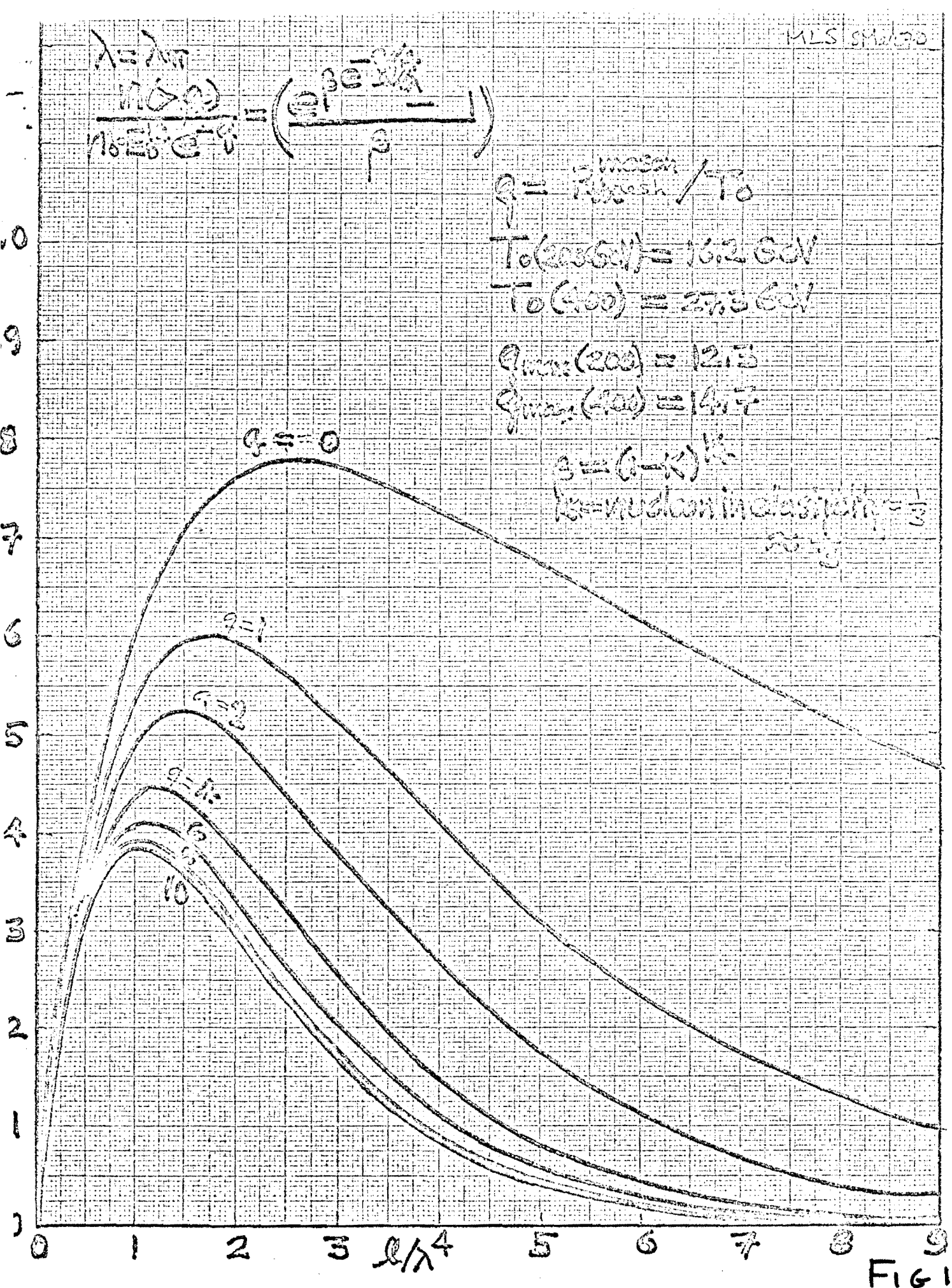
MLS SM-30
$\frac{\lambda=\lambda_m}{n(\lambda_m)} = \left(\frac{e^{\beta\varepsilon-\lambda_m}-1}{e^{\beta\varepsilon}}\right)$
$q = p_{max}/T_0$
$T_0(238GeV) = 10.2\ GeV$
$T_0(400) = 23.8\ GeV$
$q_{max}(238) = 12.5$
$q_{max}(400) = 14.5$
$\beta = (1-K)/k$
k = Nucleon inelasticity = $\frac{1}{3}$
$q=0$
$q=1$
$q=2$
$q=4$
$q=6$
$q=8$
$q=10$
0 1 2 3 λ/λ_4 5 6 7 8 9
1.0 .9 .8 .7 .6 .5 .4 .3 .2 .1

FIG 10

NAL PROPOSAL No. 9-A

Correspondent: M. L. Stevenson
Experimental Physics
Lawrence Radiation Lab
Berkeley, Calif. 94720

FTS/Commercial 415-843-6301

Proposal for a High-Energy Neutrino Experiment In The NAL 30 m^3 H_2, D_2 Bubble Chamber

R. Cence, F. Harris, M. Peters, V. Peterson, D. Yount
University of Hawaii

S. Meyer
Northwestern University

M. Alston-Garnjost, R. Birge, G. Goldhaber
J. Kadyk, S. Parker, M. L. Stevenson, G. Trilling
Lawrence Radiation Laboratory

June, 1970

PROPOSAL FOR A HIGH-ENERGY NEUTRINO EXPERIMENT IN THE NAL 30 m^3 H_2, D_2 BUBBLE CHAMBER

University of Hawaii (R. Cence, F. Harris, M. Peters, V. Peterson, D. Yount)

Northwestern University (S. Meyer)

University of California, Lawrence Radiation Laboratory (M. Alston-Garnjost, R. Birge, G. Goldhaber, J. Kadyk, S. Parker, M.L. Stevenson*, G. Trilling)

June 1970

ABSTRACT

We propose to study high-energy neutrino interactions in the NAL 30 m^3 bubble chamber. A slight alteration of the chamber design will allow a large-solid-angle quantameter to be placed just outside the thin (1/2 inch steel) wall of the bubble chamber. A detector designed to identify the muon of the interaction is placed outside the vacuum tank. With this hybrid system we can reconstruct the neutrino's energy, the lepton momentum transfer squared, Q^2, the lepton energy transfer ($\nu = E-E'$), and measure many features of the final hadron state. This sytem detects with high efficiency over the entire range of variables and is well suited to making a detailed general survey of neutrino interactions in the neutrino energy range 15 to 80 GeV. A million-picture exposure would yield tens of thousands of neutrino interactions with circulating protons at 200 GeV. A similar number of events should be obtained with protons at 500 GeV. Table I summarizes the preliminary cost estimates.

*correspondent

PROPOSAL FOR A HIGH-ENERGY NEUTRINO EXPERIMENT
IN THE NAL 30 m^3 H_2, D_2 BUBBLE CHAMBER

University of Hawaii, Northwestern University,
Lawrence Radiation Laboratory

I. INTRODUCTION

We propose an experimental program for studying the interactions of neutrinos on hydrogen and deuterium for neutrino energies above 15 GeV. This program includes measurements of:

a. the total cross section to see if it saturates or remains linear in neutrino energy,

b. distributions in the deep-inelastic region to test scale invariance and various models such as Pomeron exchange and the parton hypothesis,

c. the elastic differential cross section to learn more about nucleon form factors,

d. interactions involving W mesons, if they exist.

A detector similar to the 14-foot BNL bubble chamber, suitably altered to detect π^{o}'s, neutrons, and muons electronically, seems ideal for neutrino energies up to 80 GeV.

The proposal parallels experiments on elastic and "deep-inelastic" electron scattering: the neutrino provides an independent probe of nuclear structure with, we believe, comparable sensitivity to the electron, while the bubble-chamber technique makes possible a detailed analysis of the final-state hadrons.

In the case of neutrinos, only the direction of the incident lepton is known, and it is necessary to determine its energy E. This can be done by measuring the energies of all final π^{o}'s, charged hadrons, neutrons, and leptons (muons). Provided we identify which of the final particles is the outgoing lepton (energy E'), we can make the same analysis as in deep-inelastic electron scattering. The total and the "elastic scattering" cross sections will also be measured.

Bubble-chamber detection of neutrino events provides precise information on the location of the interaction vertex as well as the momenta of all charged outgoing particles. Photons from π^o's are detected with essentially 100 $^o/_o$ efficiency by a proportional quantameter (lead plates with wire coordinate planes in the gas gaps), and spatial information as well as the total electromagnetic energy is obtained. A "hadrometer" (optical spark chamber buried in a massive concrete absorber 10-15 collision lengths thick) stops all hadrons and makes nuclear cascades visible. Neutrons are detected in the hadrometer by their nuclear cascades, whose energy can be determined by spark counting. Muons are identified when they penetrate this hadron absorber. Backgrounds are suppressed by the time resolution of the trigger logic, by the energy discrimination of the quantameter and hadrometer, and by detailed track analysis in the bubble chamber, quantameter, and hadrometer.

There are several major advantages of the hybrid system consisting of the bubble chamber and electronic detectors. First, the bubble chamber permits an accurate (to $\pm$ 3 $^o/_o$) determination of the charged-hadron and lepton energies through track curvature, while the quantameter determines the total electromagnetic energy to about the same precision. The energy appearing in the form of neutrons is detected with the hadrometer to somewhat less accuracy, but this component is normally a small fraction of the total. Detailed vertex information is a second advantage, as already mentioned. Third, the angular acceptance is large, and a wide range of lepton-momentum and lepton-energy transfers is sampled with good efficiency. Finally, since the muon energy is determined in the bubble chamber, the thickness of the muon detector

is much less than the muon range.

In Section II we discuss some of the measurements that might be made in the neutrino energy range from 15 to 80 GeV. We use these considerations as the basis for designing detectors. Section II also contains specifications required for the neutrino beam and a summary of the components of the neutrino facility that participants in this proposal could help to develop. Technical design considerations are discussed in Section III. Finally, in Section IV we suggest a possible schedule for obtaining one million events during both 200-GeV and 500-GeV phases of the accelerator operation.

II. HIGH-ENERGY NEUTRINO INTERACTIONS

A. Kinematics of $\nu + N \rightarrow$ lepton + hadrons

We adopt the notation of Bjorken and Paschos.[1] Fig. 1 then summarizes much of the kinematics where Q^2 is the square of the momentum transfer to the leptons, and ν is the difference in initial and final lepton energies. The solid parallel lines are the loci of equal invariant hadron mass W, given in terms of the nucleon mass M by the following equations:

$$Q^2 = 2M\nu + M^2 - W^2, \tag{1}$$

$$\nu = E - E', \tag{2}$$

$$\gamma_W = (E_H = M + \nu)/W, \tag{3}$$

$$\sin^2 \frac{\theta}{2} = \frac{Q^2}{4EE'}, \tag{4}$$

$$\sin^2 \theta_H = \left[\frac{E'}{E} \frac{\cos^2 \frac{\theta}{2}}{1 + \frac{2\nu}{Q^2}}\right]^{\frac{1}{2}}, \tag{5}$$

where θ and θ_H are the laboratory angles of the final lepton and hadron systems, E is the neutrino energy and E' the final lepton energy.

The loci of equal values of γ_W, the Lorentz-contraction factor, are indicated by the dashed parabolic curves in Fig. 1. The straight lines radiating from the point ($Q^2=0, \nu = 50$ GeV) are loci of equal lepton angles for E=50 GeV. Fig. 2 is the corresponding graph for E=20 GeV.

If all the final hadrons are in thermal equilibrium, we can estimate the pion multiplicity $\langle n_\pi \rangle$, which depends only on W. The opening angle for the hadron jet is of order γ_W^{-1}. The rising parallel lines in Figs. 1 and 2 correspond to different values of $\langle n_\pi \rangle$. We believe this model provides an upper limit to the multiplicity and serves to emphasize the scope of the experimental task in detecting neutral pions.

B. Dynamics

1. Differential Cross Section

The differential cross section for the interaction of neutrinos on hadrons can be written in terms of the quantities just defined as

$$\frac{d^2\sigma}{dQ^2 d\nu} = \frac{G^2}{2\pi}\frac{E'}{E}\beta\left\{1 - \frac{Q^2}{4EE'} + \frac{\nu^2+Q^2}{2EE'}\left[(R)+(L)\right] + \frac{E+E'}{2EE'}\sqrt{\nu^2+Q^2}\left[(L)-(R)\right]\right\} \tag{6}$$

where

$$\beta = W_2 = \frac{1}{2\pi}\frac{Q^2}{\nu}\left(\frac{1}{1+\frac{Q^2}{\nu^2}}\right)\left(1-\frac{Q^2}{2M\nu}\right)(2\sigma_S + \sigma_R + \sigma_L) \tag{7}$$

$$(R) \equiv \frac{\sigma_R}{2\sigma_S + \sigma_R + \sigma_L}, \qquad (L) \equiv \frac{\sigma_L}{2\sigma_S + \sigma_R + \sigma_L} \tag{8}$$

where σ_R, σ_L and σ_S are cross sections for the appropriate helicity states.

For $Q^2 << \nu^2$, Eq. (6) becomes

$$\frac{d^2\sigma}{dQ^2\, d\nu} = \frac{G^2}{2\pi}\,\frac{E'}{E}\cdot\beta\left[1+\frac{\nu}{E'}(L)-\frac{\nu}{E}(R)\right] \qquad (9)$$

or

$$\frac{d^2\sigma}{dx\,dy} = \frac{G^2 M E}{\pi}\nu\beta\left[(1-y)+\frac{y^2}{2}((R)+(L))+y\left(1-\frac{y}{2}\right)\{(L)-(R)\}\right] \qquad (10)$$

where

$$\nu\beta = \frac{Q^2}{2\pi}(1-x)(2\sigma_S+\sigma_R+\sigma_L) \qquad (11)$$

and $$x \equiv \frac{Q^2}{2M\nu}, \quad y \equiv \frac{\nu}{E}, \qquad (12)$$

$$0 \le x \le 1,\ 0 \le y \le 1.$$

Some motivation for the use of the variable χ can be seen if one supposes that the neutrino might scatter off only a fraction, χ, of the nucleon. The kinematics of quasi-elastic scattering is obtained by replacing M by χM. It would be represented in Fig. 1 by a radial line from the origin with a slope χ times that of the one for $Q^2=2M\nu$. Bjorken has shown that at high incident energies if the parts are point-like the σ_R, σ_L, and σ_S are functions of χ only (scale invariance). Consequently, when one integrates equation (10) over χ and y one obtains σ = (constant)·E, a relation that we can test experimentally provided we detect all final states.

2. "Spin-$\frac{1}{2}$-Parton" Model

To obtain a feeling for where events would lie in the Q^2 – vs – ν plane for the "spin-$\frac{1}{2}$-parton" model, we have set $\nu\beta$ = (constant)·$(1-\chi)$ and $\sigma_R = \sigma_S = 0$. Fig. 3 shows how 1000 50-GeV neutrino interactions would be distributed under these assumptions. The important point is that all sectors contain statistically significant populations.

3. Pomeranchukon-Exchange Model

Predictions for the Pomeranchukon-exchange model can be obtained by setting ν/β = (constant) (1-X) and $\sigma_L = \sigma_R$, $\sigma_S = 0$. The distribution of 1000 events at 50 GeV for these assumptions are shown in Fig. 4.

We propose to make our detection efficiency high in all sectors of the Q^2 -vs-ν plot and consequently, to be able to measure the total cross section.

4. Fireball Model

We introduce the notion of the hadron system being in thermal equilibrium to obtain a crude idea as to what the pion multiplicity might be and how this fireball will emit its products in the lab system. It can be shown that half of the products will be emitted into a cone of half angle,

$$\theta_{cone} \approx \gamma_W^{-1} \approx \sqrt{\left(\frac{2M}{E}\right)\frac{(1-x)}{y}} \quad . \tag{13}$$

The laboratory angle for the final lepton is

$$\theta_\mu \approx \sqrt{\left(\frac{2M}{E}\right)\frac{xy}{(1-y)}} \quad . \tag{14}$$

and for the laboratory direction of the hadron system is,

$$\theta_H \approx \sqrt{\left(\frac{2M}{E}\right)\frac{x}{y}\,(1-y)} \quad . \tag{15}$$

In order to summarize the production and decay processes, we distort the triangular sectors of Fig. 3, 4 into rectangular ones. Within the rectangular sectors we draw pictures of how the events might look. The kinematics of the outgoing hadron system and final lepton are shown for some of the sectors in Fig. 5a. Most hadrons will be obtained within the shaded cones; the vector is the outgoing lepton momentum. Fig. 5b summarizes the corresponding information at E=20 GeV. The hadron

cones are constructed with pessimistic (it predicts too many π^0's with cone angles too large) assumptions, namely, those of a fireball model for the hadron system. The Pomeranchukon-exchange model would predict cones with smaller opening angles and smaller meson multiplicity.

Bjorken and Paschos[1] point out that the difference, $\sigma_\nu - \sigma_{\bar{\nu}}$, is very model dependent. We wish to expose the chamber to both ν and $\bar{\nu}$.

C. Event Rate

In estimating the event rate, we assume the radial distribution for the neutrino beam at the detector obtained from the spectra of D. Carey, et al.[2], (reproduced here as Fig. 6c). We then integrate Eq. (10) over X and y, assuming σ_R, σ_L, and σ_S are functions only of X. The resulting total cross section is proportional to the neutrino energy E. The event rates are calculated for two assumptions: a.) the linear relation, $\sigma = 0.8$ E GeV x 10^{-38} cm^2, holds for all energies; and b.) the cross section saturates at E = 10 GeV and remains constant at 8×10^{-38} cm^2, for higher energies.

The lower set of curves in Fig. 6a indicates the number of neutrino interactions per GeV per 10^6 beam pulses (at 2×10^{13} protons/pulse) per 10^{-38} cm^2. The upper set of curves in Fig. 6a is for assumption a, $\sigma = 0.8$ E (GeV) x 10^{-38} cm^2, while curves for assumption b with a saturated cross section at 8×10^{-38} cm^2 are shown in Fig. 6b. Also shown in Figs. 6a, b are histograms for the number of interactions per 10^6 pulses that lie within 1 meter of the beam axis. Because there is so much uncertainty about K^- yields and hence $\bar{\nu}$

flux, we show no corresponding curves for antineutrinos.

D. Measurement of $\frac{d N_{\nu,\bar{\nu}}}{d E_{\nu,\bar{\nu}}}$

1. Neutrino Energy Spectrum

In determining cross sections, one must first find the energy spectrum of the incident neutrinos. This spectrum, normalized with the data obtained from the neutrino flux monitor, gives the number of neutrinos incident in each energy interval during the course of the experiment. Neutrino events occurring in the bubble chamber can then be assigned to the appropriate intervals once the total energy of the final-state particles has been measured.

2. Measurement of Meson Production by Protons

As part of an initial beam survey, measurements should be made of meson production by protons of 200 GeV from targets of H_2, D_2, Li, Be, and Al. Data are needed for pion momenta above 20 GeV/c and laboratory angles between zero and 20 milliradians. Similar studies should be carried out at 500 GeV as soon as protons of this energy become available.

We feel that our understanding of the production mechanism would be significantly enhanced if a bubble chamber of modest size were exposed to primary protons at 200 and 500 GeV. Attention would be focused on low-energy charged kaons and pions corresponding to the backward jet in the center-of-mass system. We therefore endorse, and some of us would like to participate in, the bubble-chamber survey proposed by G. Snow.[3] We suggest that NAL investigate the possibility of making the bending magnets of area 2 capable of bending 500 GeV protons. Exposure of only 10 to 20 protons per pulse are needed.

The quadrupoles could remain at their 200 GeV values.

3. Meson-Focusing System

The meson-focusing device should maximize the neutrino flux at 35 GeV with incident protons of 200 GeV. To reduce systematic errors in the cross sections resulting from uncertainties in the neutrino energy and thus the neutrino flux, the meson-focusing device should simultaneously minimize the logarithmic derivative, $\left| d \ \ell n \frac{d N_\nu}{d E_\nu} / d \ \ell n \ E_\nu \right|$. This can be accomplished by eliminating those mesons that produce low-energy neutrinos ($E < 15$ GeV) and by focusing those mesons that produce neutrinos near 35 GeV. The low-power, high-band-pass devices proposed by Frisch and Kang[4] and by Palmer[5] appear to be well suited to the neutrino energy selection required. For our hybrid system a one-millisecond beam spill would be ideal, that is, short enough for the bubble chamber and long enough for the electronic devices. (We anticipate of order 1 neutrino interaction per pulse in the quantameter and of order 100 per pulse in the hadrometer. The "deadtime" of these instruments is less than 1 μ sec.)

4. Neutrino Flux Monitor

Wachsmuth[6] has described a monitoring system for the neutrino flux which measures essentially the longitudinal and radial distributions of muons within the muon shield in front of the bubble chamber. We believe such a system is necessary for reliable operation of the neutrino beam, as well as for the flux determinations required in obtaining cross sections.

E. Measurement of the Neutrino Energy

1. Curvature and Total Energy of Charged Hadrons

The neutrino energy, E or E_ν, $\bar{\nu}$, is determined for each event

by measuring the energies of all outgoing particles. The energy of the charged-hadron component is given most precisely by track curvature in the 30-KG field of the bubble chamber, while a less-precise check is obtained from the hadron calorimeter associated with muon identification. The hadrometer is limited primarily by the statistics of hadron cascades in which, unlike electromagnetic cascades, a significant and variable fraction of the energy is lost to secondary neutrinos, slow neutrons, and nuclear binding energy.[7] Fluctuations in these losses are characteristic of all hadron calorimeters, and they point up one of the major advantages of the bubble chamber as a tool for doing neutrino physics. Curvature should give the charged-hadron energy to $\pm 3\ ^{o}/_{o}$, while the hadrometer resolution and precision for single events may be about $\pm 10^{o}/_{o}$ at 35 GeV.[7]

2. Total Energy of π^{o}'s via Proportional Calorimeter

Considerable thought has been given to ways in which neutrals could be detected in the large H_2, D_2 bubble chambers.[8] For chambers of volume exceeding 100 m^3, it is possible to place track-sensitive inserts of H_2 or D_2 into mixtures of H_2-N_e and obtain effective volumes* of order 30 m^3 for neutrino physics. NAL has proposed a chamber smaller than 100 m^3, namely 30 m^3, similar to the proposed BNL 14-foot chamber. The effective volume of inserts into this 12-foot-diameter sphere are less than 3 m^3, a volume that would yield too few events in the high-energy region.

*"Effective volume" is the volume of the insert multiplied by the efficiency for detecting all of the photons from neutral pions in the H_2-N_e mixture.

To permit the necessary determination of the neutral pion energy, we propose to take advantage of a special feature of the NAL 15-foot (30 m^3) bubble chamber design -- namely the thin exit wall of 1/2" steel, less than one radiation length. The thin wall implies that photons from π^o decay can be detected efficiently and the total shower energy measured precisely by a cylindrical π^o quantameter[9] at the downstream end of the chamber. A possible arrangement is shown schematically in Figs. 7 and 8. The quantameter itself is described in more detail in Section III. The total-energy resolution should be better than $\pm 3\ ^o/_o$ for events in which the total energy into neutral pions is above a few GeV. Precise calibration would then permit an absolute determination of the π^o component in a single event to about the resolution limit.

We propose to install the quantameter in a special reentrant well constructed in the vacuum tank downstream of the hydrogen volume. This location, shown in Fig. 8 requires that the coil diameter be extended about 1/2 meter. These modifications, in addition to permitting a quantameter of 15 to 20 radiation lengths thickness, would preserve the <u>entire</u> useful volume of the bubble chamber. The volume assumed in calculating the yield histograms of Figs. 6a, b is a cylinder of 1-m radius, intercepting a sphere 3.6 m in diameter, and yielding a fiducial volume of 10 m^3. The volume outside this cylinder could be used as a blanket of H-N_e mixture to detect wide-angle photons.

3. Total Energy of Hadrons via Proportional Calorimeter

The total energy of the charged hadrons (charged pions, protons and

antiprotons) would be obtained most accurately from track curvature in the bubble chamber; the nuclear cascades in the hadrometer furnish another, less accurate, measure of charged hadron energy. However, the hadrometer will catch neutrons, which escape bubble chamber detection, and will measure their energy. All hadrons will be absorbed within 15 interaction lengths. Optical spark chamber planes at various depths would sample particle trajectories and indirectly measure ionization. Muons above 2 GeV would penetrate the hadrometer. Thus the hadrometer serves three purposes: it stops hadrons permitting muon identification, it measures hadron energy, including the energy of any neutrons emitted from the neutrino vertex, and it follows tracks spatially.

The hadrometer would be located just outside the bubble-chamber magnet as close to the magnet as practical. It's configuration might approximate a vertical half-cylinder, similar to the quantameter, although rectangular modules, such as those shown in Fig. 8, appear to be more practical.

4. Lepton Total Energy

The momentum of the final lepton is measured by curvature. Like the curvature measurements of the charged-hadron energy, this possibility is a major advantage of the bubble-chamber approach: peripheral equipment is required only to identify escaping muons, not to stop them or otherwise determine their energy. Final electrons are identified in the quantameter. Thus the hadrometer or absorber used with the bubble chamber is much thinner than the full muon range. This, in turn, permits much larger solid-angle detection for muons at an acceptable cost -- a feature well matched to intrinsically large solid angle of the bubble chamber.

Any particle penetrating 10-15 collision lengths of hadrometer is almost certainly a muon. Proportional (Charpak) chambers[10] or wire chambers can be used to locate the muon path with high spatial resolution. The muon may be identified by projecting each track from the vertex through the quantameter and hadrometer and testing whether its location at the final muon detector is consistent with location at the observed track. We propose to build into the quantameter and hadrometer a number of coordinate-sensitive planes to follow each track in detail, tracing each detected muon backwards into the bubble chamber.

F. Measurement of Structure of Hadronic State

The bubble chamber is ideally suited to studies of the final hadronic system. Hadrons, like muons, trapped in the magnetic field can usually be identified by their interactions in the hydrogen of the chamber. A much larger class of events can be studied in detail by tracing individual tracks through the quantameter and into the hadrometer where energetic nucleons in the final state may possibly be identified.[11]

Similarly, detailed information on individual π^o's and η^o's can be obtained from a knowledge of the vertex location and the origins of correlated γ showers. In many cases, for example, the π^o energy can be determined from the photon opening angle, and in some cases a separation of π^o and η^o decays should be possible.

A procedure of the type just discussed requires extensive use of coordinate-sensitive planes. The proportional-calorimeter design described in Section III permits several planes per gap or per

plate without interfering in any way with the determinations of neutral pion or hadron energy. This option is a major advantage of the proportional (Charpak) chamber.[10]

G. Possible Hadronic Decay Modes of the Intermediate Vector Boson (IVB)

If the mass of the IVB is large many decay modes are possible.[8] Again the high measurement accuracy of the bubble chamber makes it an ideal instrument for detecting these modes. Provided the mass of the IVB is not too large, its width is likely to be much smaller than the experimental resolution function of the bubble chamber. Thus the signal/noise will be improved with increased measurement accuracy.

We list below in diagramatic form some examples of the possible hadronic decay modes of the IVB.

Baryon-Antibaryon

$$W^{\pm} \rightarrow \bar{H}_8\left(\tfrac{1}{2}^+\right) + H_8\left(\tfrac{1}{2}^+\right)$$
$$\rightarrow \bar{H}_8\left(\tfrac{1}{2}^+\right) + H_{10}\left(\tfrac{3}{2}^+\right)$$

Boson-Antiboson

$$W^{\pm} \rightarrow \bar{H}_8\left(0^-\right) + H_8\left(1^-\right)$$

The symbol $\bar{H}_8\left(\frac{1}{2}^+\right)$ represents an antibaryon of the $\frac{1}{2}^+$ octet, etc.

Only those pairs of final particle-antiparticle states that are nearest neighbors in the Y —vs— T plot of Fig. 9 are allowed under the $\Delta S=0$ and $\Delta S=\Delta Q$ rules. For neutral IVB's (if neutral lepton currents exist) the nearest neighbors joined by the dashed lines would be possible decay products.

For low-momentum-transfer production the IVB would receive most of the energy of the incident neutrino. Consequently, the decay fragments would be thrown into a forward cone of half angle $M_W/2E$.

The quantameter would easily detect the π^o's that might be among the decay products.

III. EXPERIMENTAL EQUIPMENT

A. Neutrino Beam

1. Targets

The enhancement of the high-energy portion of the neutrino spectrum requires thin targets consisting of light nuclei. Fig. 10 (Fig. 4a of TM 218)[12] summarizes how the number of neutrinos above a certain energy depends upon the target thickness. Our requirement is for $q \geq 2$, thus the optimum target thickness is about 1 mfp. The detrimental effects on the high-energy neutrino spectrum of multiple interactions of the incident nucleon within a complex nucleus provide strong motivation for developing targets of very light nuclei. Experimentation and design studies for the neutrino target should begin as soon as possible.

2. Meson-Focusing System

We wish to participate in the design and testing of a meson-focusing device[4,5] to produce those special qualities in the neutrino beam alluded in Section II D.3.

3. Neutrino Flux Monitor

The CERN neutrino spectrum was measured by placing emulsions and ionization chambers at various depths and radial positrons in the muon shield to determine the muon flux at these points. Wachsmuth[6] asserts that if the pion and kaon spectra are known and the shield measurements taken, $\frac{d N_\nu}{d E_\nu}$ at the bubble chamber can be determined to about 5 %. The importance of determining $\frac{d N_\nu}{d E_\nu}$ is

so great for this experiment that some of us would like to participate in these measurements.

While the equipment relating to the neutrino beam would be part of the NAL facility, members of this proposal are prepared to participate in the design and development of this apparatus.

B. Hybrid Detector System

1. 30 m^3 H_2, D_2 Bubble Chamber

The detector has already been discussed briefly in Section II, dealing with the type of measurements one might make. The hybrid system shown in Fig. 8 is built around the NAL bubble chamber and offers these advantages:

a. precision on $E_\nu = E_{\pi^o} + E_H + E_\mu$ to $\pm 3\,^{o}/_{o}$,

b. vertex information of the bubble chamber,

c. absorber (hadrometer) thickness much less, than the muon range

d. large solid angle,

e. simplicity.

Of these, the first four follow immediately from the use of the bubble chamber itself, particularly its ability to measure E_H and E_μ, once the muon has been identified. Supplementary information on E_H, including identification of baryons, is provided by the hadrometer, while E_{π^o} is given solely by the quantameter. The advantage of simplicity follows partly from the relatively thin absorber required (since the bubble chamber measures E_μ) and partly from the use of porportional calorimeters to be described.

The reentrant cylindrical tank housing the quantameter is an

important change in the preliminary bubble-chamber design and necessitates an increase in the coil diameter of about 1/2 meter; this change will greatly increase the effectiveness of the bubble chamber for both strong and weak interaction physics, particularly in reactions involving final π^o's.

2. Ionization and Proportional Calorimeters

Parallel-plate ionization calorimeters, such as the quantameters[9] widely used in monitoring photon beams, have several intrinsic properties that are essential in determining E_{π^o} and E_H accurately. First, the response depends only upon the relative ionization in the gas gaps as compared to the ionization in the plates; tolerances of a few percent in these parameters are easily met and insure a uniform response to the same level. Second, since the ratio of gap to plate is independent of track angle in a parallel plate chamber, such a device is intrinsically isotropic. Third, the output of an ionization calorimeter is linear in the energy absorbed over a wide range. Fourth, an ion chamber is operated as a one-parameter device; there is one high-voltage setting and one output signal proportional to the total energy deposited in the chamber as sampled periodically via the ionization in the gas gaps. This last feature greatly simplifies the operation of the calorimeter and results in a highly reproducible instrument.

In the case of electromagnetic showers (E_{π^o}), virtually all of the energy appears ultimately in the form of ions, which are sampled directly in the ionization calorimeter thereby avoiding such questions as the response of scintillation or Cerenkov counters.

In the case of hadronic cascades, a certain portion of the energy is lost to neutrinos, slow neutrons, and nuclear binding, as mentioned previously.[7] A typical loss might be 20-30 $^{o}/_{o}$ at 35 GeV, although for some events the loss may be catastrophically large. Within the statistical uncertainties of this process, the response is similar for all hadrons, including high-energy neutrons, providing the absorber thickness is sufficient to contain the cascade. The actual gain can be determined by calibration with hadrons of various energy.

The only serious limitation of ionization calorimeters, as far as the present application is concerned, is their relatively low gain, typically[9] 4×10^3 ions per GeV absorbed with 1-atm of A-CO_2. This small signal appears across the relatively large capacity of the parallel plate structure and is not easily detected.

A much higher gain is possible by using the high electric fields surrounding small-diameter (20-100μ) wires to induce proportional avalanche multiplication. Proportional calorimeters[10] retain the uniformity, isotropy, and linearity of ion chambers, and if the signals from the high-voltage plates are added, there is one high-voltage setting and one output signal. The gain of a proportional chamber, unlike an ion chamber, varies exponentially with the high voltage, but good reproducibility can be obtained.

Proportional chambers cease to be linear when the space charge in single avalanches appreciably distorts the electric field near the wires. This occurs typically at 5×10^6 ions, and the high voltage is normally set low enough so that this condition is not

exceeded.

A crucial point in our application is that the primary ionization of the shower, consisting of some 4000 ions/GeV, in the gas, is distributed over several hundred tracks in perhaps 10 gaps. As many as 10^3 avalanches may be thus involved so that an output of 5×10^9 ions or more can be obtained without exceeding the linear response region. This largely compensates for the greater capacity of a pair of plates or of an entire chamber, as compared with the capacity of a single wire, and it yields an output voltage within one or two orders of magnitude of that normally obtained on a single wire of a multiwire proportional chamber. Such a net signal can easily be measured, and if necessary, one can afford sensitive amplifiers since only a small number of total-energy outputs are involved. (The situation is quite different when one must read 10^3 to 10^4 separate wires.)

3. Proportional Quantameter

We presently envision the proportional quantameter to consist of 15 lead plates and a similar number of gas gaps totaling 15 radiation lengths of lead, about 9 cm. A sector $90^0 \times 90^0$ measured from the center of the bubble chamber would be about 4 meters high with a 3-m arc and would weigh about 12 tons. Each double gap would consist of a single wire plane centered between two lead plates and defining a total gap of 2x.5 cm = 1.0cm. Fifteen of these gaps would add an additional 15 cm to the quantameter thickness. Allowing an additional 5 cm for flanges and windows, we obtain a total quantameter thickness of about 30 cm. A 35-cm-wide reentrant tank would

allow, in addition, the installation of a couple of scintillation counters or possibly a two-gap spark chamber. Note that the steel walls of the bubble chamber and the reentrant wall will amount to 1-2 radiation lengths and may be considered as the first plate of the quantameter, while the quantameter at 1 collision length may be considered the first plate of the hadrometer. The quantameter itself might then begin with a sensitive gap followed by the first lead plate.

The wires of the proportional quantameter will be read out to provide spatial resolution. A wire diameter of 50μ and a spacing of 2mm is probably convenient[10] although 1mm seems feasible if one is willing to try hard enough. Vertical wires are straight forward in the cylindrical configurations, but horizontal wires may force a modular quantameter design with flat parallel plates.

4. Hadrometer

The hadrometer would consist of about 20 walls of heavy concrete (density = $3.5 \frac{gm}{cm^2}$) 25 cm. thick, separated by 2-gap optical spark chambers. This thickness of concrete provides 14 collision lengths (and 67 radiation lengths) of absorber. The 12-cm lead of the quantameter is equivalent to about 1 collision length for hadrons. The copper coils of the bubble chamber magnet amount to several collision lengths but do not seriously limit the accuracy of the hadron-energy determination for most event types.

We presently envision a hadrometer subtending vertical and horizontal angles of about 90° by 90° as measured at the center of the bubble chamber. The volume of concrete would then be 8mx8mx5m and the weight about 1200 tons. The full 180° azimuth in the bending plane

could be covered (thinner at wide angles) with 2000 tons.

Optical spark chambers with 90° stereo viewing would be used to record muon tracks and nucleonic cascades within the hadrometer. We presently plan 20 planes distributed in an optimum manner to record the maximum number of sparks per cascade. Neutron-initiated cascades will be distinguished from charged pion/proton cascades by lack of incident track. Calibration of total sparks/GeV can be done using protons. Since the typical neutron energies is expected to be a small fraction of the total only, crude energy resolution (± 30 %) is required to retain overall ± 5 % precision in hadron energy.

Muons tracks should be quite distinctive due to lack of interaction in the hadrometer.

"Accidental" neutrino-induced background within the hadrometer should be distinct from neutron-induced cascades, due to muon secondaries. Assuming that the beam is spilled over 1 millisecond, these accidentals (occurring within spark-chamber sensitive time) should be rare.

5. Range Detector for Muons Leaving the Bubble Chamber

Highly non-peripheral events produce muons at large angles and at sufficiently low momenta that the muons can be trapped in the bubble-chamber magnetic field. Muons of a few GeV and more pass through the 14 collision lengths of photon and hadron absorber and can be identified in that way. A single plane of scintillators downstream of the hadrometer might suffice, while the last several gaps of the hadrometer could provide the spatial resolution necessary to permit muon tracks to be traced back to the bubble chamber. Events with muons in an inter-

mediate energy range, for example the range from 1 to 3 GeV, may frequently remain ambiguous, as far as muon identification is concerned unless the hadrometer subtends a very large solid angle and unless individual tracks are followed through each plane of the hadrometer until they stop.

6. Triggering Options

Signals should be available from the quantameter and hadrometer

within 100 ns of the occurence of an event and with a time jitter of less than 50 ns.[10]. These signals, in coincidence with scintillator planes, could be used to develop a trigger requiring an interaction having total energy above, for example, 10 GeV. Four scintillator planes might suffice: an anticounter in front of the bubble chamber, a yes-counter in front of the quantameter and another in front of the hadrometer, and finally the muon counter plane already mentioned. The trigger could be used to flash the bubble chamber illumination or fire peripheral spark chambers, or it could simply be recorded for use in analyzing the bubble-chamber film. We presently favor the last option, at least during the early stages of the experiment.

IV. SCHEDULES AND PARTICIPATION

A. Design and Development of Equipment

We shall explore ways in which the participating groups, and particularly LRL as a service to other users, can participate in the design and development of the neutrino beam, quantameter, hadrometer, counters and modifications of the bubble chamber. Arrangements for sharing the cost should be negotiated between our groups NAL, and AEC.

B. LRL Development

Work should begin immediately on some of the special items just mentioned. Among these is the design of the reentrant tank for the quantameter, which could be carried out by LRL mechanical engineers skilled in cryogenic equipment. The design could proceed at Berkeley in close collaboration with W. Fowler and his group at

NAL. In addition, the shop and experimental facilities of LRL could be made available to the University of Hawaii group and others involved in developing the quantameter and hadrometer.

C. Participation of Our Personnel at NAL.

The development of the neutrino beam equipment would best be done at NAL. We would hope to make the experience of graduate students stationed at NAL as broad as possible. Thus, while a major fraction of their time would be devoted to development of the neutrino facility and bubble chamber, their direct participation in construction and other activities of the accelerator should be encouraged.

D. Beam Survey Experiment

The meson production measurements should start as soon as the survey beam (10^{10} proton/pulse) is available in Area 2. Here, we could provide experienced personnel and some equipment to aid groups that have made specific survey proposals involving major hardware commitments.

A survey bubble chamber of the type suggested by Snow[3] should be available at the turn-on date of Area 2. The present film and data-analysis equipment at our participating institutions is adequate to handle exposure of several hundred thousand pictures on both hydrogen and deuterium. The information from the yield measurements could be used to up-date the operating parameters of the meson-focusing device. Early exposures to 500-GeV protons would be very useful in designing the focusing for the 500-GeV phase. Since only ten or twenty protons per pulse are required, one might consider

designing the bending magnets of Area 2 (super conducting?) to bend 500-GeV protons, allowing the quadrupoles to remain set at their 200-GeV design values. At the low intensities required, no radiation damage would result to the beam transport equipment, and no additional shielding would be required. Reliable, fail-safe intensity-control equipment would, however, be necessary.

E. Million-Picture Exposure at 200 GeV

The experimental program of preparing the neutrino beam for this application could easily occupy the first year or more after beam turn-on. The accelerator operation in its second and third years is likely to be more reliable, and the bubble chamber will be better understood. We therefore propose that a one-million picture exposure to hydrogen of both neutrinos and anti-neutrinos of high energy be made in the second or third year of operation at NAL. Similar exposures to deuterium would come later.

F. Million-Picture Exposure at 500 GeV

Our reason for requesting an exposure at higher accelerator energy is to allow the energy at which we have a low value of $\left| d \ln \frac{d N_\nu}{d E_\nu} / d \ln E_\nu \right|$ to be increased significantly. This, in turn, would raise the central neutrino energy from 35 GeV to 70 GeV for an acceptable uncertainty in the number of neutrinos incident. The 500-GeV exposure would occur at a much later date.

V. PRELIMINARY COST ESTIMATE

A preliminary cost estimate is given in Table I. The principal assumptions are:

A. Geometry shown in Fig. 8

B. $.50/pound for lead plates (container 18K),

C. all wires readout, 2-mm wire spacing, 15 planes/chamber, $5/wire to readout, $1.50/wire to fabricate the quantameter,

D. $250/per cubic yard for heavy concrete.

TABLE I

Preliminary Cost Estimates (All Wires Read Out)

			Cost K$	Cost K$
1.	Modifications of Bubble Chamber Coils and Vacuum Tank		300	300
2.	Quantameter:	Lead Plates and Container	40	
		15 Wire Planes	30	
		15x4m/2mm=30,000 Readouts x $5/wire	150	220
3.	Hadrometer:	Concrete (1200 tons at $250/yds.^{3})	100	
		Optical Spark Chambers	100	
		Camera and Mirrors	100	300
4.	Counter Planes:	4mx4m Anti (8 scintillators 16 PMS)	20	
		4mx4m Yes at Quantameter In	20	
		8mx8m Yes at Hadrometer In (16 scintillators, 32 PMS)	40	
		8mx8m Yes at Hadrometer Out	40	120
5.	Computer Interfacing		50	50
6.	Fast Logic, Slow Logic, etc.		50	50

TOTAL = $1040K ($90^\circ$x$90^\circ$ Hadrometer)

REFERENCES

1. J.D. Bjorken and E.A. Paschos, SLAC-PUB-678, December, 1969 (Lectures by Bjorken at 1969 Summer Study).

2. D. Carey, Y.W. Kang, F.A. Nezrick, and R. Stefanski, TM-222 "A Note on the 200-GeV Neutrino Design."

3. G.A. Snow (correspondent) "Preliminary Proposal to Study Multiparticle p-p and π-p Interactions from 75 to 200 GeV/c (and higher momenta as soon as they become available), April 23, 1970. University of Maryland High Energy Physics Group.

4. D. Frisch and Y.W. Kang, "D.C. Horn for Very-High-Energy Spark-Chamber Neutrino Experiments," 1969 NAL Summer Study 1, 389.

5. R.B. Palmer, "The Design of Long-Pulse Monopole Focusing Elements," 1969 NAL Summer Study 1, 383.

6. H. Wachsmuth, "Neutrino Spectrum Determination from Muon Flux Measurements," 1969 NAL Summer Study 1, 367.

7. V.S. Murzin, Progress in Elementary-Particle and Cosmic-Ray and Cosmic-Ray Physics, (North-Holland Publishing Company, Amsterdam, The Netherlands, 1967), Vol. IX, p. 245.

8. See for example M.L. Stevenson, "High-Energy Neutrino Physics $\leq E_\nu >$ 20 GeV and the Constraints Placed on Detectors," 1969, NAL Summer Study 2, 121.

9. R.R. Wilson, Nucl. Instr. 1, 101 (1957). A high-energy (multi-GeV) quantameter is described by D. Yount, Nucl. Instr. Methods 52, 1 (1957).

10. G. Charpak, D. Rahm, and H. Steiner, "Some Developments in the Operation of Multiwire Proportional Chambers," CERN Preprint.

11. A. Pais, "Weak Interactions at High Energies," Presented at the Conference on "Expections for Particle Reactions at the New Accelerators," University of Wisconsin, 1970; S.D. Drell and Tung-Mow Yan, "Final Particle Correlations in Deep Inelastic Lepton Processes," Phys. Rev. Letters 24, 855 (1970).

12. M.L. Stevenson, "Targets for the Neutrino Beam: Concepts," NAL Report TM 218.

13. D.D. Jovanovic, R. Palmer, and B. Roe, "Muon Detectors after the 25-foot Chamber" NAL 1969 Summer Study, 2, 207.

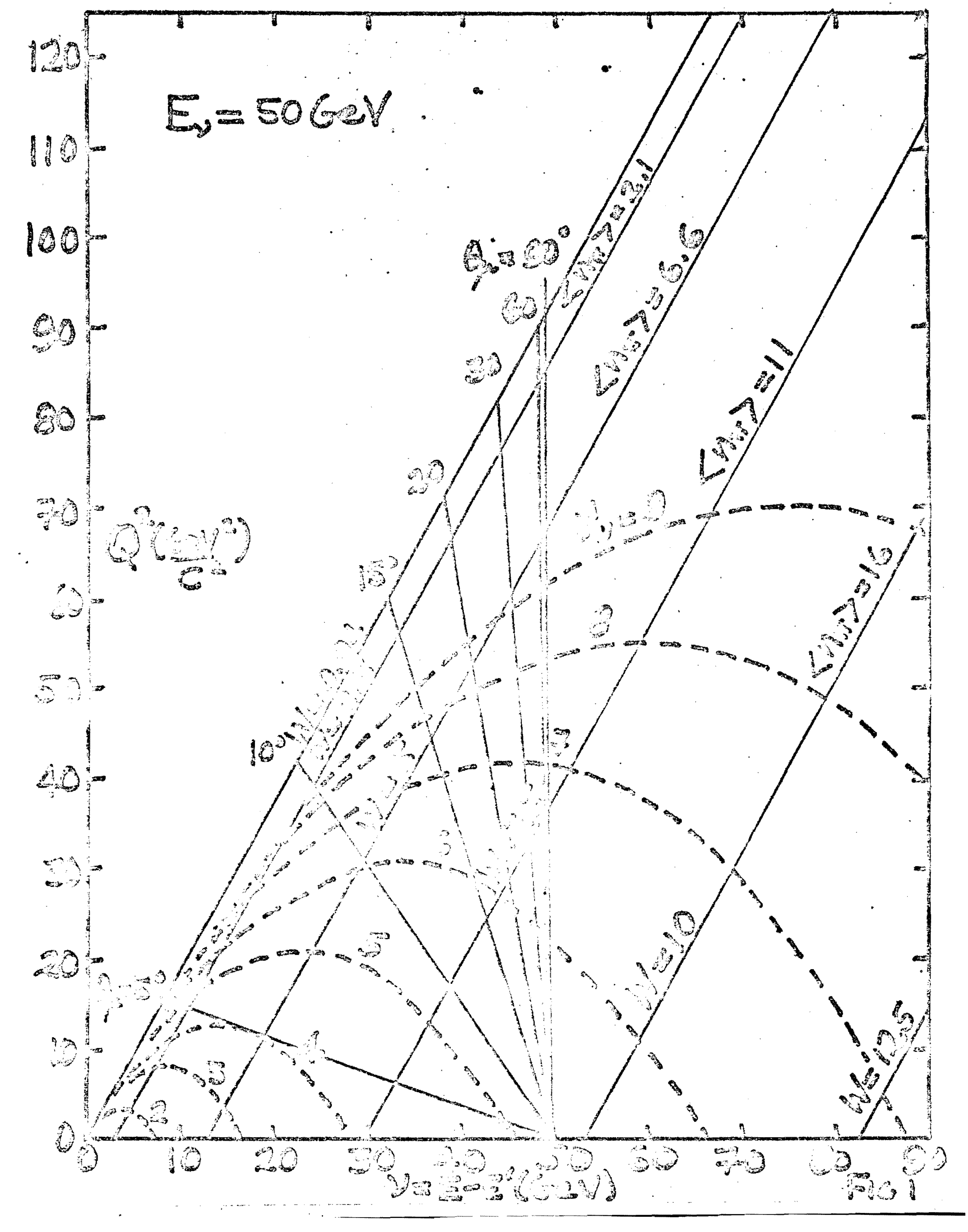

$E_\nu = 50$ GeV
Q^2 (GeV²/c²)
$\nu = E - E'$ (GeV)
θ = 90°
60
30
20
15
10°
<n> = 3.1
<n> = 6.6
<n> = 11
<n> = 16
W = 10
W = 12.5
120
110
100
90
80
70
50
40
20
0
10
20
30
60
70
80
90
Fig 1

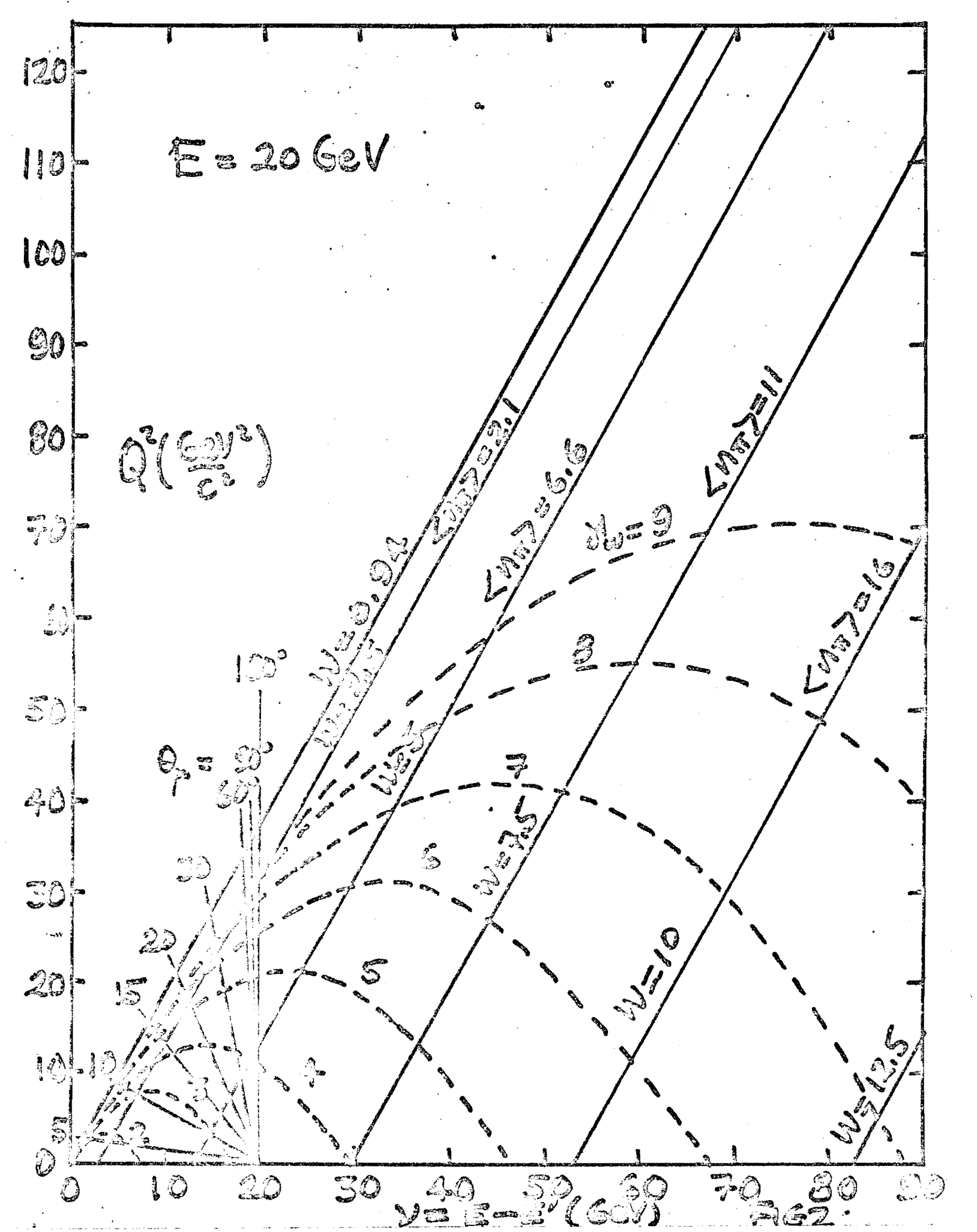
E = 20 GeV
$Q^2\left(\frac{GeV^2}{c^2}\right)$
W=0.94
W=3.5
W=5.6
W=7.5
W=9
W=11
W=10
W=12.5
θ = 10°
θ = 20°
θ = 30°
θ = 40°
θ = 50°
θ = 60°
θ = 70°
θ = 80°
θ = 90°
θ = 100°
θ = 110°
θ = 120°
$\nu = E - E' \left(\frac{GeV}{c^2}\right)$

FIG 2.

Distribution of 1000 Events

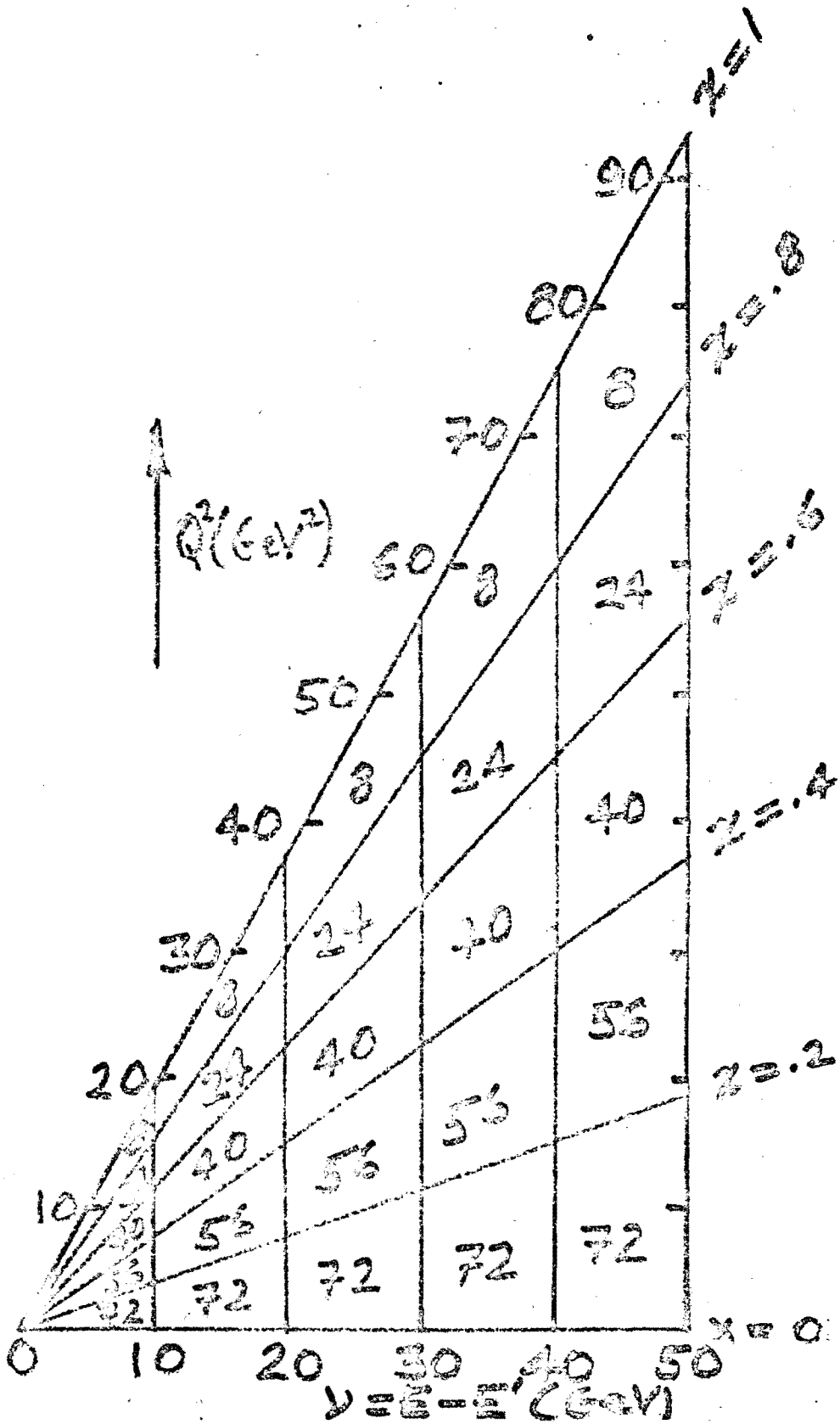

$E_\nu = 50$ GeV

for $\nu_3 = K(1-x)$

$\sigma_R = \sigma_S = 0$

SPIN $\frac{1}{2}$ PARTONS

$M_W = \infty$

FIG 3

Distribution of 1000 Events

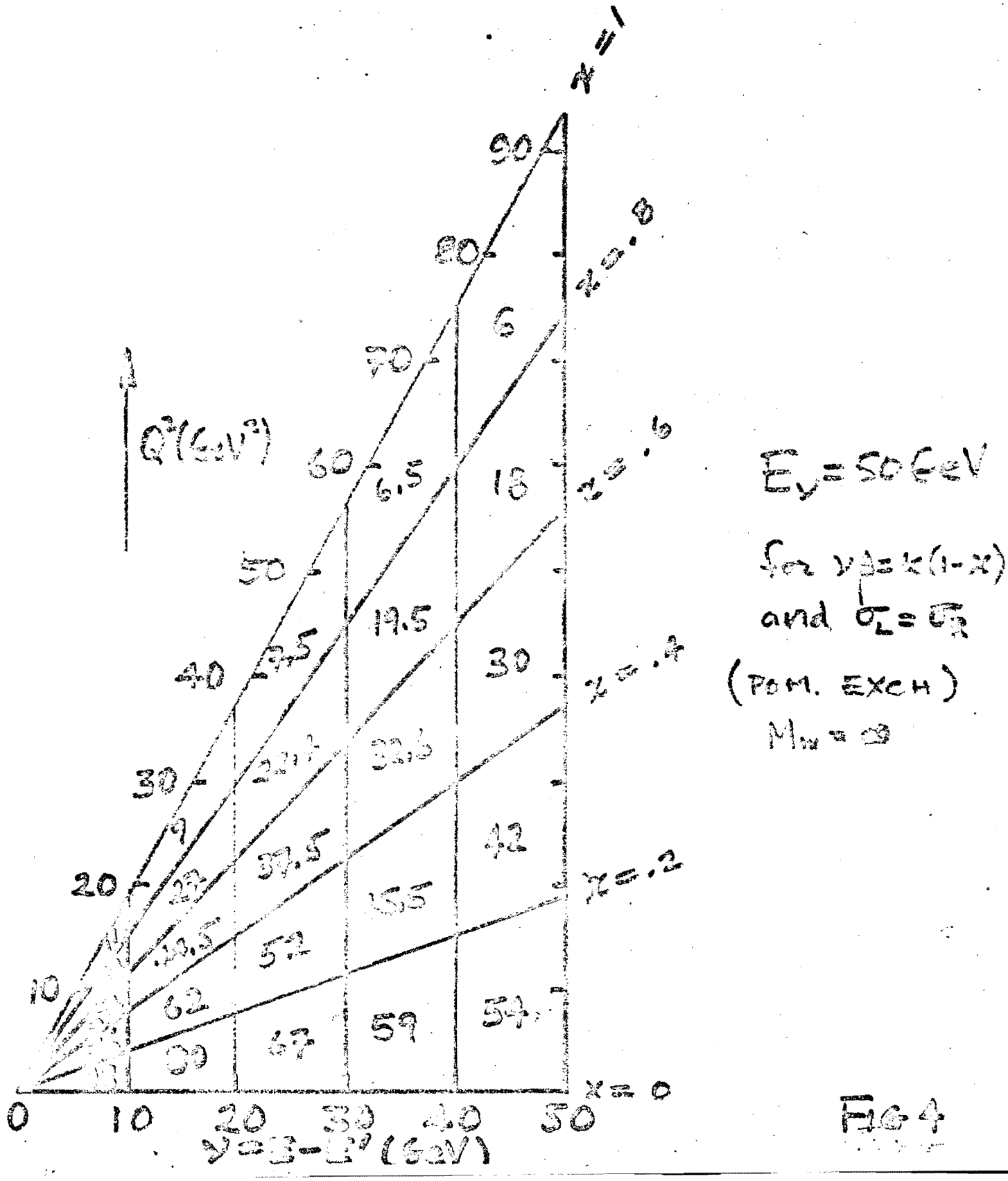

Fig 4

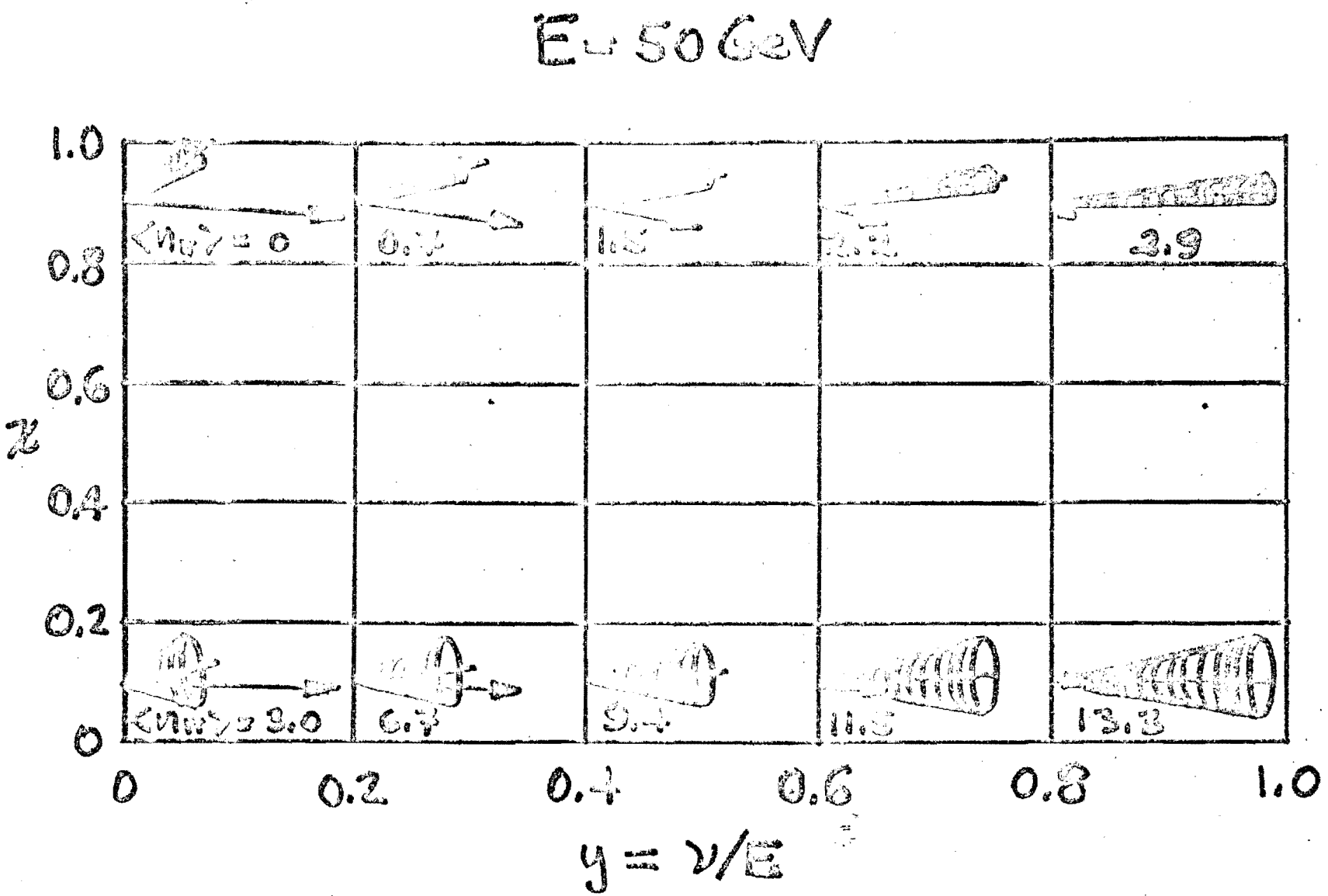

FIG 5a

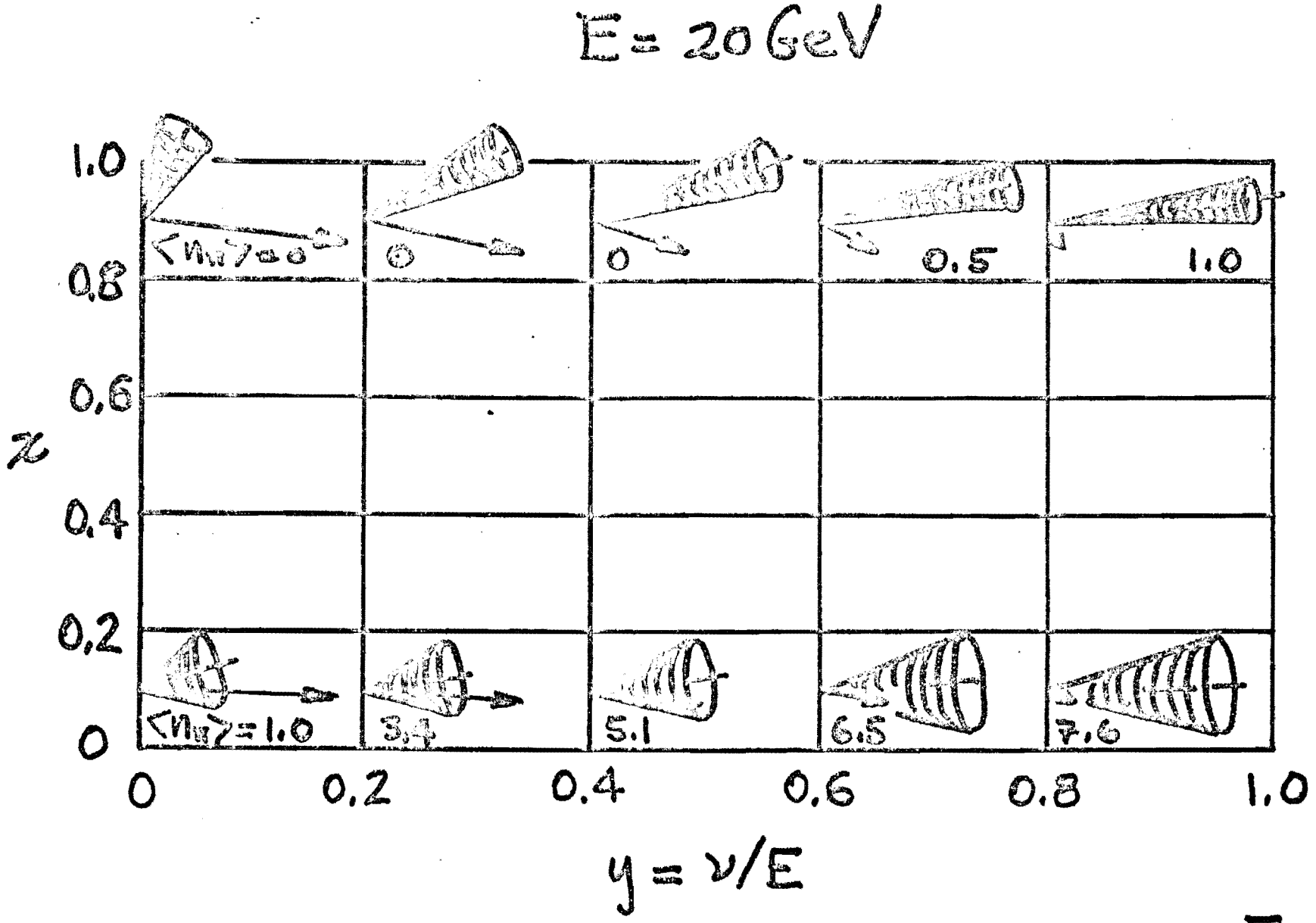
E = 20 GeV
1.0
0.8
0.6
0.4
0.2
0
x
0
0.2
0.4
0.6
0.8
1.0
y = ν/E
⟨nμ⟩=0
0
0.5
1.0
⟨nμ⟩=1.0
3.4
5.1
6.5
7.6

Fig. 5b

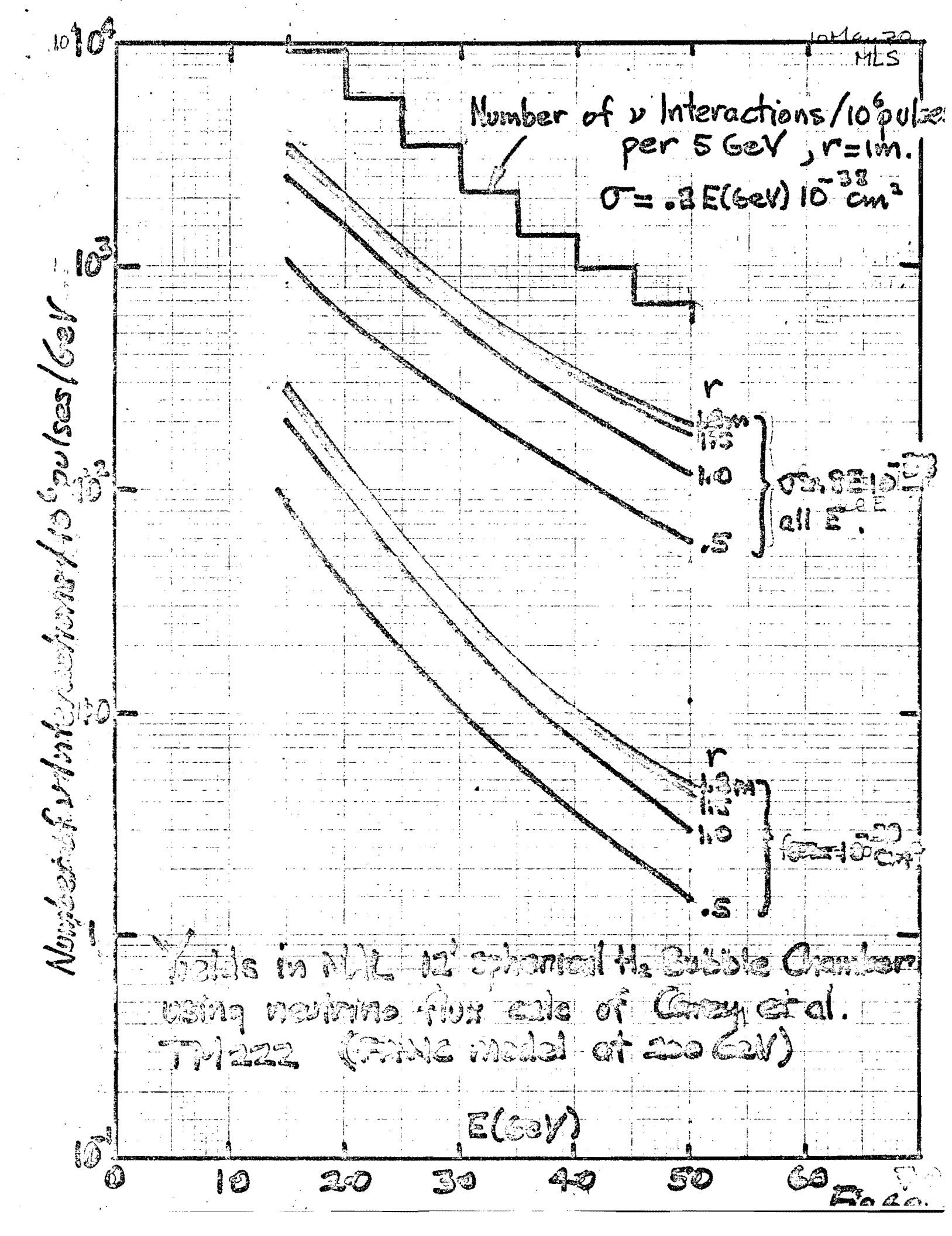

Yields in MIT 12' Spherical H_2 Bubble Chamber using neutrino flux calc of Carey et al. TM222 (FNAL model at 200 GeV)

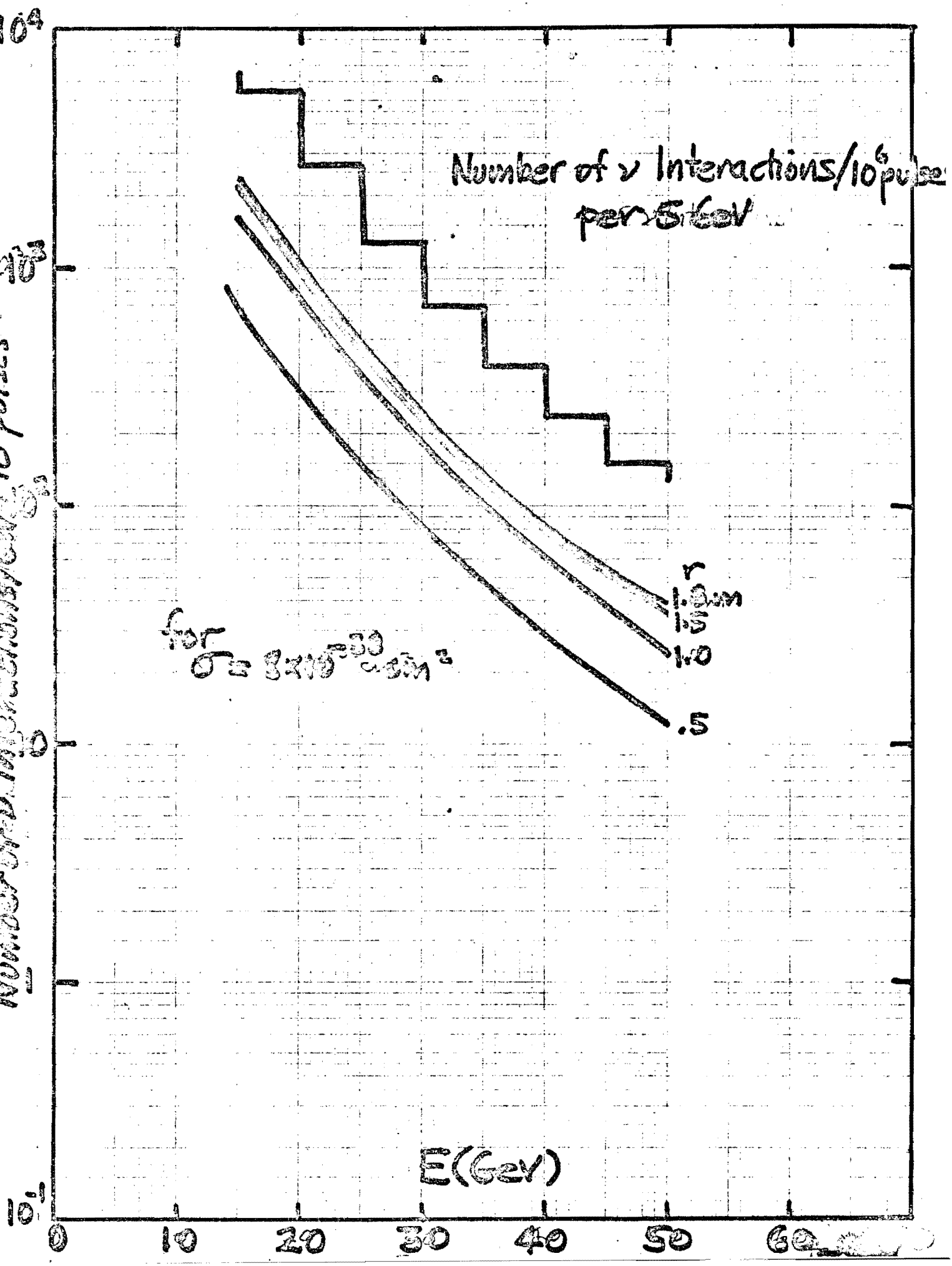
Number of ν Interactions/10⁶ pulses per 5 GeV
for σ = 8×10⁻³³ cm²
1.5
1.0
.5
E(GeV)
0
10
20
30
40
50
60

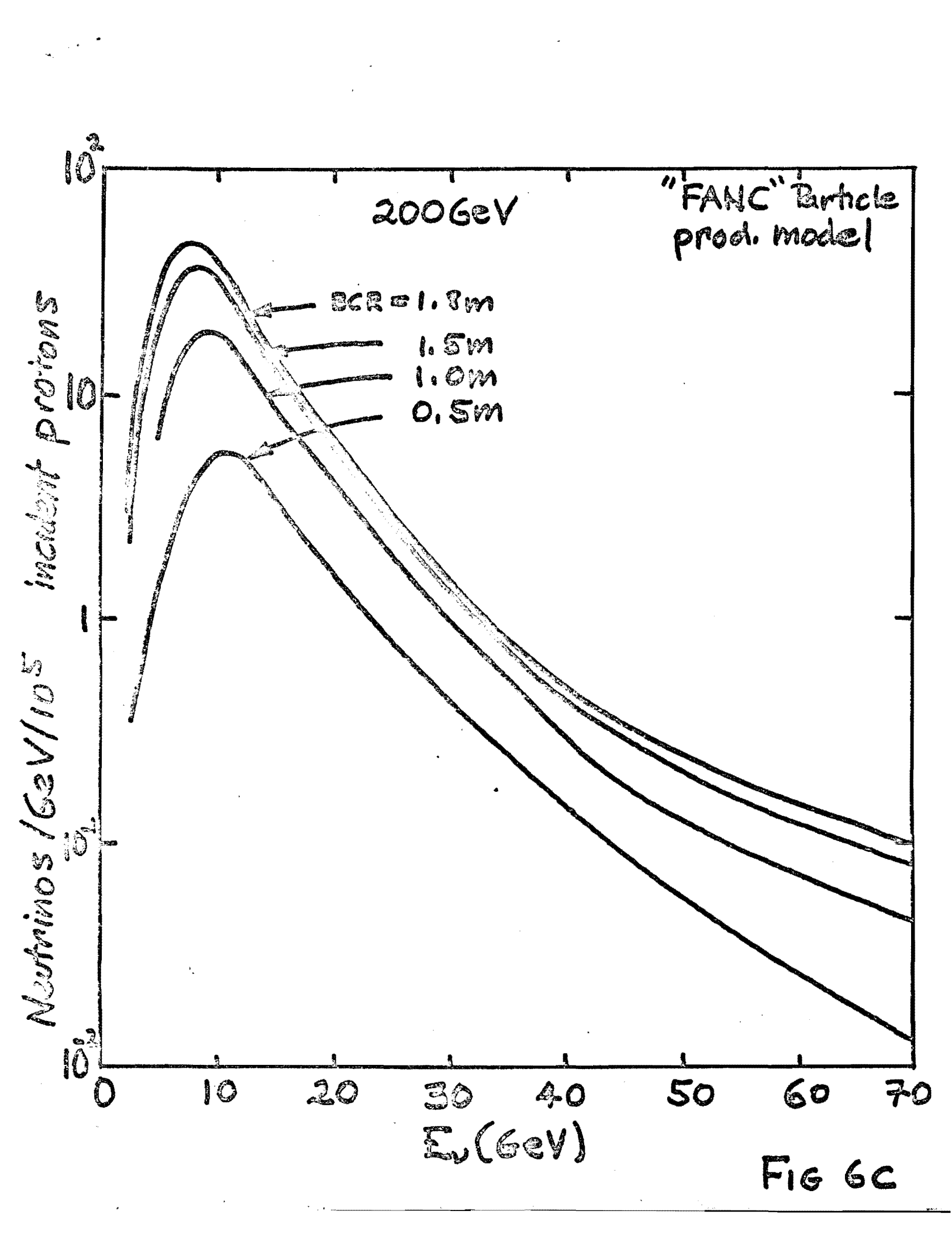
200GeV
"FANC" Particle prod. model
BCR = 1.8m
1.5m
1.0m
0.5m
Neutrinos/GeV/10^5 incident protons
10^2
10
1
10^-1
10^-2
0
10
20
30
40
50
60
70
E_ν (GeV)

Fig 6c

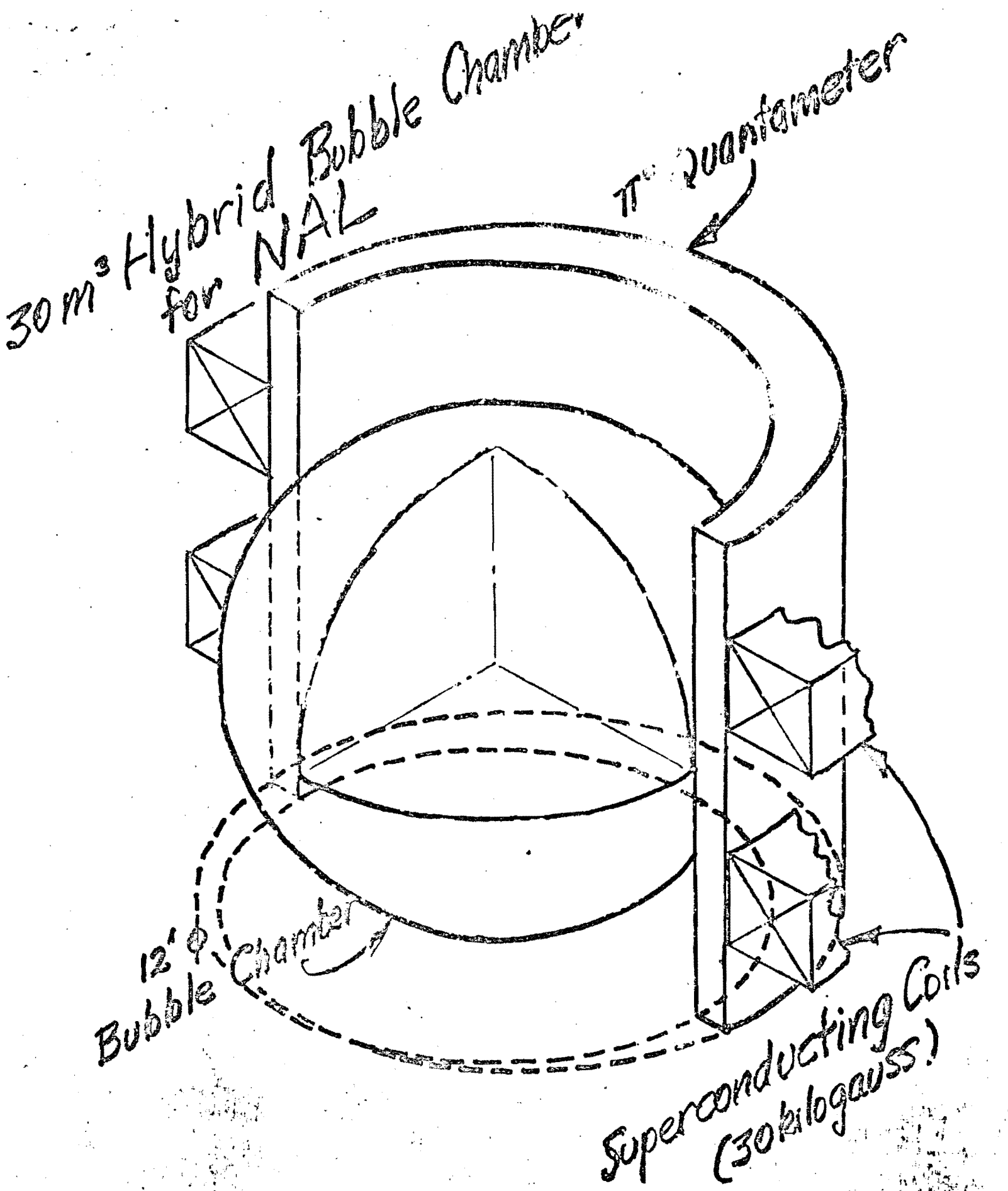
30 m³ Hybrid Bubble Chamber for NAL
π° Quantameter
12' ϕ Bubble Chamber
Superconducting Coils (30 kilogauss)

Fig. 7

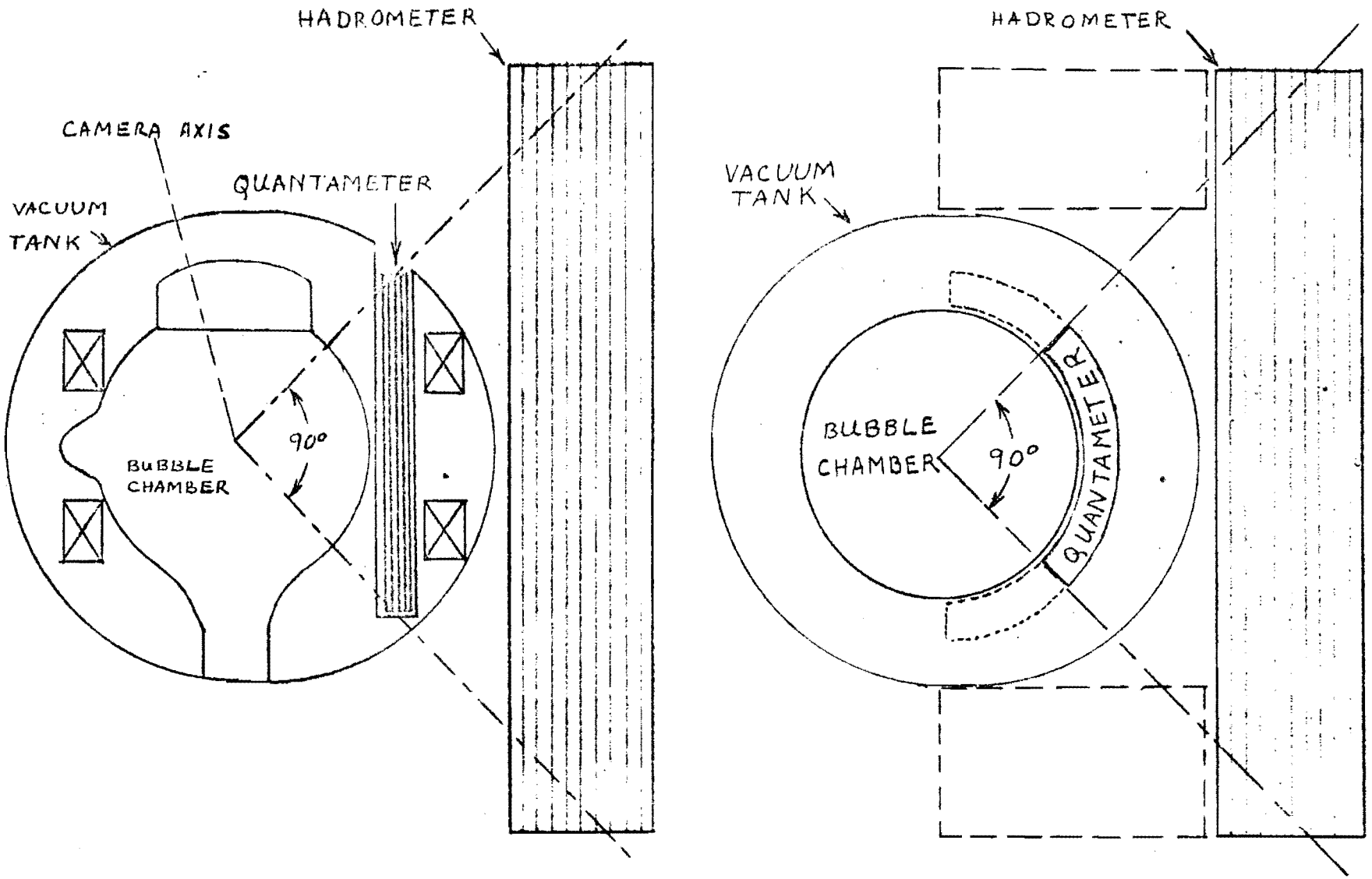
HADROMETER
CAMERA AXIS
QUANTAMETER
VACUUM TANK
BUBBLE CHAMBER
90°
SIDE VIEW
HADROMETER
VACUUM TANK
BUBBLE CHAMBER
90°
QUANTAMETER
TOP VIEW

FIG. 8

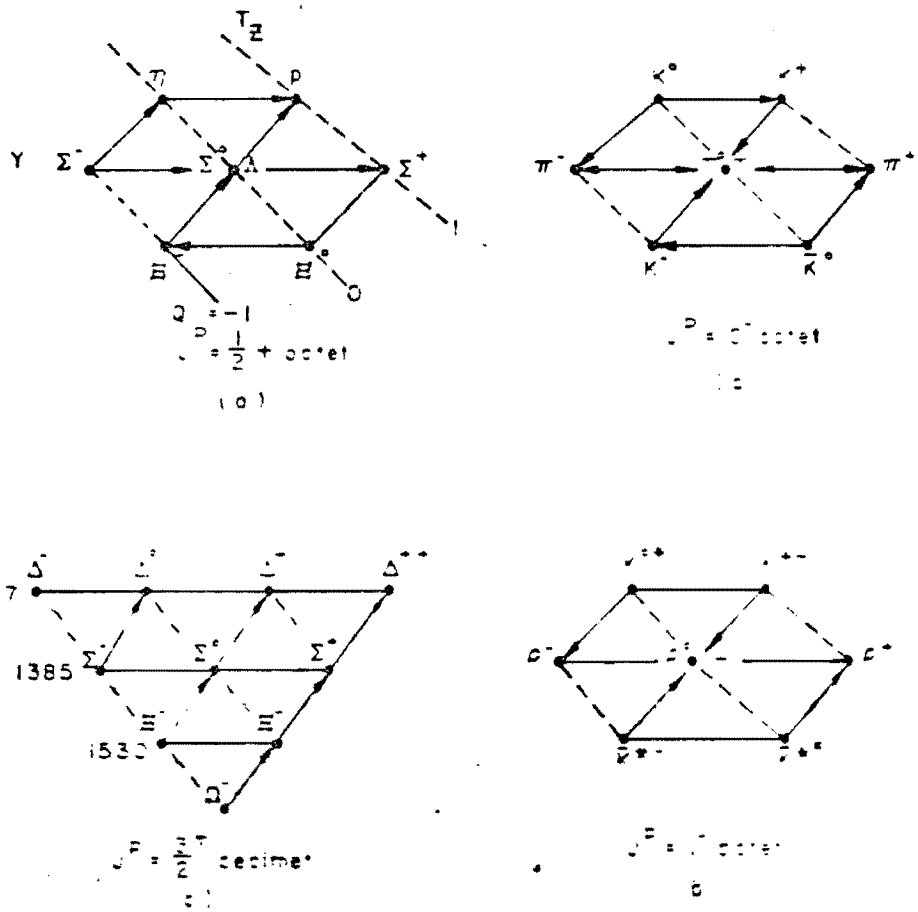
T_z
n
p
Y
Σ^-
Σ^0
Λ
Σ^+
Ξ^-
Ξ^0
Q = −1
Q = 0
$J^P = \frac{1}{2}^+$ octet
(a)
K^0
π^-
π^+
K^-
$\bar{K}^0$
$J^P = 0^-$ octet
(b)
1237
1385
1530
Δ^-
Δ^{++}
Σ^-
Σ^0
Σ^+
Ξ^-
Ω^-
$J^P = \frac{3}{2}^+$ decimet
(c)
D^-
D^+
$J^P = 1^-$ octet
(d)

9
FIG 10

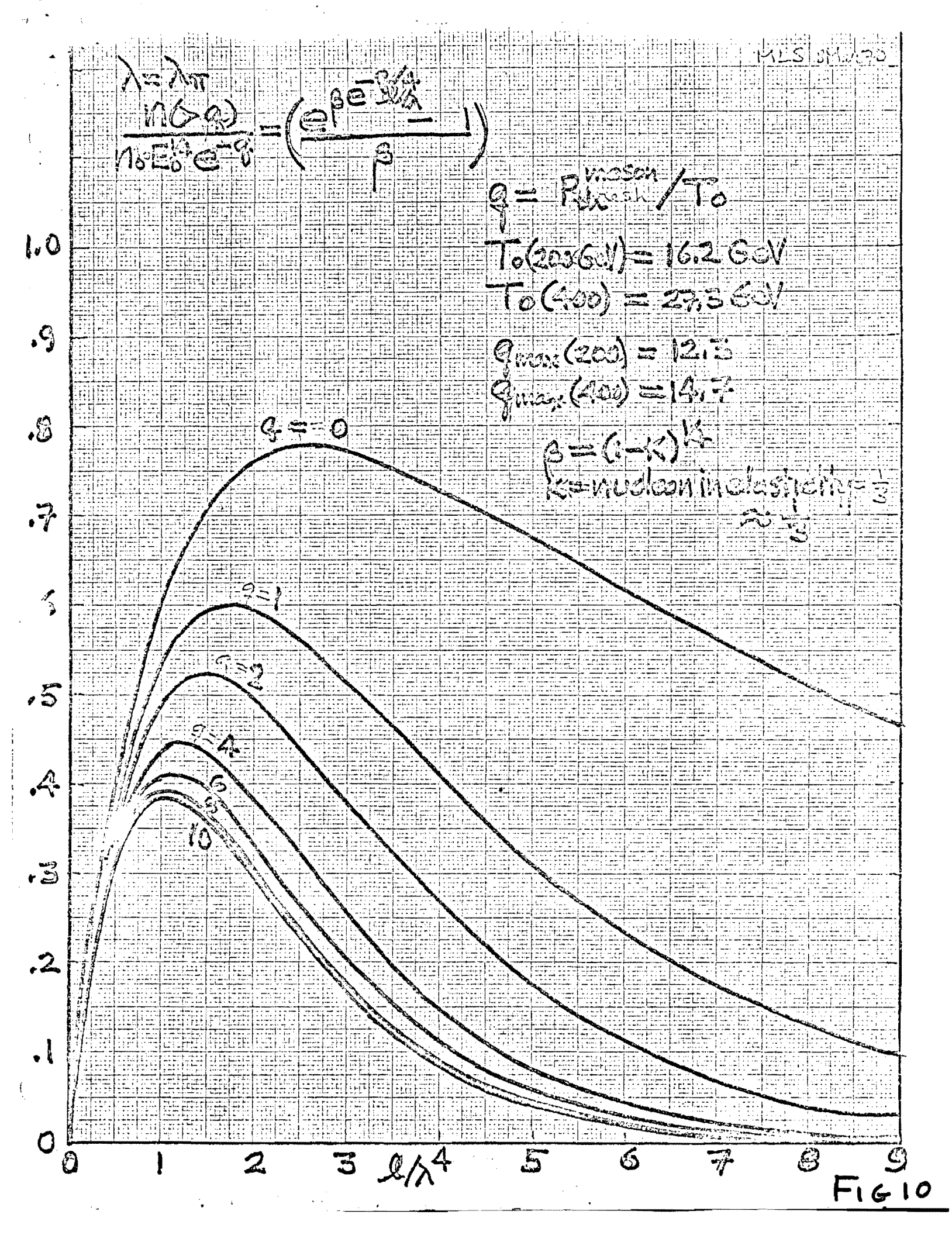
$\frac{\lambda = \lambda_T}{n(>q)} = \left(\frac{e^{\beta e^{-q/\lambda}} - 1}{\beta}\right)$
$n_0 E_0^{-\gamma} e^{-q}$
$q = P_{Nucleon}^{meson} / T_0$
$T_0(200) = 16.2$ GeV
$T_0(400) = 29.3$ GeV
$q_{max}(200) = 12.3$
$q_{max}(400) = 14.7$
$\beta = (1-K)^{\frac{1}{3}}$
K = nucleon inelasticity = $\frac{1}{2}$
q = 0
q = 1
q = 2
q = 4
q = 6
q = 8
q = 10
1.0
.9
.8
.7
.6
.5
.4
.3
.2
.1
0
0 1 2 3 ℓ/λ_A 5 6 7 8 9

FIG 10

MASTER

NAL PROPOSAL # 9A

SUPPLEMENT TO NAL PROPOSAL (#9) FOR A HIGH ENERGY NEUTRINO EXPERIMENT IN THE NAL 30m^3 H_2, D_2 BUBBLE CHAMBER

University of Hawaii (R. Cence, F. Harris, M. Peters, V. Peterson, D. Yount)

Northwestern University (S. Meyer)

University of California, Lawrence Radiation Laboratory (M. Alston Garnjost, R. Birge, G. Goldhaber, J. Kadyk, S. Parker, M.L. Stevenson*, G. Trilling)

July 1970

We wish to respond here to some of the misunderstandings and criticisms of our proposal to make the NAL 30m^3 bubble chamber a hybrid system consisting of a fifteen radiation length quentameter and a fourteen collision length hadrometer.

I. Why Hydrogen and Deuterium?

We admit that our preference for using these targets is subjective. It is formed from years of observing strange and unexpected phenomena while scanning hydrogen and deuterium bubble chamber film. One is much more likely to strugele for an explanation to a peculiar event if it occurred on hydrogen. When the target nucleus is more complex one can usually invent many superfluous explanations for the event. Therefore, we believe it is essential to study high energy ν and $\bar{\nu}$ interactions on H_2 and D_2 in a bubble chamber where the interaction vertex is seen and the momentum of all charged tracks measured. The understanding of the unexpected H_2 events will aid in untangling peculiar events in D_2. Observations must be made over all possible kinematic variables. Two important questions must then be answered; 1) Which charged track is the lepton, and 2) What is the momentum of the neutral system? The hybrid system provides the answers.

*correspondent

II. Why Build the Hybrid System When Track Sensitive Targets (TST) are Planned for the NAL $30m^3$ Chamber?

The motivation that led us to develope the hybrid system was our awareness of how marginal the usefulness of TST's for high energy neutrino plysics became when the size of the NAL chamber was reduced from $100m^3$ to $30m^3$. The reason for the marginality is that at least two conversion lengths of Ne-H_2 mixture must blanket the TST. When the chamber volume is reduced, the TST volume reduces at a much greater rate. The solid curves of Fig. 1 summarize the effective TST volumes* for 0, 1, 2, and $3\pi^o$ physics as a function of bubble chamber diameter (in feet). The transverse distribution of neutrinos is assumed to be uniform. Pure Ne is used as the blanket. The design using a 12 foot diameter chamber described by Roe et al in NAL proposal number 44 is used as normalization.

Our original proposal (June 1970) for the development of a hybrid system called for an enlargement of the coils to allow the Quantameter to be inserted. We now believe a much better solution both for TST's and for Quantameter accuracy is to enlarge the chamber to fill the space and to slice two feet off the rear portion of the chamber as shown in Fig. 2. The reasons are discussed on pages 8-10 of Appendix 1. The solid curves of Fig. 3 show the fiducial volume of the hybrid system as a function of the bubble chamber diameter for two possible neutrino transverse distributions. The fiducial volume of the hybrid system is defined to be that space in which a neutrino event can occur and all π^os be detected. The dashed curves of Fig. 3 show the TST effective volumes that could be placed in a truncated sphere of that diameter. The broken curve of Fig. 3 is the estimated bubble chamber cost. This number is based upon \$0.2 million/ft ∅ incremental coil cost. Chambers within the range of 10' ∅ to 14' ∅ will fit in the 22' ∅ vacuum tank, use the same expansion system, and the same optics.

* "Effective volume" is defined to be the product of TST volume and the probability of converting all γ's of all π^os.

We add \$0.1 million/ft Ø to take account of added bubble chamber body cost. This brings the total cost differential to \$0.3 million/ft Ø. The percentage bubble chamber-cost-increase per foot Ø is $\tilde{\sim}$ 4.3%/ft Ø. The percentage increase in fiducial volume is 65%/ft Ø for TST's in the truncated spheres and is 30%/ft Ø for the hybrid system. The large percentage increase in TST effective volume per foot Ø is the reason for our belief that the present 12' Ø design is very marginal for TST's.

The hybrid system with a 12' Ø truncated sphere has (12/4.1 = 3) times the effective volume for one π^o physics with TST's in a complete 12' Ø sphere and (12/2.3 = 5.2) for three π^o physics. These factors become (12/3.3 = 3.6) and 12/1.6 = 7.5), respectively, for TST's in a truncated 12' Ø sphere.* The cost of the Quantameter is approximately \$0.35 million. In summary, for modest incremental chamber costs (4.3%/ft Ø) great gain in usefulness both for TST's (65%/ft Ø) and the hybrid system (30%/ft Ø) can be obtained. We urge NAL to expand the chamber size to correspond to a truncated sphere of 14 foot diameter (total volume $\tilde{\sim}$ 30m^3).

III. Determination of the Momentum of the Neutral System

The Quantameter

A. How can we determine the γ's energy when we have no information about the showers in the first two radiation lengths? This is a natural question for heavy liquid bubble chamber physicists to ask. The quantameter operates on a much different principle. It is well established that for photons of energy

*The hybrid system has an advantage for doing "no π^o" physics over the bubble chamber without TST's. With "no π^o" events there is an ambiguity where the event can have a π^o moving directly downstream or directly upstream. The quantameter can rule out the downstream π^o. The upstream π^o ambiguity usually involves low energy π^o's.

greater than 1 GeV more than 96% of its energy appears in the form of ionization beyond the first two radiation lengths. Details are given in Appendix I.

B. Is the preliminary cost estimate for the electronic readout realistic?

The proposed multi-wire proportional chamber (MWPC, or "Charpak chamber") measures the position (and ionization) of each charged particle in the Quantameter. An area of 25 meters^2 corresponds to 180° x 90° coverage. We assume an average of 10 gaps (5 to 15 gaps, depending on position) of cm each. Thus 250m^2 of area is to be digitized. Position accuracy to ±1 mm in two coordinates is desired; in addition, pulse height to ±3% is required.

Standard techniques (one amplifier/wire) are very expensive. However, recent developments in higher gain in proportional multiplication (Charpak et al, 1970) and delay-line readout (Perez-Mendez et al., 1970)[1] make possible simplifications. The delay-line can readout 500 wires with one amplifier. Using the positive induced pulses on steps in the negative planes (oriented, say at ±45 deg to the positive wires) one can readout both x- and y-coordinates in a single gap.

A module of 100 cm width and 300 cm height will require about 2000 center wires (at 45°) and two Mylar planes with 2 mm wide aluminized strips to readout x- and y- into orthogonal delay lines. The estimated cost of delay line readout is $5000/module,[2] including pulse-height; 70 molules would cost about $350K.

IV. Identification of the Lepton

The primary purpose of the hadrometer is to absorb all hadrons, permitting the muons to pass through and be identified. Further details are given by Mukhin and Yount.[3]

How can the hybrid system deal with mesons that decay into muons? Fast pions of momentum P can decay into muons whose momenta range from 1/2P to P. Thus accurate momentum measurements (±3%) within the H_2-D_2 bubble-chamber should be able to detect more than 90% of π-μ decays within the chamber. Decays outside

the chamber (in Q, or in H, or between) are more difficult to detect, except that for low momenta (<2 GeV/c) π-μ decays will usually give anomalously short ranges in the hadrometer for the measured momentum.

Thus despite the long average pion decay distance from production vertex to the hadrometer center ($\tilde{\sim}$ 5 meters), corresponding to 9% (at 1 GeV/c) to 1% (9 GeV/c) decay fractions, range and momentum measurements will detect most of these π-μ decays. Full use of the H_2 volume for momentum measurements along a suspected muon track is essential.

The "ambiguous" region includes mainly the quantameter (35 cm) and space between quantameter and hadrometer ($\tilde{\sim}$100 cm).

V. Trigger Rate for Quantameter and Hadrometer

The electronics trigger will require (a) an anti against incident charged particles (or charged particles from the upstream coil), (b) one or more tracks passing through the Quantameter and (c) a muon (penetrating particle) leaving the Hadrometer. This signature rejects muons from the shield, cosmic ray muons, neutrino interactions in the Quantameter or Hadrometer, and neutron interactions. It strongly favors neutrino interactions in the hydrogen.

The Quantameters's proportional chamber is continuously sensitive with fast readout which can be combined with scintillation logic to decide on spark-chamber triggers in <1 μsec. Thus the Hadrometer is fired only when the signature is complete.

If the trigger rate exceeds one per burst, it is possible to refine the Quantameter and/or scintillator logic to define the penetrating muon trajectory more precisely. Multiple electronic "events" per burst can be handled if necessary. This would require more than one vidicon camera (with electronic shutter) for the Hadrometer.

VI. Why Don't the Quantameter and Hadrometer Subtend More Solid Angle?

We have the possibility at a later date to increase the hadrometer to cover 180° thereby detecting muons below 4GeV. The addition of a TST cylinder that runs the full length of the chamber can also be added later.

VII. How Does One Take Account of Hadron Interactions in the Quantameter?

Most of the γ's from a π^{o} are confined in a cone of full angle $2/\gamma$. If a charged pion has a large probability of being emitted into this cone then it will pose some problems for us. However, we wish to give some crude arguments to suggest that this is not the case. Under these circumstances we can track the charged hadron through the quantameter, not being bothered by the γ showers, and get a good measure of the energy it deposits in the quantameter.

The argument is based on a fireball type model [4] where one assumes that a substantial number of pions come into thermal equilibrium at a temperature $kT \tilde{\approx} 0.18$ GeV. Their energy distribution is a Planck-like one. The "overlap" problem is best considered in the rest frame of this fireball. Suppose for the moment that all the pions were neutral, each with its γ ray cone subtending a solid angle of π/γ^{2}. Here γ is the energy of the pion, E, divided by the pion rest energy μc^{2}. The fraction of the total solid angle, 4π, that is "used up" by all the γray cones is,

$$f = \frac{\langle n_{\pi} \rangle X_{o}^{2}}{4} \; \frac{\int_{X_{o}}^{\infty} \frac{1}{X} \frac{\sqrt{X^{2} - X_{o}^{2}}}{e^{X} - 1} \, dx}{\int_{X_{o}}^{\infty} \frac{X}{\sqrt{X^{2} - X_{o}^{2}}} \frac{}{e^{X} - 1} \, dx} \; ,$$

where, $X_{o} \equiv \frac{\mu c^{2}}{KT}$, $X \equiv \frac{E}{kT}$

Evaluation of the integrals yields, $f = \frac{\langle n_{\pi} \rangle}{27}$

Usually, one third of the mesons will be neutral, in which case

$$f_o = \frac{\langle n_\pi \rangle}{81}$$

Let us consider the worst possible case.

From Fig. 1 of our original proposal (#9) one sees that for Eν = 50 GeV, $\langle n_\pi \rangle < 15$, $f_o < 0.18$ for 50 GeV nutrinos.

The probability that all charged pions miss these cones is $(1-f_o)^{n_{ch}}$. for $\langle n_\pi \rangle = 15$ this probability is $(.82)^{(\frac{2}{3}\cdot 15 = 10)} = 0.14$

The probability that all but <u>one</u> pion miss

$$\text{is} = \frac{\langle n_{ch} \rangle !}{(\langle n_{ch} \rangle - 1)!\,1!}(1-f_o)^{\langle n_{ch} \rangle - 1} f_o^1 = \left(\frac{10!}{9!} = 10\right)(.82)^9(.18)$$

$$= (10)(.168)(.18) = 0.30$$

that all but <u>two</u> pions miss is,

$$\frac{\langle n_{ch} \rangle !}{(\langle n_{ch} \rangle - 2)!\,2!}(1-f_o)^{\langle n_{ch} \rangle - 2} f_o^2 = \left(\frac{10!}{8!\,2!} = 45\right)(.82)^8(.18)^2$$

$$= 45(.204)(.0324) = 0.30$$

that all but <u>three</u> pions miss is,

$$\frac{\langle n_{ch} \rangle !}{(\langle n_{ch} \rangle - 3)!\,3!}(1-f_o)^{\langle n_{ch} \rangle - 3} f_o^3 = \frac{10!}{7!\,3!}(.82)^7(.18)^3 = 0.174$$

and so on. Each charged pion that strikes a cone has a probability of $e^{-1} = .368$ of <u>not</u> interacting in the quantameter.

In the proposal we assumed that the entire final hadron state comes into thermal equilibrium. In this way we obtain an upper limit on the multiplicity. For Pomeranchuk exchange $\langle n_\pi \rangle$ would be much lower than these.

In Table I we summarize for various multiplicities, $\langle n_\pi \rangle$, a) the probability that no charged pion strike within the "γ-cones", and b) the probability that no charged pion interacts in the Quantameter within the "γ-cones".

At this stage we feel confident of our ability to deal with this problem.

We intend to demonstrate capability of the Quantameter to perform the function we describe in our proposal by doing a modest experiment.

TABLE I

$\langle n_\pi \rangle$	Probability that all charged pions miss cones	Probability that no charged pion interact within γ cones.
3	0.928	0.928 + 0.0262 + ... = 0.954
6	0.735	0.735 + .087 + .004 + ... = 0.83
15	0.140	0.140 + 0.110 + 0.040 + 0.009 = 0.30

REFERENCES

(1) "Electromagnetic Delay Line Readout for Proportional Wire Chambers", by R. Grove, K. Lee, V. Perez-Mendez, and J. Sperinde, UCRL-19858, July 1970. Appended to this note.

(2) See LRL Engineering Note F.ET-1361 (July 1, 1970), "Digitizing System for Proportional Chambers Using Delay Line Readout", by F.A. Kirsten for component costs ($0.47 per wire for 512 wire chamber), including scalers, amplifiers, and delay line.

(3) A. Mukhin and D. Yount, "External versus Internal Muon Identification in the 15-Foot Bubble Chamber" 1970 NAL Summer Study.

(4) M.L. Stevenson "The Role of the Planck Distribution in Understanding the Constancy of the Transverse Momentum in High Energy Nucleon-Nucleon Collisions NAL Internal Report TM-219, and Y.W. Kang and M.L. Stevenson "Properties of the Neutrino Beams at a 400 GeV Accelerator" TM 217, page 6.

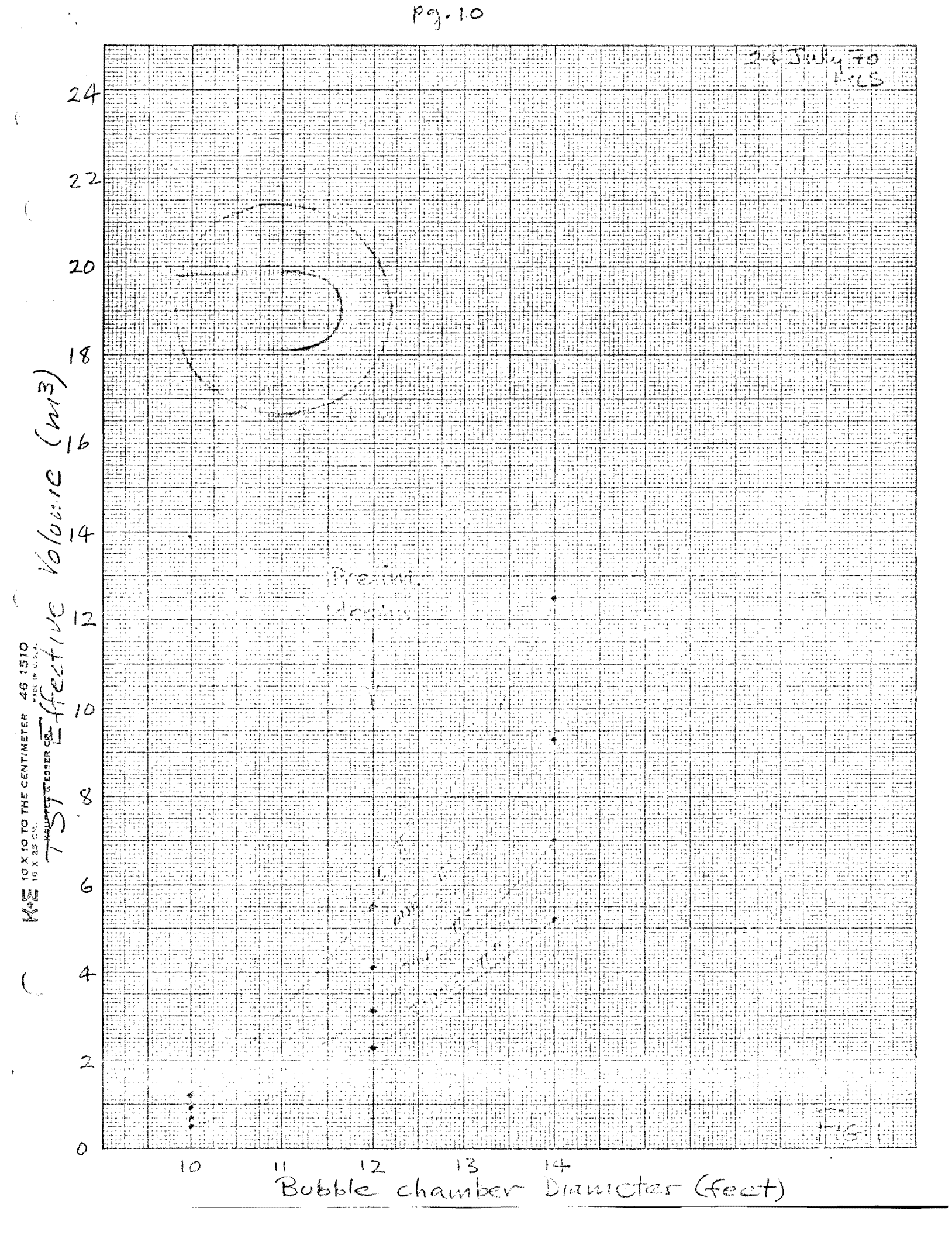
24 July 70
M.C.S.
Preliminary
Design
Effective Volume (m^3)
0
2
4
6
8
10
12
14
16
18
20
22
24
10
11
12
13
14
Bubble chamber Diameter (feet)
FIG 1
KE 10 X 10 TO THE CENTIMETER 46 1510
18 X 25 CM.
KEUFFEL & ESSER CO. MADE IN U.S.A.

23 July 70
FIG 2

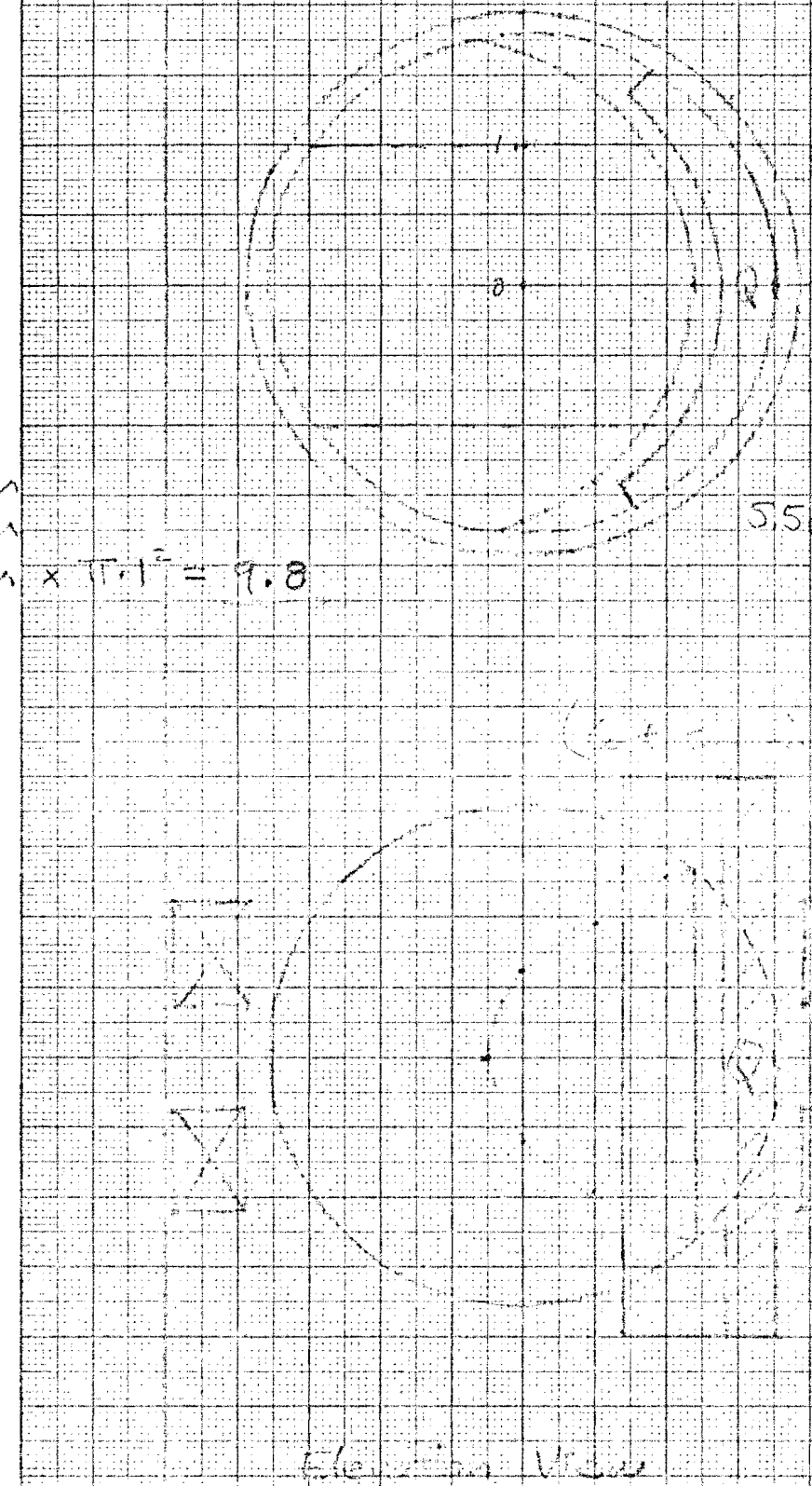

For a shield of equal mass, the fiducial vol is a factor of 1.5 larger.

FIG. 2

SQUARE 10 X 10 TO THE CENTIMETER AS-6014-67
KEUFFEL & ESSER CO. GRAPHIC TECHNICAL CORPORATION Bronx, New York Printed in U.S.A.

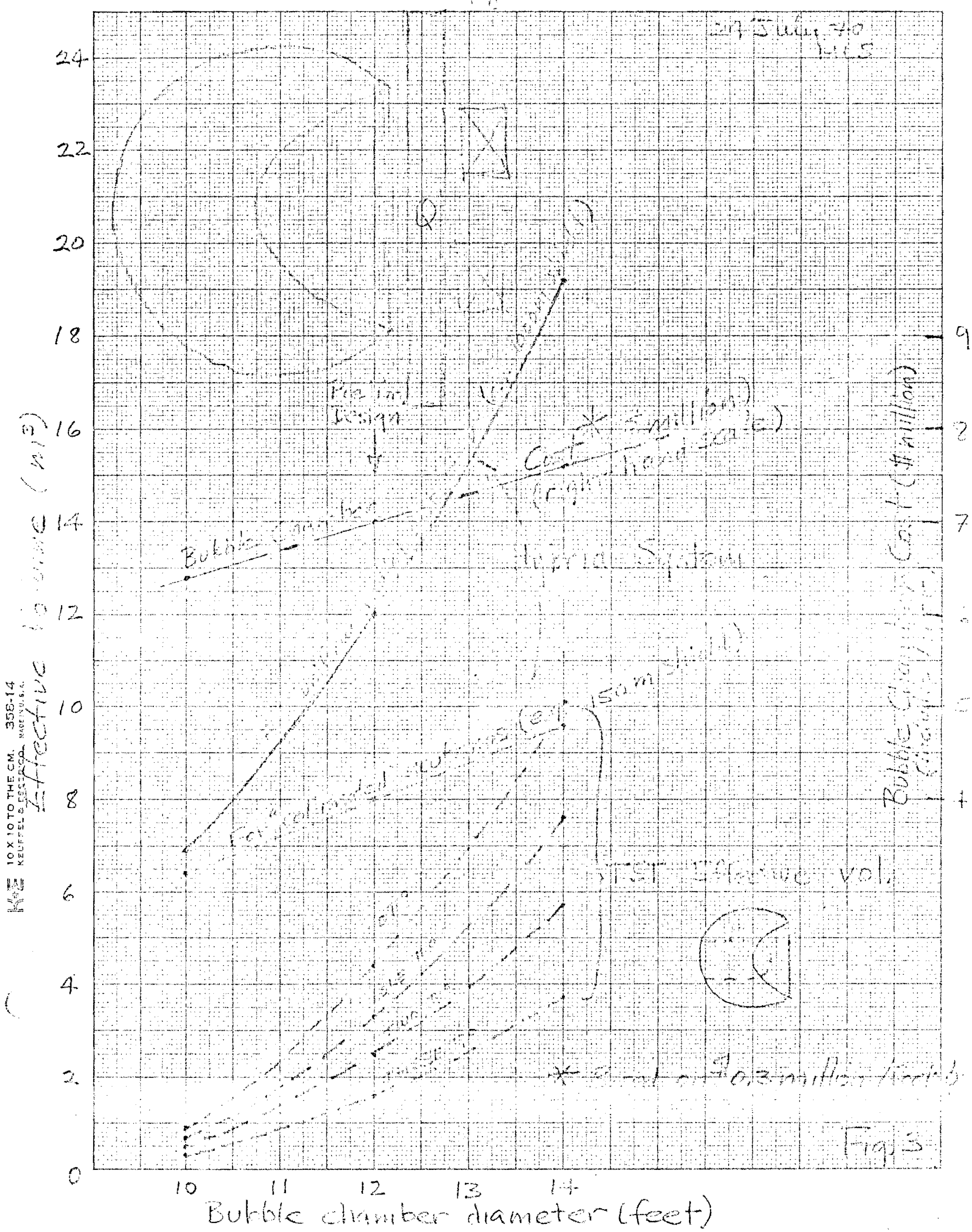
27 July 70
HCS
Effective Volume (m³)
Bubble chamber diameter (feet)
Bubble Chamber Cost ($ million)
Bubble Chamber
Cost
(right hand scale)
Hybrid System
Fiducial volume
TST Effective vol.
Fig. 3
0
2
4
6
8
10
12
14
16
18
20
22
24
10
11
12
13
14
7
8
9
10 X 10 TO THE CM. 358-14
KEUFFEL & ESSER CO. MADE IN U.S.A.

APPENDIX 1

PROPORTIONAL QUANTAMETER FOR THE 15-FOOT BUBBLE CHAMBER

D. Yount

University of Hawaii

ABSTRACT

The performance of a quantameter to detect and measure the energy of the neutral pions produced by neutrino interactions in the 15-foot bubble chamber is evaluated.

INTRODUCTION

Since the neutrino energy spectrum is broad, measurement of the νp and νd total cross sections requires that the full energy of each interaction be determined. Essentially, there are four components: charged hadrons, charged leptons, neutrons, and neutral pions. The charged component can be found with high precision (± 3%) from track curvature in the 15-foot H_2, D_2 bubble chamber, although additional equipment is required to identify leptons, particularly muons, with good efficiency. The neutron component may be small for most interactions and can probably be determined with an external hadrometer to sufficient accuracy that the uncertainty in the total energy is not dominated by this source. The most efficient method for measuring the photon energy from neutral pion decay appears to be the lead-plate quantameter: the purpose of this note is to estimate the resolution and precision of this type of detector, thereby emphasizing

the importance of allowing for such a device in the bubble-chamber design.

Typically half the energy in a neutrino interaction appears in the form of charged leptons. Perhaps 1/3 of the total hadron energy appears in the form of neutral pions, which therefore account for 1/6 of the total neutrino energy. The fraction is large enough so that neutral pions must be detected with good conversion efficiency in any total-cross-section experiment; it is small enough so that even a modest accuracy (± 10% of the neutral-pion component) would imply that the dominant error results from track curvature. It may therefore be possible to determine the total neutrino energy to ± 3% in the hybrid H_2, D_2 bubble chamber, while an estimate of ± 5% has been given in an NAL proposal.[1] Corresponding estimates for the neon bubble chamber range as high as ± 20%.[2]

Parallel-plate ionization calorimeters, such as the quantameters[3] widely used in monitoring photon beams, have several intrinsic properties that are essential in determining the neutral-pion energy accurately. First, the response depends only upon the relative ionization in the gas gaps as compared to the ionization in the plates; tolerances of 1% or less in these parameters can be met and insure a uniform response to the same level. Second, since the ratio of gap to plate is independent of track angle in a parallel-plate chamber, such a device is intrinsically isotropic. Third, the output of an ionization calorimeter is linear in the energy absorbed over a wide range.

Fourth, an ion chamber is operated as a one-parameter device; there is one high-voltage setting and one output signal proportional to the total energy deposited in the chamber as sampled periodically via the ionization in the gas gaps. This last feature greatly simplifies the operation of the calorimeter and results in a highly reproducible instrument.

In the case of electromagnetic showers, virtually all of the energy appears ultimately in the form of ions, which are sampled directly in the ionization calorimeter thereby avoiding such questions as the response of scintillation or Cerenkov counters using phototubes. The SLAC quantameter,[4] for example, has been shown to be linear in energy to ± 0.2% from 1 GeV to 14 GeV, the highest energy at which linearity was tested. The response for incident electrons or positrons[5] was found to be the same to about ± 0.3%, and the reproducibility over long periods of time is also on this level. The SLAC quantameter has been calibrated with a Faraday cup so that it can be used as an absolute monitor to a few tenths of one percent. One simply fills the chamber with a standard gas and sets the high voltage.

The precision, linearity, and reproducibility of ionization quantameters under very favorable circumstances are clearly excellent. The performance of a large proportional quantameter in detecting the electromagnetic energy in a single neutrino-induced event from the bubble chamber can be estimated by considering those factors which cause the response to deteriorate, as compared with ordinary quantameters used in beam

monitoring. The analysis below indicates that a statistical uncertainty of ± 3% (1000 tracks for 10 GeV neutral-pion energy) results from shower sampling every 1/2 radiation length, while sampling every radiation length would give ± 4%. When systematic effects are taken into account, the overall accuracy should be better than ± 6% for 10 GeV neutral-pion energy or about ± 1% of the total neutrino energy in a 60-GeV event. Unlike the neon bubble chamber, which has a radius of about 3 radiation lengths, the quantameter improves with energy, the accuracy varying roughly as $1/\sqrt{E_{\pi^0}}$.

SHOWER STATISTICS

The gain of the SLAC quantameter with 1-atm argon-CO_2 filling is about 4000 ions per GeV incident.[4] The copper plates are 0.963 cm = 0.72 radiation lengths thick with an average gas gap of 0.476 cm. An output of about 40 ions/track would result from a single minimum ionizing particle passing through such a gap indicating that the number of tracks sampled is of order 100/GeV. For a total π^0 energy of 10 GeV, 1000 tracks would be expected yielding a statistical uncertainty of about ± 3%. Monte Carlo calculations for electron-photon showers in lead[6] predict about 600 electrons above 1.5 MeV for a 6-GeV shower sampled at intervals of 1/2 radiation length. This is equivalent to 1000 electrons at 10 GeV, consistent with the first estimate. (The quantameter plates are somewhat thicker than 1/2 radiation

length, but particles of less than 1.5 MeV are detected.)

SHOWER SAMPLING AFTER 2 RADIATION LENGTHS

A recent 15-foot bubble-chamber design specifies a thin exit wall of 1/2 inch steel, equivalent to about 0.7 radiation lengths. The front wall of the reentrant tank would be of comparable thickness. Photons originating at the center of the bubble chamber will pass through about 0.3 radiation lengths of liquid hydrogen, so that the total thickness before entering the quantameter is about 1.7 radiation lengths. This may be considered as the first plate of the quantameter, which would begin with a thin window followed by a sensitive gas gap. Since photon cascades are displaced in the direction of the shower axis by about 1 radiation length with respect to electron cascades,[6] photon-shower sampling beginning after 2 radiation lengths should be excellent.

Quantitatively, only about 0.5% of the total ionization in a photon shower at 6 GeV occurs in the first radiation length, while at 1 GeV the value is the same to 0.2%. Less than 4% of the ionization occurs in the first two radiation lengths, the difference in 1 and 6 GeV being less than 1%. The shower multiplicities versus thickness in lead for these two energies are shown in Figure 1 to illustrate this point.[6] Since the quantameter will be calibrated, only the linearity is in question: this appears to be of order 1% for photons above 1 GeV, even

if sampling begins after 2 radiation lengths. Clearly, it makes negligible difference if 10 GeV reaches the quantameter as two photons or a dozen. In fact, the thickness after which sampling begins can be varied from 0 to 2 radiation lengths without affecting the quantameter output by more than 4%.

SHOWER PENETRATION

The shower penetration in percent depends on the incident photon energy and could affect the energy linearity if the quantameter is too thin. About 7% of the ionization in a 6-GeV photon shower occurs after 15 radiation lengths, while less than 2% appears after 20 radiation lengths.[6] In ionization quantameters,[3] the spacing of the last gas gap is usually made large enough to "compensate" for shower penetration, reducing this loss by perhaps one order of magnitude. Compensation is also possible in the proportional quantameter: for example, the gain of the last gap can be increased so that the signal from this gap is proportional to the penetrating ionization rather than simply the ionization of one gap at the particular thickness in radiation lengths. In any case, it is straight forward to design a quantameter for which shower penetration alters the energy linearity by less than 1%. The back-scattered energy from a 6-GeV photon cascade in lead is about 0.12% of the total.[6]

7.

SHOWER DATA

Before considering other systematic effects peculiar to the hybrid application, it is useful to compare the estimates of intrinsic quantameter performance with existing data. An energy resolution of ± 19% (HWHM) has been obtained at 200 MeV by counting sparks in a lead plate chamber with plates 0.15 radiation length thick.[7] Scaling to 1 radiation length and 10 GeV would give

$$19\%/\left[\frac{10\ \text{GeV}}{50\ \text{MeV}} \times \frac{0.15\ \text{r.l.}}{1.0\ \text{r.l.}}\right]^{\frac{1}{2}} = \pm\ 7.4\%$$

as compared with the statistical limit of ± 4%. The scaling is pessimistic for two reasons: 1. tracks observed in a photon shower at intervals of 0.15 radiation lengths are not independent in a statistical sense, and 2. spark counting is less efficient than a direct ionization measurement.

Backenstoss et al.[8] have measured the resolution of a lead-scintillator shower counter consisting of 20 lead plates each 0.8 radiation lengths thick. Their result at 10 GeV is ± 4.9%, which scales to ± 5.4% at 1 radiation length. This value is more applicable to the quantameter configuration than that obtained by scaling track-counting results, but it is still somewhat pessimistic since it involves phototube resolution, light attenuation in plastic scintillator, etc.

Hofstadter and Hughes have studied the resolution in a Pb-NaI array as a function of the thickness of lead.[9] Their results for incident electrons at 8 GeV are shown in Figure 2. The resolution is observed to vary from ± 1% (HWHM) with no lead to ± 6% with 0.75 inches, about 3 radiation lengths, in front of each successive crystal. Since the NaI crystals are 7 inches = 7 radiation lengths thick, the results are not directly applicable to the thin gas gaps of a proportional quantameter. They do, however, illustrate that even very crude sampling of an electromagnetic shower at high energy can yield excellent resolution.

MAGNETIC FIELD

Electrons and positrons from photon conversion in the 0.7-radiation-length exit wall of the bubble chamber must pass through a magnetic field of 30 kG before reaching the quantameter. Since the H_2,D_2 container is spherical and the reentrant quantameter tank cylindrical, as presently envisioned, the distance traveled in the magnetic field depends upon where conversion occurs. A reasonable approximation is

$$s = 5 \text{ cm} + 200(1 - \cos\theta) \text{ cm}$$

where s is the separation, 5 cm is assumed to be the separation in the median plane, 200 cm is the approximate radius of the bubble chamber, and θ is the angle between the median plane and a line from the center of the bubble chamber to the place on the 1/2-inch-steel wall where photon conversion occurs. A track with radius equal to the separation will just miss the quantameter. The momentum cutoff for detection is then given by

$$p(\text{GeV/c}) = 3\ B(\text{kG})\rho(\text{cm})$$
$$= 100s.$$

Values of s and p are plotted versus the height above the median plane of the bubble chamber in Figure 3a.

Assuming the distribution function for the fraction of the total energy given to an electron or positron is constant, energy losses occur in $2(p/p_o)$ of the conversions where p_o is the incident photon energy. The mean energy carried away when a particle is lost is $(p/p_o)/2$ so that the average for all photon conversions is $(p/p_o)^2$. The average energy loss in percent, computed in this way, is plotted versus the height above the median plane in Figure 3b for several photon energies. This model, while exceedingly crude, suggests that measurements of the total π^o energy can be made with accuracy of a few percent or better over most of the quantameter area when the total energy is above a few GeV. The losses in the median plane

are small even at quite low photon energies, and this property could be extended to the entire quantameter by matching bubble-chamber and quantameter geometries, either making the back of the bubble chamber cylindrical or making the quantameter locally spherical. Nine modules 1 m square in a 3 m x 3 m array would approximate a spherical surface nicely if a reentrant tank of suitable shape were made to contain them.

INCIDENT CHARGED LEPTONS

Muons penetrating the quantameter would contribute to the total ionization about one track per gap. For 20 radiation lengths and 40 gaps, this amounts to about 40 tracks/1000 tracks = 4% of the signal from a 10-GeV neutral-pion shower. A correction of this magnitude is straight forward once the penetrating muon has been identified, for example, by a hadrometer in the hybrid system.

Electrons or positrons entering the quantameter will be detected with exactly the same response as incident photons. If the electrons arise from conversion of π^o photons in the bubble chamber or steel vacuum tank, the resulting signal should be combined directly with that due to π^o photons, a case already discussed. Electrons from an electron-neutrino ν_e vertex can be identified by associating a shower in the quantameter with

with a charged track in the bubble chamber: spatial resolution in the quantameter is required. The energy of the identified electron can be determined from track curvature in the bubble chamber and can be subtracted from the total quantameter signal, leaving the neutral pion component intact. Dalitz decays are rare and yield pairs of electrons which can be identified in the quantameter and retained in the neutral pion signal.

NEUTRONS AND INCIDENT CHARGED HADRONS

Corrections of order 4% per hadron can be made to the quantameter signal for charged hadrons that penetrate without interacting. No correction is necessary for neutrons that do not interact. For interacting hadrons the correction may be comparable with the neutral pion signal, and it can only be made by analyzing each event in detail, taking into account the incident hadron energy, the penetrating hadron energy (determined, for example, by a hadrometer), and the spatial information provided by the wire readout of the proportional quantameter.

A thickness of 15 - 20 radiation lengths of lead is equivalent to about 1 collision length for strongly interacting particles. Perhaps a third of the energy in each collision goes into neutral pions,[10] which shower and are detected with good efficiency by the quantameter unless the interaction occurs in the last few radiation lengths. Depending upon the

event configuration, it may be necessary to determine the neutral pion component from the neutrino vertex by track counting rather than by measuring the total quantameter signal. Since the sum of the π^0 and interacting-hadron energies is measured absolutely by the quantameter, only the relative numbers of tracks in various showers is required. An accuracy approaching the statistical limit might still be possible in this case, but the analysis would become more complex. A modular quantameter design would substantially reduce the probability for more than one shower signal to occur in a single readout.

SHOWER POINTING ERROR

Experimental data on the accuracy with which the direction of a photon shower can be determined are shown in Figure 4.[11] The results suggest that the pointing error improves slowly after 1 GeV, while the variation with plate thickness may be $t^{1/2}$. The result, scaled to a plate thickness of 1 radiation length, is a pointing error of about $\pm 10^{o}$. This should be sufficient to associate individual showers detected in the quantameter with particular events seen in the bubble chamber when more than one event occurs during an expansion. It would also exclude photons from interactions in the coils upstream of the bubble chamber in most cases and would permit pairs or single electrons and positrons to be associated with photons converting in the

1/2-steel wall of the bubble chamber.

PROPORTIONAL READOUT

The primary ionization from a single electromagnetic shower at 10 GeV is not sufficient to produce a practical signal across the high capacitance of a large parallel-plate quantameter. In the proportional chamber[12] several orders of magnitude additional amplification can be obtained through avalanche formation in the high electric field surrounding wires 20 - 50 u in diameter and spaced 1 - 3 mm apart. In the proportional quantameter[1] shower formation and avalanche multiplication combine to yield a signal across the full capacity of one gap or of one chamber that is comparable with the single-avalanche signal across the capacity of one wire. Furthermore, since a small number of signals are involved in a total-energy measurement, high quality amplifiers can be used to preserve the output linearity and stability. The performance of a proportional quantameter, as compared with an ionization quantameter, appears, therefore, to be limited mainly by such considerations as the wire uniformity, the characteristics of avalance formation, and the time distribution and time interval sampled. Each of these effects should be greatly reduced in the statistical average over 1000 tracks. A rough guess is that collection times of several tens of nanoseconds would be sufficient to permit reproducibility, uniformity, and

energy linearity approaching the statistical limit (± 4% for 1-radiation-length plates at 10 GeV).

DISCUSSION

It appears that a lead-plate proportional quantameter of 15 - 20 radiation lengths thickness and a similar number of gaps could be used to determine the neutral-pion energy from individual neutrino interactions in the 15-foot bubble chamber with an accuracy well under ± 10%. Certain classes of events, particularly those in which hadrons interact in the quantameter, would require detailed analysis, including shower-track counting, before this level could be reached. Since on the average only 1/6 of the energy in a neutrino interaction is expected to go into neutral pions, an uncertainty as large as ± 10% in this component would contribute a smaller error to the measurement of total neutrino energy than results from track curvature in the H_2,D_2 bubble chamber, ± 3%. In this sense, it seems clear that a lead-plate proportional quantameter would be highly useful, even if its resolution is several times worse than presently seems feasible.

REFERENCES

1. M. L. Stevenson et al., "Proposal for a High-Energy Neutrino Experiment in the NAL 30 m^3 H_2,D_2 Bubble Chamber," NAL Proposal Number 9.

2. C. Baltay, R. B. Palmer, and N. P. Samios, "Search for the Intermediate Boson, Lepton Pair Production, and a Study of Deeply Inelastic Reactions Utilizing High Energy Neutrino Interactions in Liquid Neon," NAL Proposal Number 53.

3. R. R. Wilson, Nucl. Instr. 1, 101 (1957).

4. D. Yount, Nucl. Instr. Methods 52, 1 (1967).

5. D. Yount, Symposium on Beam Intensity Measurement (Daresbury, England, 22-26 April 1968, V. W. Hatton (Ed.)) pp. 75-96. (See DNPL/R-1.)

6. H. Nagel, Zeitschrift fur Physik, 186, 319 (1965); U. Völkel, DESY Report 65/6, July 1965.

7. R. Cence (Private Communication) July, 1970.

8. G. Backenstoss, B. D. Hyams, G. Knop, and U. Stierlin, Nucl. Instr. Methods 21, 155 (1963).

9. E. B. Hughes, "Observations on the Total Absorption of Electrons and Pions in Matter at GeV Energies," HEPL 603, June, 1969.

10. V. S. Murzin, Progress in Elementary Particle and Cosmic Ray Physics (North-Holland Publishing Company, Amsterdam, The Netherlands, 1967), Vol. IX, p. 245.

11. V. Peterson (Private Communication) July, 1970.

12. G. Charpak, D. Rahm, and H. Steiner, Nucl. Instr. Methods 80, 13 (1970).

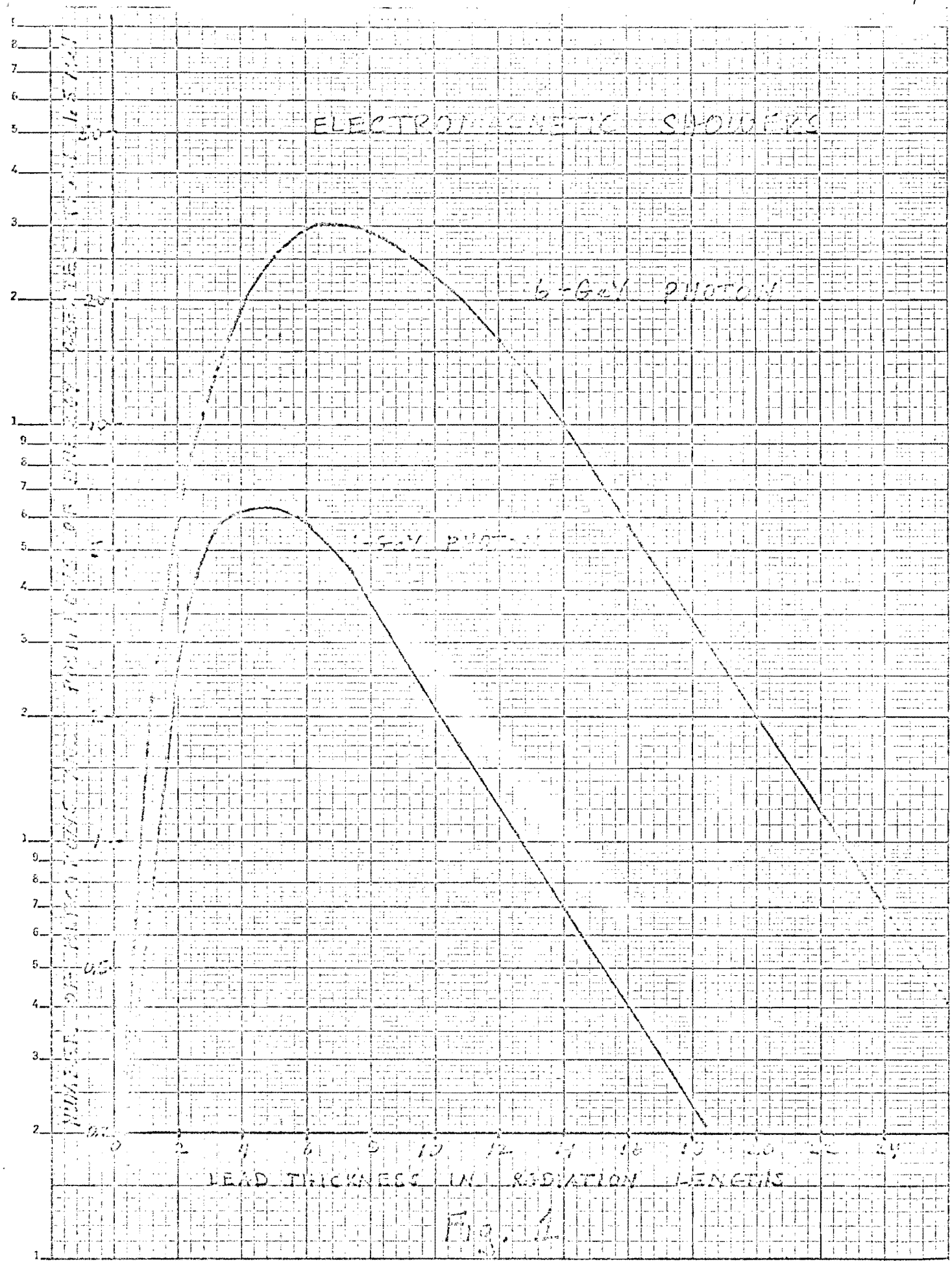
ELECTROMAGNETIC SHOWERS
6-GeV PHOTONS
1-GeV PHOTONS
LEAD THICKNESS IN RADIATION LENGTHS

Fig. 4

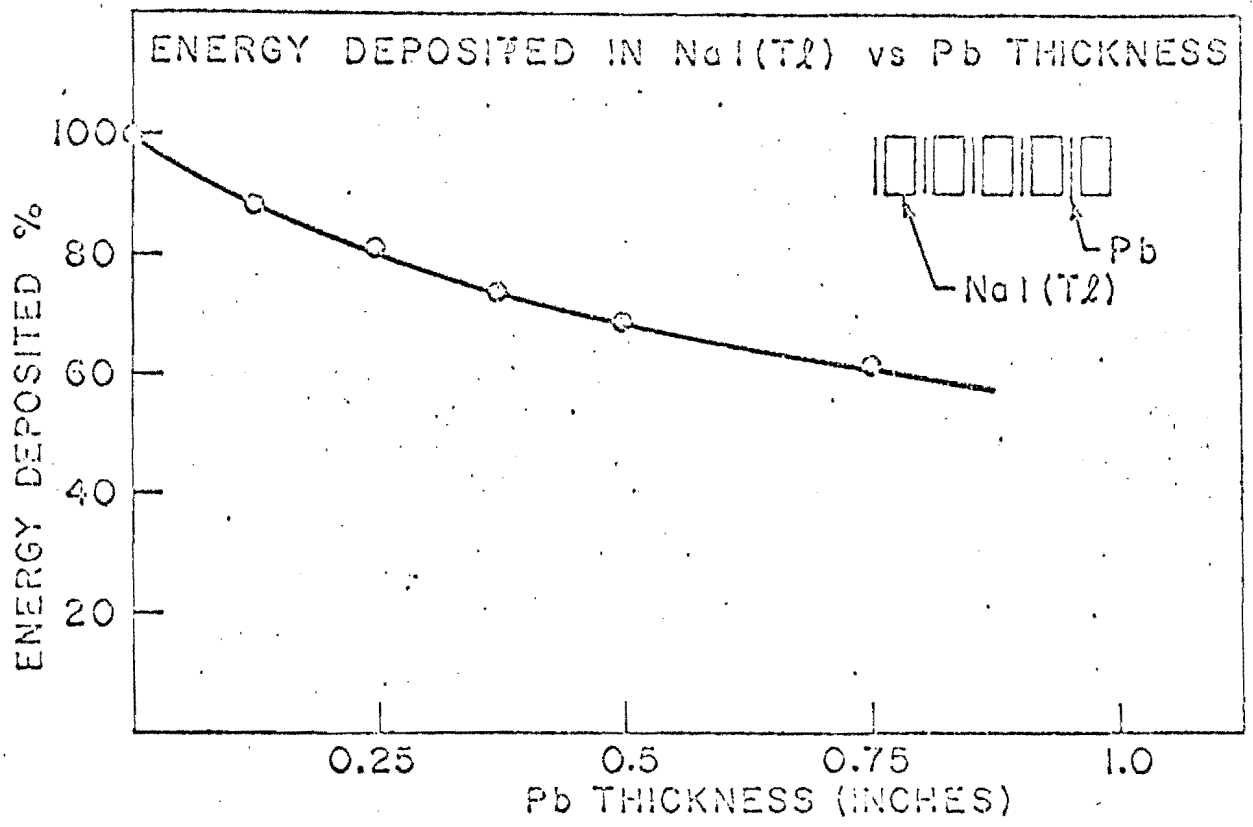
ENERGY DEPOSITED IN NaI(Tℓ) vs Pb THICKNESS
ENERGY DEPOSITED %
100
80
60
40
20
NaI(Tℓ)
Pb
0.25
0.5
0.75
1.0
Pb THICKNESS (INCHES)

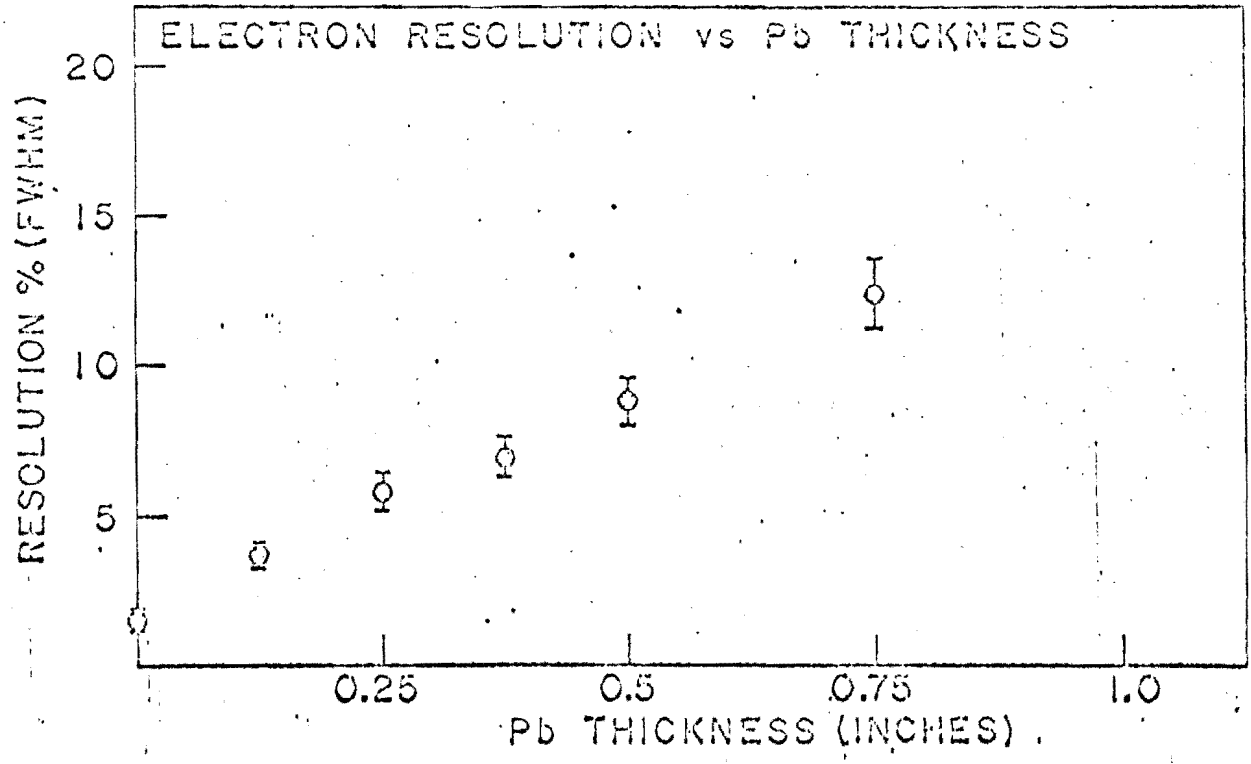
ELECTRON RESOLUTION vs Pb THICKNESS
RESOLUTION % (FWHM)
20
15
10
5
0.25
0.5
0.75
1.0
Pb THICKNESS (INCHES)

Fig. 2

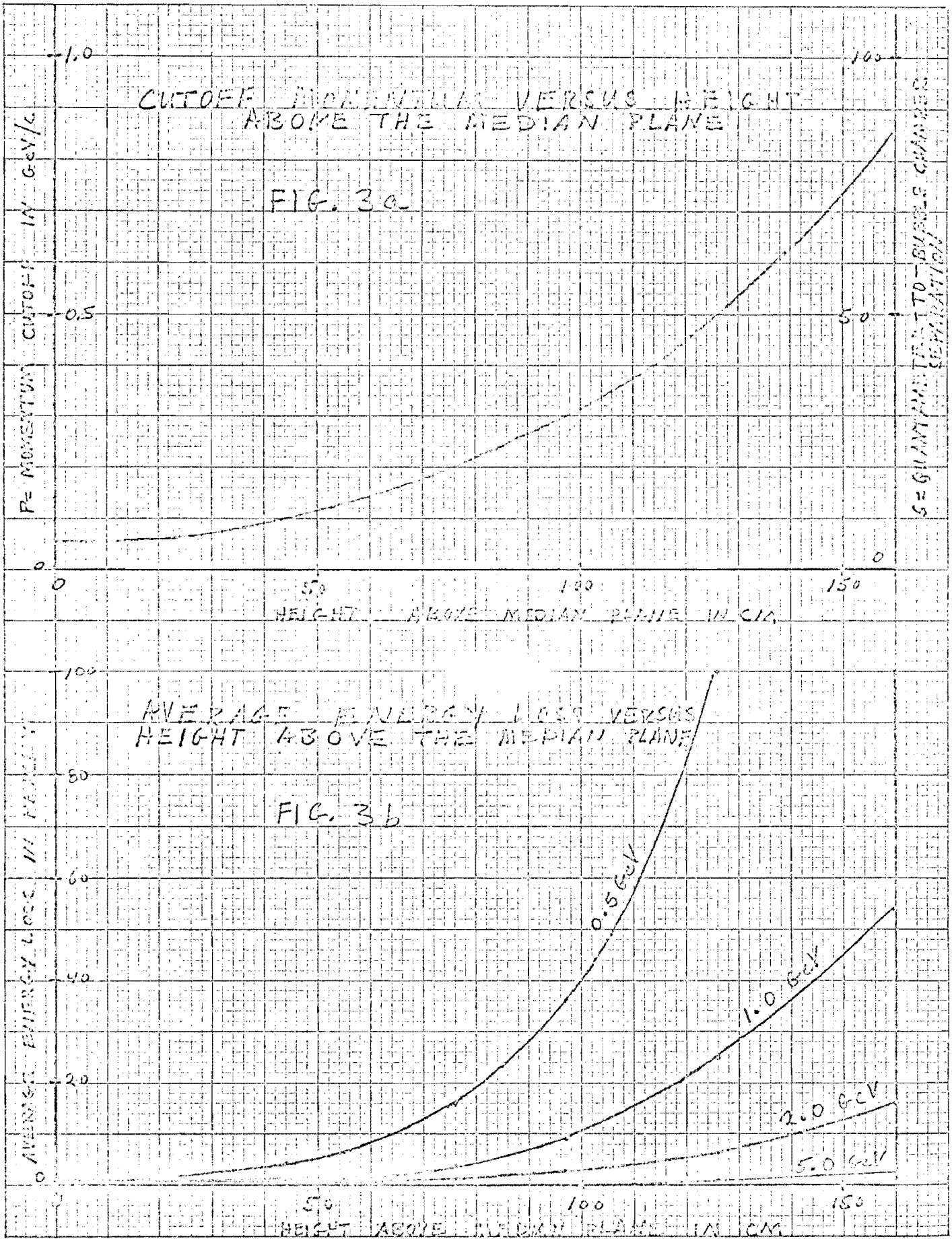

5 X 5 TO THE CENTIMETER 46 1010
10 X 10 CM
KEUFFEL & ESSER CO.

5 X 5 TO THE CENTIMETER 46 1610
10 X 24 CM. MADE IN U.S.A.
KEUFFEL & ESSER CO.

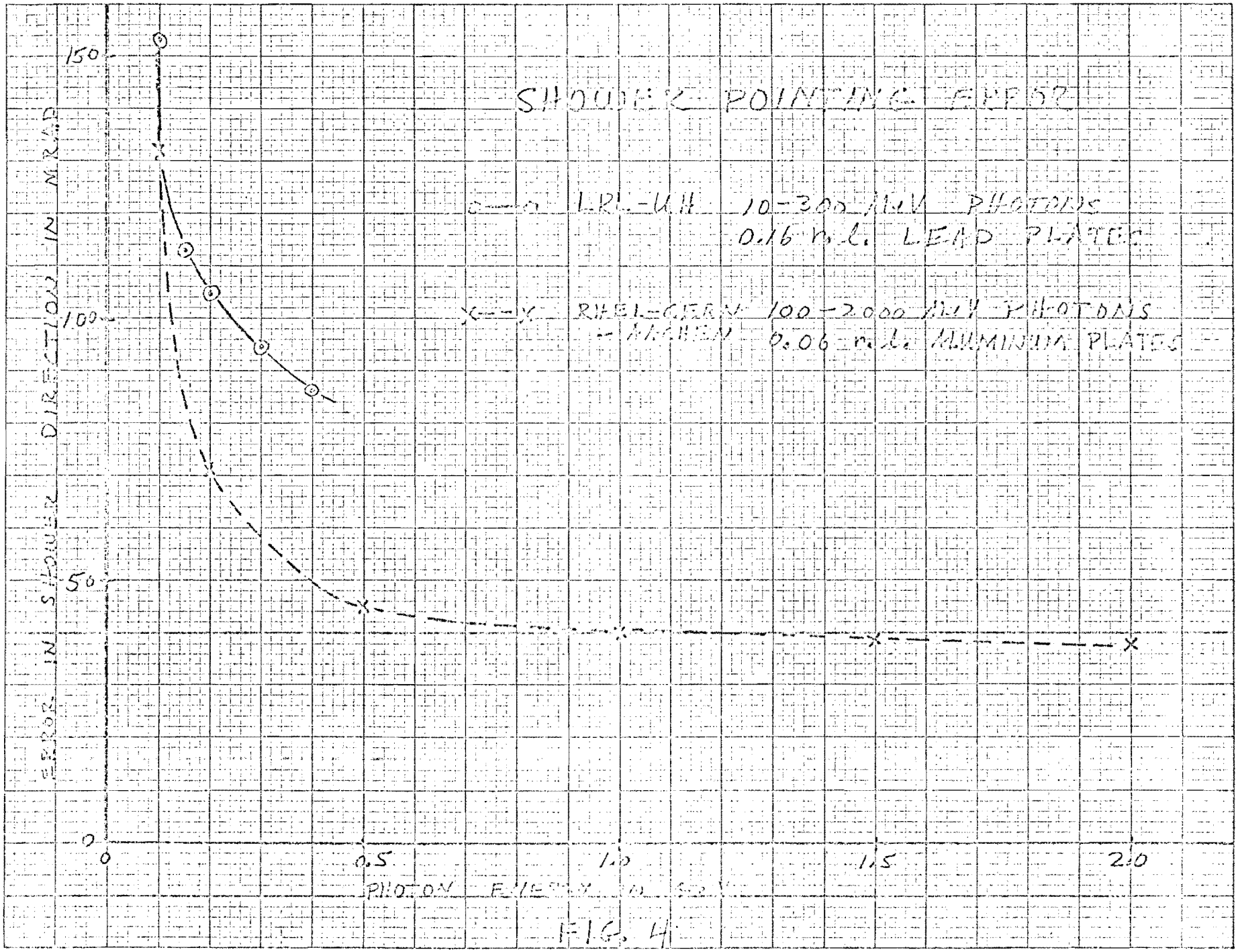

FIG. 4

Submitted to Nuclear Instruments and Methods

UCRL 19858

UNIVERSITY OF CALIFORNIA

Lawrence Radiation Laboratory

Berkeley, California

ELECTROMAGNETIC DELAY LINE READOUT FOR PROPORTIONAL WIRE CHAMBERS

R. Grove, K. Lee, V. Perez-Mendez and J. Sperinde

ELECTROMAGNETIC DELAY LINE READOUT FOR PROPORTIONAL WIRE CHAMBERS*

R. Grove, K. Lee, V. Perez-Mendez and J. Sperinde
Lawrence Radiation Laboratory
University of California
Berkeley, California

June 25, 1970

ABSTRACT

We describe the use of electromagnetic delay lines to read out the position of ionizing events in multi-wire proportional chambers. The delay line used is a ceramic core (non-magnetic) type with a delay of 80 nanosec/cm. The readout accuracy achieved depends on the wire plane which is read out: for the positive plane which forms the electron avalanche, the accuracy is ± 1 mm. (half the wire spacing). For the negative plane, which records the induced signal produced on a number of adjacent wires by the positive ions, the interpolation property of the delay line permits an accuracy of ± 0.15 mm.

I. INTRODUCTION

Multi-wire proportional chambers are now coming into extensive use in nuclear and elementary particle physics. Their main advantage over wire spark chambers is the ability to record events at high rates whereas the spark chambers are limited by the recovery time of the chamber. The main difficulty with wire proportional chambers so far has been the readout--which in the simplest case is done by using an array of amplifiers and storage logic elements connected to the individual wires. In a previous paper[1] we showed that a readout scheme using an electromagnetic delay line could be made which was

considerably cheaper and simpler than the amplifier array method. The delay line that we used was a ferrite loaded delay line to which the individual wires of the chamber were coupled by coils: the positioning accuracy that we were able to achieve was approximately 3 mm. which was the same as the spacing of the wires. In this paper we discuss a similar readout scheme using a different type of electromagnetic delay line without any ferrite or magnetic material in it. This type of delay line has a number of advantages. The ratio of delay to rise time of a pulse and the delay per unit length are higher than in the ferrite line. Furthermore the dispersion of the signal per unit delay is smaller. The combination of these properties makes it possible to use a readout scheme which achieves a position accuracy better than ± 0.15 mm. and can be used in the presence of magnetic fields of any strength.

II. DELAY LINE CHARACTERISTICS

For this project we have been using a commercially available ceramic core delay line of a type that is well described in the literature.[2] Fig. 1 shows the construction of the delay line.[3] The center conductor consists of silver painted longitudinal strips on a ceramic core which is non-magnetic. The outer conductor consists of a copper winding as shown in the figure, made of insulated copper wire 0.09 mm. in diameter with 100 turns/cm. The line is wound in 3 mm. sections with each section overlapping the previous one by 1.5 mm (see Fig. 1 insert). All turns of the winding are in the same direction. This type of delay line has the following characteristics: Delay = 80 nanosec/cm., band pass = 3.6 Mc/sec, attenuation = 1.5 db/microsec delay.

The readout methods described below depend on the high coupling possible through external coils (current coupling) or through external conducting

straps wrapped around the line (capacitative coupling). Both of these coupling schemes are possible due to the fact that the center conductor of the line is operated as the grounded conductor.

The efficiencies of these coupling methods are shown in Fig. 2. Fig. 2a shows the amplitude of the output signal for different rise times of current pulses and various numbers of turns in the coupling coils: Fig. 2b shows the corresponding curves for the capacitative coupling.

An important point to consider is the effect of the external coupling on the delay line characteristics, since we want to maintain an accuracy of timing of the pulses to within 1-1.5 nanoseconds. This loading effect is shown in Fig. 3 for both couplings; it is seen that the capacitative coupling introduces less dispersion and 'ringing' than the coil coupling. Since it is also considerably easier to construct mechanically and electrically, by wrapping plastic with conducting strips etched on it around the delay line, it is the method we prefer to use.

III. PROPORTIONAL CHAMBER MEASUREMENTS

Our measurements were done on chambers with three wire planes: a central plane consisting of wires 25 microns in diameter, spaced by 2 mm. which collected the electrons and whose field gradient produced the avalanches. The positive ion collecting planes were made of wires 100 microns in diameter, spaced by 2 mm. and with the wires oriented at 90° relative to those of the central plane. We collected signals from both the central and the outside planes. The arrangement we used is shown schematically in Fig. 4. For timing purposes we used a zero-cross [4] method.

The positioning accuracy attainable with this delay line depends on the following: (a) the amplitude of the signals above the noise level of the

electronics (b) the polarity and wire spacing of the plane which is being read-out. The zero-cross electronics will locate the pulse with a jitter of less than 1 nanosec for pulse amplitudes at the output of the delay line above 400 micro-volt. This corresponds to an output of 10-20 millivolts from the chamber wire. This amplitude is attainable with an Argon-Isobutane (70% Ar: 30% Isobutane) gas mixture with the total number of electrons pairs in the avalanche equal to $\approx 5 \times 10^6$.

The accuracy of spatial distribution depends on the polarity of the plane which is being readout due to the asymmetry in the signals induced on the electron collecting wires or on those that receive the displacement current due to the positive ions. Since the signal produced on the delay line is a composite of the signals from a number of wires adjacent to the source of ionization, interpolation between wires is possible if the amplitude of these pulses falls off monotonically with distance. Fig. 5 shows the electric lines of force. An ionizing event will produce an avalanche on wires a or b depending on whether it occurs in the region AA or AB. The position of the avalanche along the wire has a displacement error which is due mainly to diffusion of the electron trajectory due to scattering collisions in the gas. The displacement current signal induced on the positive ion collecting planes centers on the point perpendicularly opposite to the center of the avalanche, since due to the shape of lines of force there is no 'quantizing' effect.

Our measurements confirm this effect, as shown in Fig. 6, in which we plot the position of the ionizing event measured by the delay line, as a function of the position of a collimated source of 5.9 KeV γ-rays from Fe^{55}. The width of the error bars is the full width at half maximum of the distribution observed from the output of the P.H.A. This is due to source width distribution,

jitter in electronic timing and diffusion of the electrons in the gas. The difference in position accuracy and interpolation between the two planes is evident. A proportional chamber with this asymmetry is however quite useful in magnetic spectrometer experiments where the position of the particle trajectories in the plane perpendicular to the magnetic field of the deflecting magnet is usually required to the highest accuracy for the momentum determination.

If symmetry in positional accuracy in two coordinates is desired from one chamber the simplest method is to build it with the positive ion collecting planes oriented at $\pm 45^{\circ}$ relative to the central plane and which are then used for the readout.

The width of the signal pulse on the delay line, relative to the velocity of propagation determines the pulse pair resolution for two simultaneously occurring ionizing events. This is shown in Fig. 7. The results are obtained by simultaneously putting two signals on the delay line and then observing the arrival of the signals at one end of the line. The position of A is fixed and B is moved. The two dashed lines indicate the results which would be obtained for a single pulse at position A or B. Interference between the two pulses will cause the measurements to deviate from the straight lines. In the present setup the two pulse resolution is 30 mm., as can be seen from the figure. We are limited here by the simple zero-cross method of finding the pulse center. Measuring the leading edge of the pulse at each end of the delay line and a suitable coding method would improve the two pulse resolution.

IV. CONCLUSIONS

A delay line readout of the type described above has the advantages

over the individual amplifier per line scheme of greater simplicity and less expense. It is also more accurate due to the ability to interpolate among wires. The two track resolution as noted above is somewhat poorer, but can be improved.

We should also point out that electromagnetic delay lines of this type can be used for reading out wire spark chambers in magnetic fields. The signals from these chambers--current coupled or capacitatively coupled are large enough so that very little amplification is needed.

Acknowledgements

We would like to thank Ray Fuzesy and Herb Steiner for their help and cooperation in constructing and lending us some of the chambers on which these measurements were made.

FOOTNOTE AND REFERENCES

* This work was done under the auspices of the U. S. Atomic Energy Commission.

1) A. Rindi, V. Perez-Mendez and R. T. Wallace, Nucl. Inst. and Methods 77 (1970) 325.

2) J. Blewett, Proc. IRE 35 (1947) 1580; W. J. Carley, Tele-Tech. and Electronic Industries 13 (1954) 74.

3) 'Mini Lines' manufactured by Columbia Technical Corp, 24-30 Brooklyn-Queens Express Way, West Woodside 77, New York.

4) We used type T140/N zero-cross discriminators manufactured by Edgerton, Germeshausen & Grier, Inc., 160 Brookline Ave., Boston, Mass., U.S.A.

FIGURE LEGENDS

Fig. 1. Perspective view of ceramic core delay line.

Fig. 2. Efficiency of coupling from the chamber to the delay line as a function of the input pulse rise time for (a) coils of 50, 75 and 100 turns and (b) copper straps 1 mm. and 2 mm. wide.

Fig. 3: Loading effect of coupling on a 10 cm. delay line for (a) capacitative coupling and (b) coil coupling. The delay lines are loaded with coils or straps, one every two millimeters.

Fig. 4: Block diagram of the electronics used for timing the pulse. The delay line is capacitatively coupled to the chamber and zero-cross discriminators are used to locate the center of the pulse.

Fig. 5: Electric lines of force in the chamber in (a) the view normal to the central wires showing the origin of the quantizing effect and (b) the view parallel to the central wires. To make the lines of force in (b) as parallel as possible flat strips should be used for the negative plane.

Fig. 6: Measurements of the position accuracy for locating ionizing events as read out by the delay line. Figure 6a shows the event location as a function of position when the delay line is connected to the electron collecting wires. Figure 6b shows a similar measurement with the event read out from the positive ion collecting plane.

Fig. 7: Output pulse separation as a function of the input pulse separation. The dashed lines represent the measured position for a single pulse at A or B.

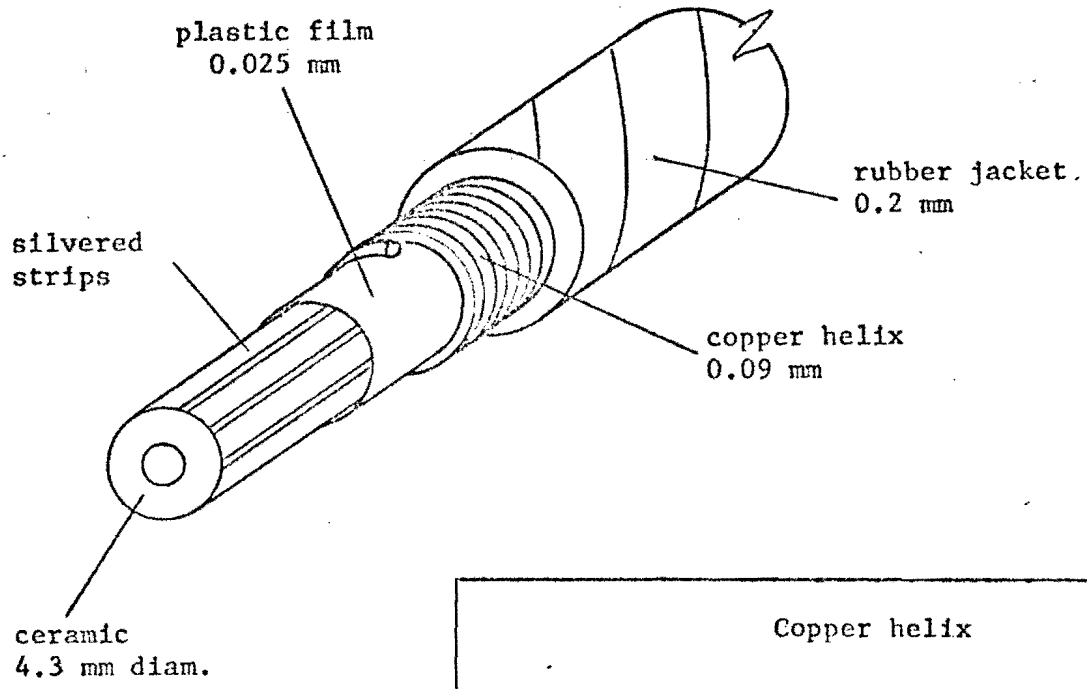
plastic film
0.025 mm
rubber jacket
0.2 mm
silvered
strips
copper helix
0.09 mm
ceramic
4.3 mm diam.

(a)

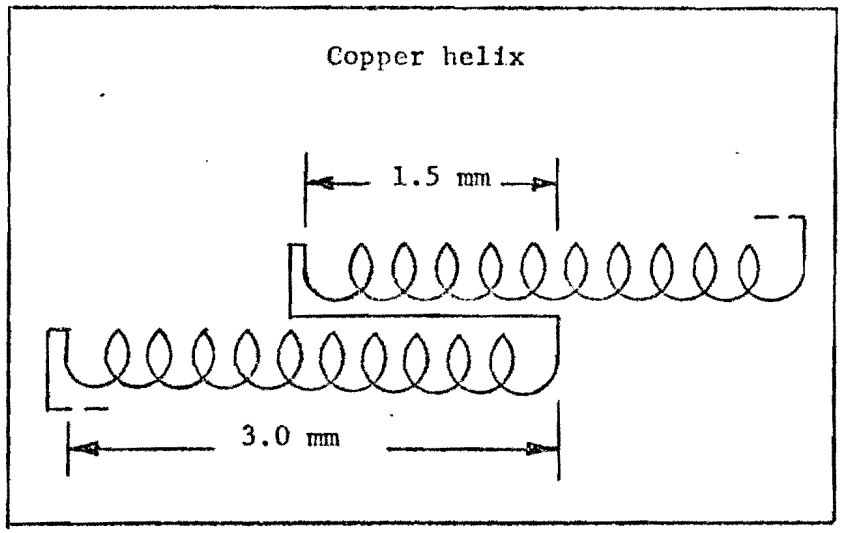
Copper helix
1.5 mm
3.0 mm

(b)

Fig. 1

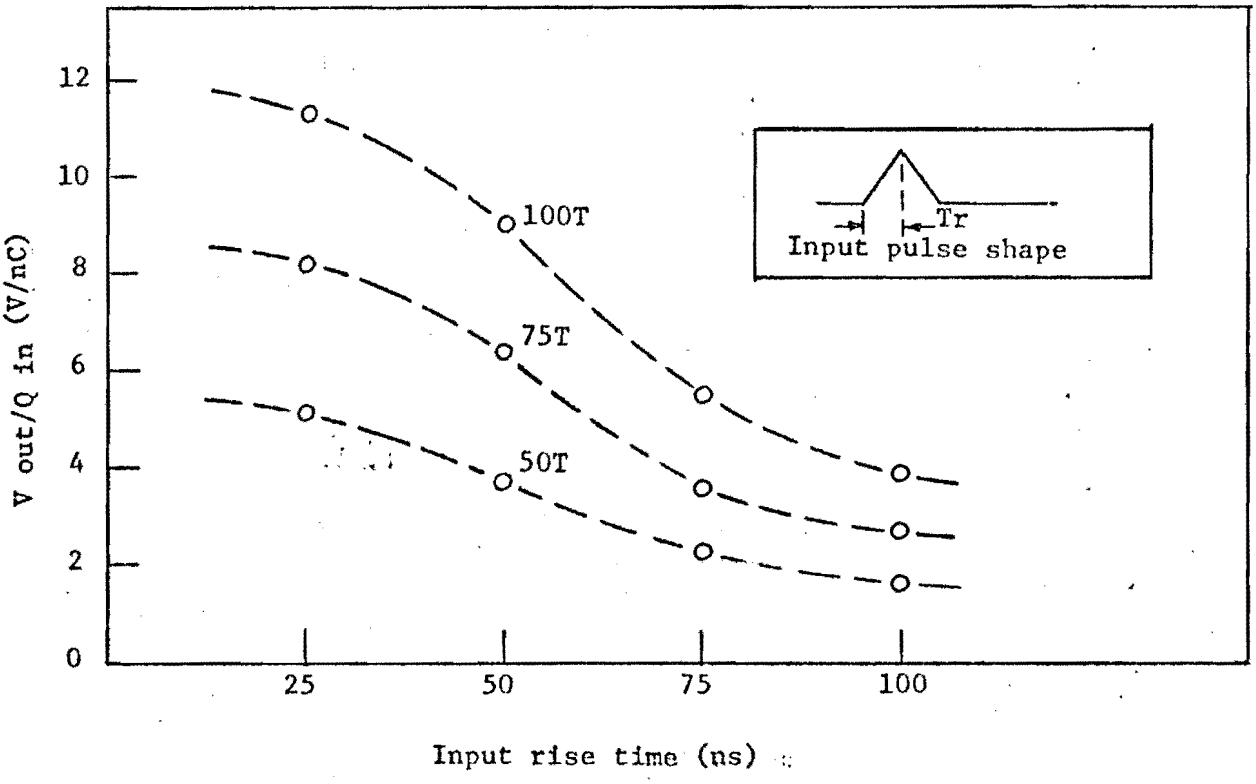
12
10
8
6
4
2
0
V out/Q in (V/nC)
100T
75T
50T
Tr
Input pulse shape
25
50
75
100
Input rise time (ns)

(a)

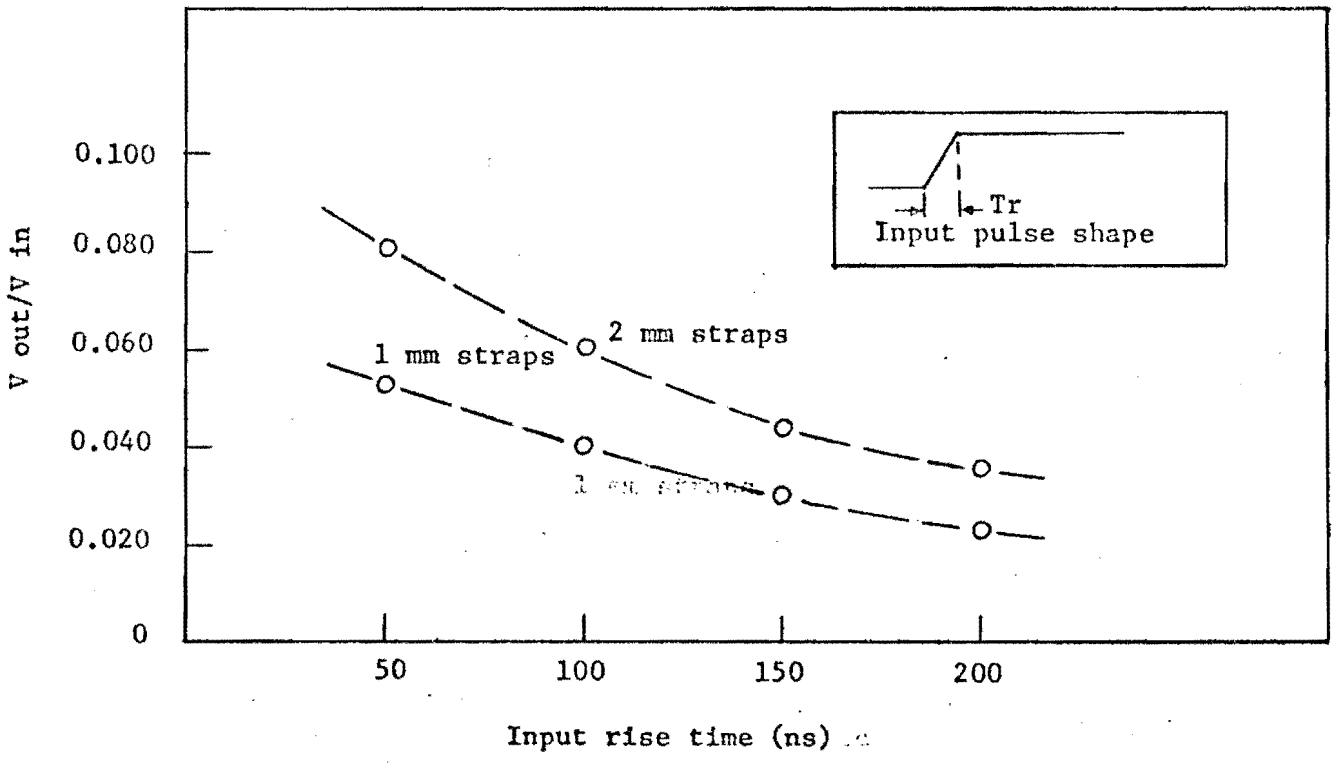
0.100
0.080
0.060
0.040
0.020
0
V out/V in
Tr
Input pulse shape
2 mm straps
1 mm straps
50
100
150
200
Input rise time (ns)

(b)

Fig. 2

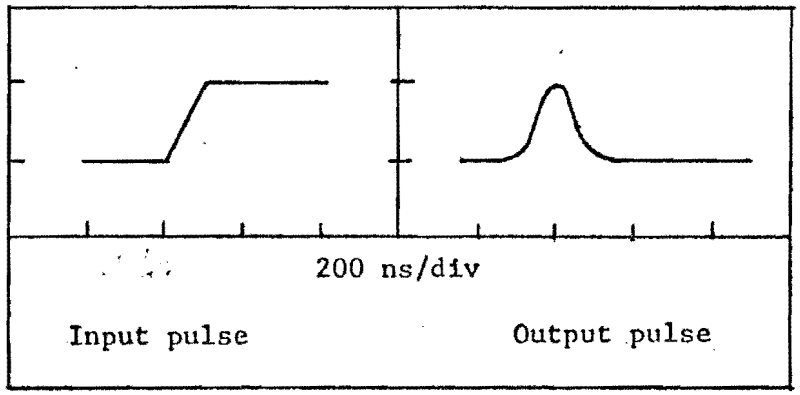
200 ns/div
Input pulse
Output pulse

(a)

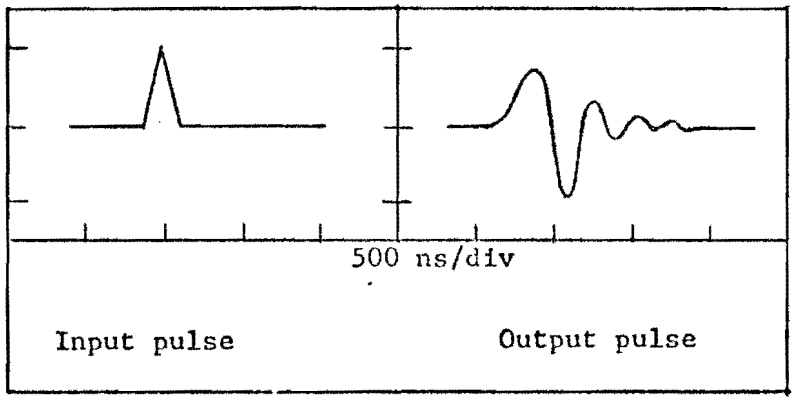
500 ns/div
Input pulse
Output pulse

(b)

Fig. 3

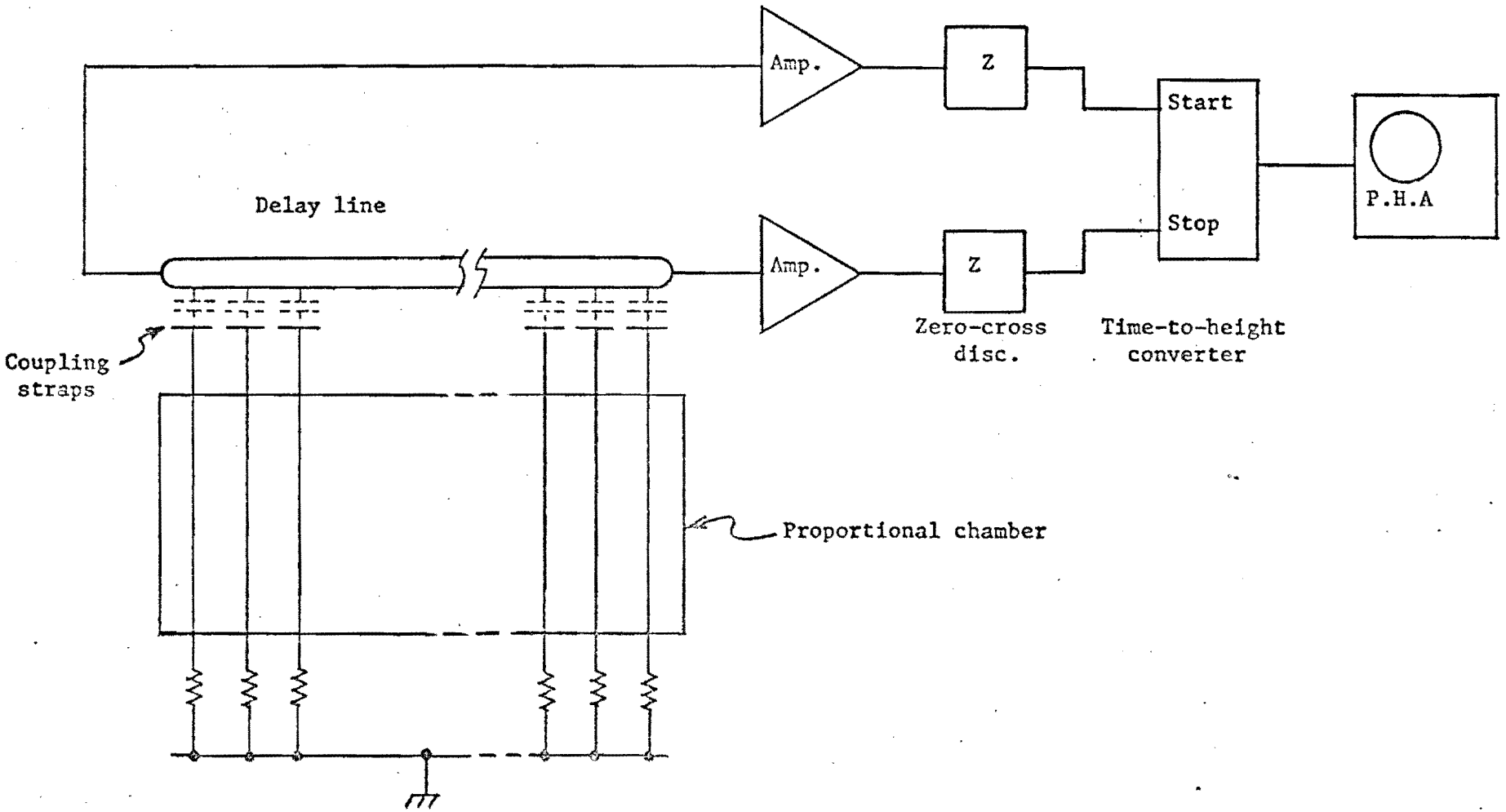
Amp.
Z
Start
Stop
P.H.A
Delay line
Amp.
Z
Zero-cross
disc.
Time-to-height
converter
Coupling
straps
Proportional chamber

Fig. 4

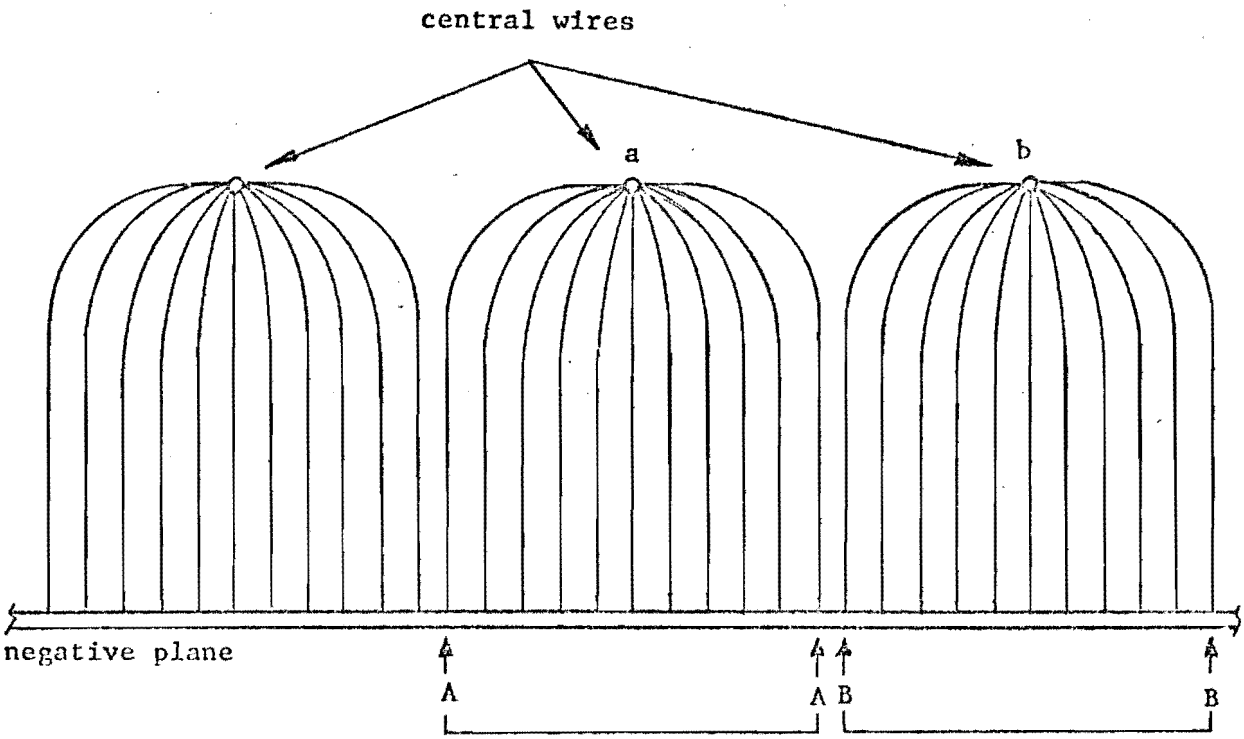
central wires
a
b
negative plane
A
A
B
B

(a)

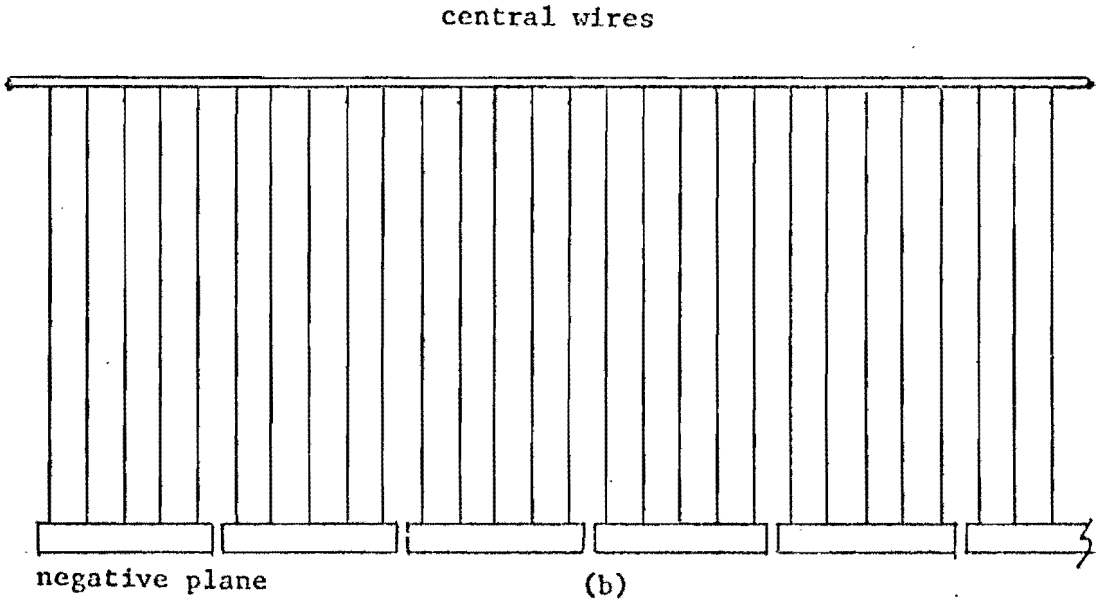
central wires
negative plane

(b)

Fig. 5

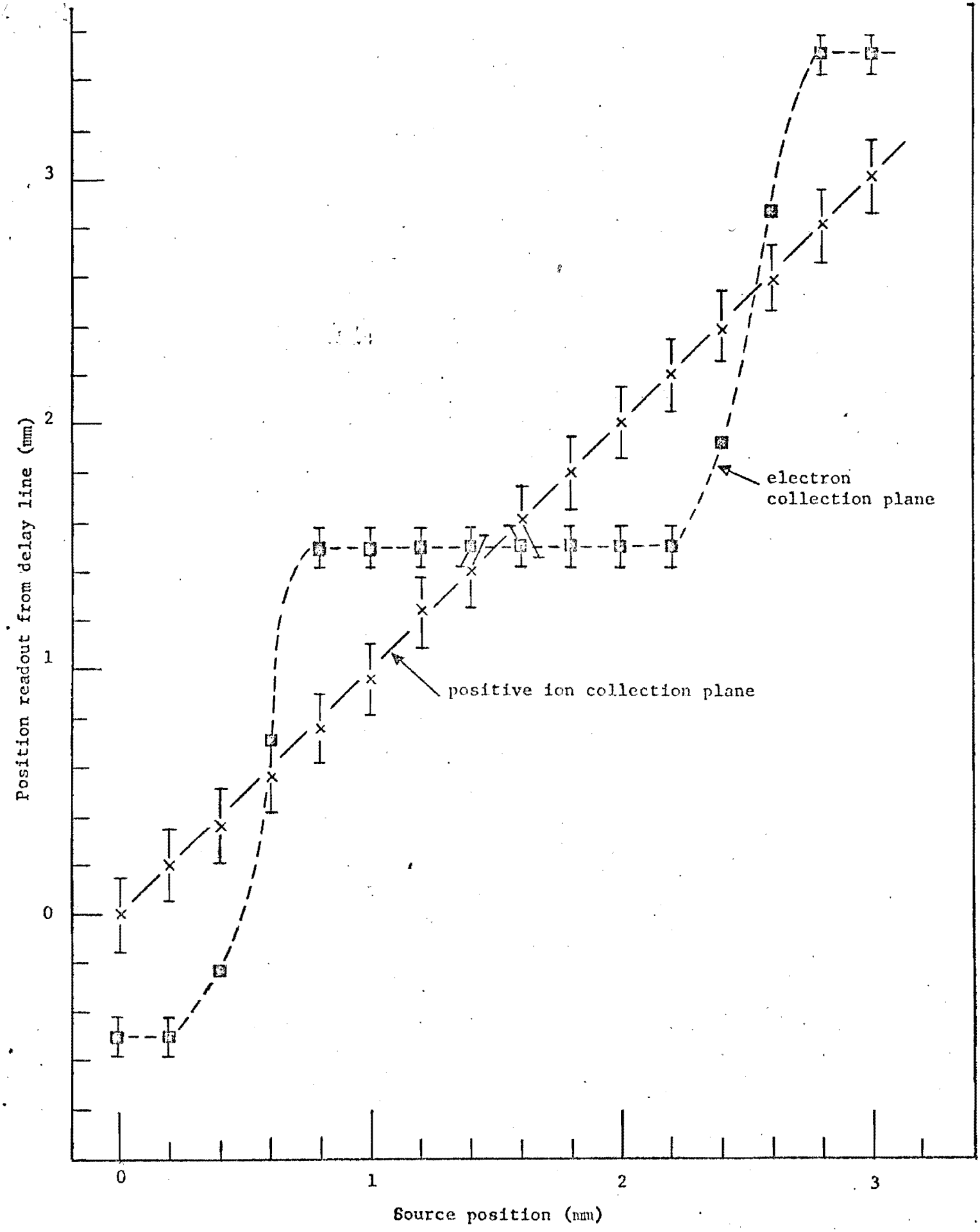
Position readout from delay line (mm)
3
2
1
0
0
1
2
3
Source position (mm)
electron
collection plane
positive ion collection plane

Fig. 6

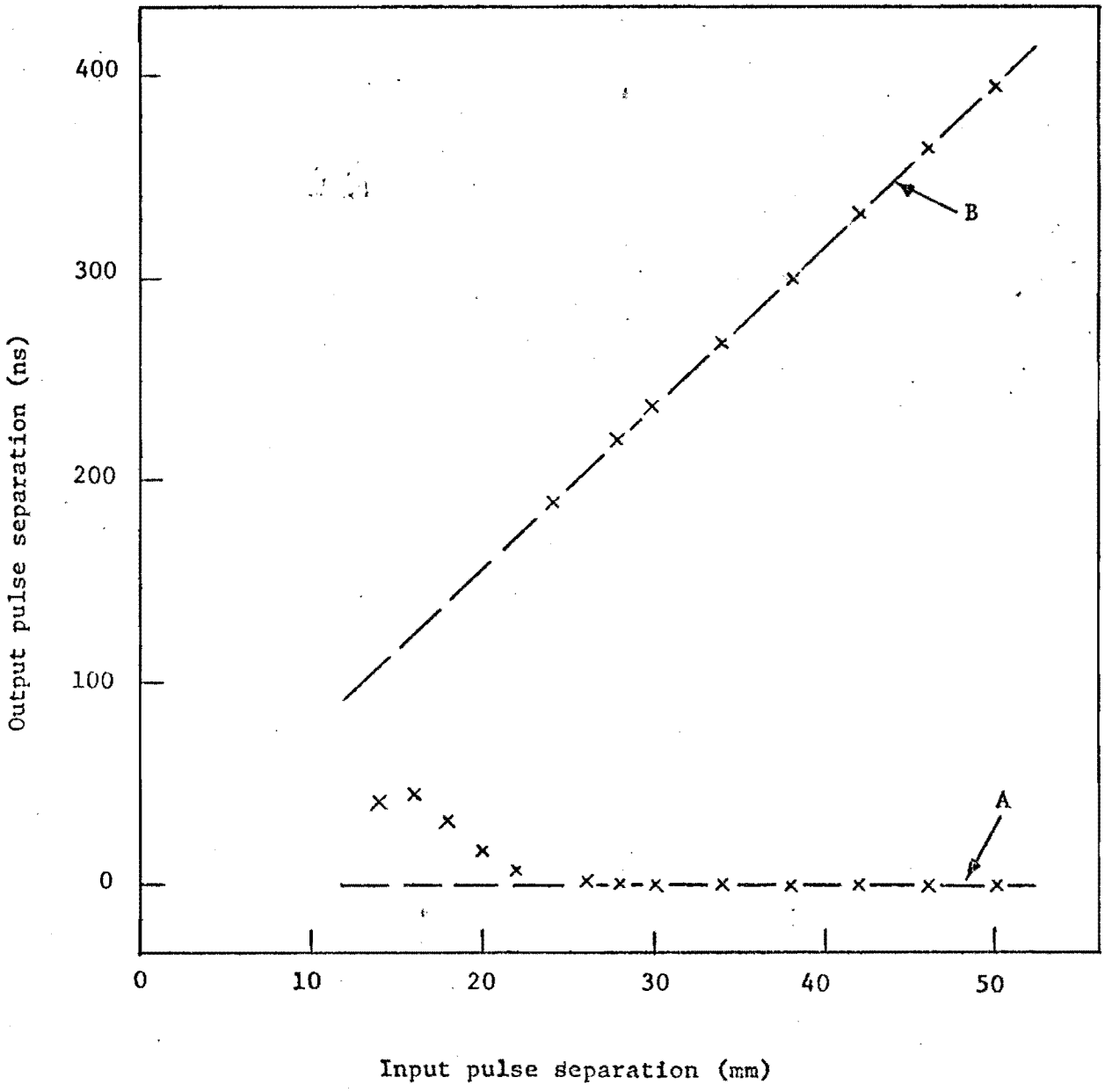
400
300
200
100
0
Output pulse separation (ns)
0
10
20
30
40
50
Input pulse separation (mm)
A
B

Fig. 7

9B

NAL PROPOSAL NO. 9B

Correspondent: M.L. Stevenson

University of California
Lawrence Berkeley Laboratory
Berkeley, California 94720
Telephone: FTS-18-415-843-6301
Commercial: 415-843-2740 Ext. 6301

PROPOSAL TO STUDY NEUTRINO INTERACTIONS IN THE 30 m^3 NAL BUBBLE CHAMBER WITH EXTERNAL MUON IDENTIFIER

R.J. Cence, F.A. Harris, M.W. Peters, V.Z. Peterson
V.J. Stenger, and D.E. Yount
University of Hawaii

M. Alston-Garnjost, S.I. Parker, F.T. Solmitz, and M.L. Stevenson
University of California
Lawrence Berkeley Laboratory

July 9, 1971

9B

PROPOSAL TO STUDY NEUTRINO INTERACTIONS IN THE 30 m^3 NAL BUBBLE CHAMBER WITH EXTERNAL MUON IDENTIFIER

ABSTRACT

We propose: 1) to participate in the development of a muon identifier external to the NAL 30 m^3 bubble chamber, 2) to use the external muon identifier with a narrow band beam and hydrogen filling to investigate, at energies above 20 GeV, neutrino total cross sections, deep-inelastic scattering, and possible W production, and 3) to use the external muon identifier with a broad-band beam and hydrogen filling to investigate individual neutrino reaction channels with good statistics over a broad range of energies. At this time, specifically, we request bubble chamber exposures yielding 5,000 neutrino events and 5,000 anti-neutrino events with the narrow-band beam and 50,000 events with the broad-band neutrino beam. Requests for exposure to deuterium and neon will be deferred until more is known about the bubble chamber operation.

I. INTRODUCTION

Our original proposal to study high energy (15-80 GeV) neutrino interactions in the 30 m^3 NAL bubble chamber (NAL Proposal No. 9) [1] contains two unique features: 1) a proportional quantameter to detect photons from neutral pions produced in neutrino interactions and 2) an external muon identifier (EMI) to detect penetrating muons. The proportional quantameter would be installed immediately downstream of the hydrogen vessel between the vessel and the magnet coils, and a significant modification of the bubble chamber would be required. The EMI would consist of detector planes having spatial resolution, these planes interspersed with absorbing walls external to the bubble chamber. The EMI could be developed essentially independently of the bubble chamber.

Since our original proposal was submitted more than one year ago, two major developments have occurred. First, the quantameter has been deferred. [2] This implies that the fraction of the neutrino energy that goes into neutral pions, and thus into photons, will not be detected with good efficiency. We therefore propose to carry out those measurements requiring a knowledge of incident neutrino energy, such as total cross sections and deep inelastic scattering, using a narrow-band neutrino beam.*

The second major development has been the approval and partial funding by NAL of the external muon identifier. This decision reflects the broad support within the bubble chamber community for a muon identifier and is due also to the considerable progress made during the last year in designing and testing an EMI that promises to be both economical and highly efficient. [3]

The simultaneous use of the EMI and a narrow-band beam will permit a determination of both the incident neutrino energy and the momentum transfer to the final muon, as required in studying deep-inelastic scattering. Neither

---

*We shall attempt to develop techniques using the wide band data to obtain approximations to the neutrino energy.

the momentum transfer squared, Q^2, nor the energy transfer, $\nu = E-E'$, can be determined without muon identification. In fact, it is in the region of Q^2 and ν where one is probing most deeply the structure of the target proton namely, large Q^2 and ν (with resulting large hadron multiplicities) that the identification becomes most difficult without an adequate EMI. The EMI will also be useful with a broad-band neutrino beam, and in this case, we propose to use the much higher broad-band flux to obtain good statistics on individual reaction channels, particularly those channels in which the final nucleon can be identified.

For the narrow-band experiment we request an exposure yielding 5000 events from π^+ neutrinos and 5000 events from π^- anti neutrinos. Pions and Kaons produced by 400-GeV protons will be selected at 100 ± 5 GeV/c to produce pion-neutrino at 43 ± 7 GeV and kaon-neutrinos at 96 ± 10 GeV.* Requests for an exposure to deuterium will be deferred until more is known about the bubble chamber operation. With 3×10^{13} incident protons per pulse on a one mean free path thick target, we estimate that for a neutrino cross section that continues to rise linearly with energy above 10 GeV, a run of 180,000 (260,000) pictures will yield 5,000 neutrino events (anti-neutrino events) in the 43-GeV bin and - 300 events in the 96-GeV bin.

For the broad-band experiment we request an exposure yielding 50,000 events. Of this number, more than 5,000 are expected to be above 30 GeV.[4] For 10^{13} interacting protons per pulse at 400 GeV, approximately 50,000 pictures will be required.

---

* It is probable that we will run part of this exposure at lower energies. The results of the counter neutrino experiments will determine the optimum energies.

II. Physics Justification

The hybrid bubble chamber with its ability to look in detail at the structure of the final hadron state in inelastic neutrino scattering can resolve many of the questions that will be raised by the early neutrino counter experiments.

The conventions and definitions used in inelastic electron scattering and by Bjorken and Paschos[5] are useful here. They are briefly:

Momentum transfer squared, Q^2,

$$Q^2 = 2M\nu + M^2 - W^2 \quad ; \tag{1}$$

where M^2 and W^2 are the invariant mass squared of the initial and final hadron states respectively.

Energy transfer, ν,

$$\nu = E - E' \quad , \tag{2}$$

where, E and E' are the initial and final lepton laboratory energies respectively.

Lepton scattering angle, θ, (laboratory)

$$\sin^2\frac{\theta}{2} = \frac{Q^2}{4EE'} \tag{3}$$

Hadron final state "scattering angle", θ_H (laboratory)

$$\sin^2\theta_H = \left[\frac{E'}{E}\,\frac{\cos^2\theta/2}{1+(\nu/Q^2)}\right]^{1/2} \tag{4}$$

From these expressions the graphical display of Figure 1 can be constructed.

The straight lines radiating from the point $Q^2=0$, ν =20 GeV are loci of equal muon scattering angles for 20 GeV neutrinos. The muon's laboratory energy can be easily found from $E' = 20-\nu$. The solid parallel lines are loci of equal invariant hadron-mass W. The numbers, $\langle n_\pi \rangle$, are crude upper limits to the total pion multiplicity to be expected from hadron states of mass W. The dashed parabolic curves give values of θ_W and can be used to derive crude upper limits to the "hadron jet" opening half-angle,

$\theta' \approx \gamma_W^{-1}$. Fig. 2 summarizes the appearance of typical events at the vertex of the interaction before the bubble chamber magnetic field sweeps them apart. The vector with the arrow is the muon momentum. The cones are for the hadron jets with half angle, γ_W^{-1}. The variables x and y are closely related to Q^2 and ν, respectively, and will be discussed in the following section. The manner in which the magnetic field sweeps these muons from their original direction is shown in Fig. 3. For emphasis we have indicated in each sub-sketch of Fig. 3 a number which is an upper limit of the expected pion multiplicity accompanying each of the muons. More will be said of their average behavior in section IV. The solid line trajectories correspond to muons produced to the left and right in the equatorial plane. The dashed trajectories are those muons produced with maximum dip angle.

A. Differential and total cross section.

The differential cross section for the interaction of neutrinos on hadrons can be written in terms of the quantities just defined as

$$\frac{d^2\sigma}{dQ^2 d\nu} = \frac{G^2}{2\pi}\frac{E'}{E}\beta\left\{1 - \frac{Q^2}{4EE'} + \frac{\nu^2+Q^2}{2EE'}\left[(R)+(L)\right] + \frac{E+E'}{2EE'}\sqrt{\nu^2+Q^2}\left[(L)-(R)\right]\right\} \quad (6)$$

where,

$$\beta = W_2 = \frac{1}{2\pi}\frac{Q^2}{\nu}\frac{1}{\left[1+(Q^2/\nu^2)\right]}\left(1 - \frac{Q^2}{2M\nu}\right)\left(2\sigma_S + \sigma_R + \sigma_L\right) , \quad (7)$$

$$(R) \equiv \frac{\sigma_R}{2\sigma_S + \sigma_R + \sigma_L} , \quad (L) \equiv \frac{\sigma_L}{2\sigma_S + \sigma_R + \sigma_L} , \quad (8)$$

where σ_R, σ_L and σ_S are cross sections for the appropriate helicity states. For $Q^2 \ll \nu^2$ Eq.(6) becomes

$$\frac{d^2\sigma}{dQ^2 d\nu} = \frac{G^2}{2\pi}\frac{E'}{E}\beta\left[1 + \frac{\nu}{E'}(L) - \frac{\nu}{E}(R)\right] \quad (9)$$

or

$$\frac{d^2\sigma}{dx\,dy} = \frac{G^2 M E}{\pi}\,\nu\beta\left[(1-y) + \frac{y^2}{2}\left[(R)+(L)\right] + y\left(1-\frac{y}{2}\right)\left[(L)-(R)\right]\right] \tag{10}$$

where

$$\nu\beta = \frac{Q^2}{2\pi}(1-x)(2\sigma_S + \sigma_R + \sigma_L) \tag{11}$$

and

$$x = Q^2/2M\nu \quad , \quad y = \nu/E$$

$$0 \leq x \leq 1 \qquad\qquad 0 \leq y \leq 1 \tag{12}$$

Some motivation for the use of the variable x can be seen if one supposes that the neutrino might scatter off only a fraction, x , of the nucleon. The kinematics of quasi-elastic scattering is obtained by replacing M by xM. It would be represented in Fig. 1 by a radial line from the origin with a slope x times that of the one for $Q^2 = 2M\nu$. Bjorken has shown that at high incident energies if the parts are point-like $Q^2\cdot(\sigma_R, \sigma_L,$ and $\sigma_S)$ are functions of x only (scale invariance). When one integrates equation (10) over x and y one obtains σ = (constant)·E, a relation that we can test experimentally provided we detect all final states. Multiplicities and the dependence on x and y will be measured and compared with the predictions of various models.

1. "Spin-1/2-Parton" Model

To obtain a feeling for where events would lie in the Q^2 - vs - ν plane for the "spin-1/2-parton" model, we have set $\nu\beta$ = (constant)·(1-x) and $\sigma_R = \sigma_S = 0$. Fig. 4 shows how 1000 50-GeV neutrino interactions would be distributed under these assumptions. The important point is that all sectors contain statistically significant populations.

2. Pomeranchukon-Exchange Model

Predictions for the Pomeranchukon-exchange model can be obtained by setting $\nu\beta$ = (constant) $(1-x)$ and $\sigma_L = \sigma_R$, $\sigma_S = 0$. The distribution of 1000 events at 50 GeV for these assumptions are shown in Fig. 5.

We propose to make our detection efficiency high in all sectors of the Q^2 - vs - ν plot and consequently, to be able to measure the total cross section. Bjorken and Paschos[9] point out that the difference $\sigma_\nu - \sigma_{\bar{\nu}}$ is very model dependent. We wish to expose the chamber to both ν and $\bar{\nu}$.

3. Possible effects of an Intermediate Vector Boson (IVB) on Scaling.

The effects of an (IVB) would be to modify the differential distribution $d^2\sigma/dxdy$ of eq. 9 by the (IVB) propagator factor $[M_W^2/(Q^2 + M_W^2)]^2$. This would produce breakdown in "scaling". Such a factor is most easily detected experimentally for large energy transfers. Fig. 6 illustrates its detectability at y=0.9 for 20 and 50 GeV neutrinos by showing how the function $\nu\beta = K(1-x)$ would be modified by an (IVB) of mass 8 GeV. It is imperative that we be able to identify the muons of low momentum that correspond to large y values. Fig. 3 shows us that we must place EMI detectors near 90 degrees in order to detect them. Very low momentum muons will be trapped in the chamber by the magnetic field.

B. Intermediate-Vector-Boson Decay Modes

Although the bubble chamber is best suited to studying the hadronic decay modes of the (IVB), it is also capable of identifying the leptonic decay modes. Calculations[8] indicate that the μ^- associated with W^+ production has a reasonable chance of having a momentum less than 1 GeV/c. It then can be trapped in a circular orbit within the chamber and will identify itself by not interacting. The μ^+ from the $W^+ \rightarrow \mu^+ \nu$ decay will be emitted at much higher energy into the forward direction and will be detected with high efficiency in the EMI. In fact, scanning for these events (produced either

in a full chamber of Ne, H, or D) is particularly simple. The signature is a trapped μ^-. If the (IVB) Mass is 5 GeV we expect 3500 (300) of them in the wide band (narrow band) exposure; and 350 if the (IVB) Mass is 8 GeV.

C. Heavy Lepton Search

The identification of a muon in the EMI allows one to form the invariant mass of this muon with other detected particles such as photons and mesons. The existence of a heavy lepton that decays into these combinations would produce a peak in the invariant mass combination.

D. Lepton Locality

It has been shown[13] that if the distribution in ϕ, the angle between the normals to the hadron plane and lepton plane, in reactions of the type

$$\nu p \rightarrow \mu^- p y^+$$

where y^+ is any meson system, is <u>not</u> given by

$$\frac{d\sigma}{d\phi} = a + b\sin\phi + c\cos\phi + d\sin 2\phi + e\cos 2\phi$$

then lepton locality is violated. Other things, (see Pais ref. 5) such as s-channel-helicity conservation, pomeron exchange, and V-A interference, can be tested with this distribution, which we propose to measure.

E. Exclusive Reactions

We will be able to study in detail several exclusive reactions. For example, consider

$$\nu p \rightarrow \mu^- (\Delta^{++} \rightarrow \pi^+ p)$$

with which the Adler condition relating the cross section at small θ_μ to that for $\pi^+ p \rightarrow \Delta^{++}$ can be tested. Other resonance production reactions can be more easily studied if one has muon identification. The invariant-mass plots will not have muons masquerading as hadrons.

F. Unusual Events

One should also be prepared for unusual and unexpected processes to occur. Hydrogen and, to a lesser degree, deuterium are the best target materials for uncovering such rare processes. Muon identification will help in bringing unusual events to our attention.

III. Yields

A. Narrow Band Beam

Nezrick[6] has described a way of producing a narrow band beam (NB) of neutrinos with a magnetic horn. It essentially focusses 70 ± 4 GeV mesons emitted with angles between 3 and 12 milliradians to produce 27 ± 3 GeV neutrinos from pion decay, and 67 ± 4.5 GeV neutrinos from kaon decay. Other versions[7] of NB beams use quadrupole magnets as focusing elements. It is not clear at this time which form will be most suitable for our purposes or which form NAL is going to develop. We shall use whatever is available.

Table I summarizes the meson yields and the number of neutrino interactions per 10^{19} interacting protons for two types of NB focusing devices, the first a Nezrick type Monohorn that accepts 100 ± 5 GeV mesons emitted between 2 and 8 milliradians, and the second a Quadrupole system that accepts 100 ± 5 GeV mesons between 0 and 4 milliradians. The latter is compared with the NAL-Cal Tech (Expt 21) system that has the same $\Delta p/p=0.1$ and has an aperature of 0 to 2 milliradians. Two meson production models are used, CKP,[9] and a new multiperipheral model of Clifford Risk[10] that fits all $\pi^{\pm}$, and K^{+} production data within 30% including the recent Argonne-Bologna-Michigan ISR results[16] at equivalent energies of 500 and 1100 GeV. Details of these calculations will be presented in a separate document.[11] Figure 7 shows the probability per meson of emitting a neutrino from the $\mu+\nu$ decay mode into the 30 m^3 NAL bubble chamber within one meter of the beam axis. The calculations are made for a drift length of 400 meters and a shield length of 1000 meters. Also shown is how the fractional full width of the neutrino energy spectrum increases as the meson momentum is increased. It shows that the energy resolution of the pion neutrino beam deteriorates rapidly for meson momenta above 100 GeV. Figure 8 is used

TABLE I

Narrow Band Event Rates

Device Type	Angular Acceptance (mrad)	Production Model		Eo	$\Delta p/p = \pm 0.1$ Meson Energy	Mesons per 10^3 Int. prots	Neutrino Energy ±HW@Base	Thousands of Neutrino Interactions per 10^{19} Interacting Protons	Thousands of Neutrino interactions per 10^{19} incident Protons on a one mean free path target.†	Thousands of pictures required to produce 5000 pion neutrino events. For 3×10^{13} incident protons per pulse.
Quad	0<θ<4	CKP	π^+	400	100	9.6	43 ± 7	9.4	4.5	370
	"	Risk				17.5		17.1	8.1	205
	* 0<θ<2	"				6.65		6.5	3.1	540
Horn	2<θ<8	CKP				11.5		11.2	5.3	310
	"	Risk				20.2		19.7	9.4	180
Quad	0<θ<4	CKP	π^-			4.8		4.7	2.2	750
	"	Risk				10.0		9.8	4.7	360
	0<θ<2	"				3.61		3.5	1.7	100
Horn	2<θ<8	CKP				5.73		5.6	2.7	630
	"	Risk				14.1		13.7	6.5	260
Quad	0<θ<4	CKP	K^+			1.92	96 ± 10	1.64	.78	
		Risk				0.90		0.77	.37	
	0<θ<2	"				0.30		0.26	.12	
Horn	2<θ<8	CKP				2.29		1.96	.93	
	"	Risk				1.43		1.22	.58	

* The CKP yield for 0 to 2 mrad is 0.423 that for 0 to 4 mrad.

† Account has been taken of the effects of meson absorption and nucleon cascading in thick target according to the prescription of reference (12). To convert from "interacting" to "incident" we multiply the "interacting" column by $\left(\frac{dn}{dq}\Big/\left(\frac{dn}{dq}\right)_{\text{Thin target}} = 0.475\right)$

to illustrate how the neutrino interaction rate varies with meson momentum. The CKP production model is used together with a Quadrupole system that has a meson angular acceptance of 0 to 4 milliradians. The neutrino cross section was assumed to be $\sigma = 0.8\ E\ (GeV) \times 10^{-38}\ cm^2$. The K^+ flux was assumed to be 0.2 that of the μ^+ at each momentum. The dashed curves are a modified version of CKP to give an approximate upper limit to the K^+ yield. The Risk model serves to give a lower limit to the K^+ yield (the model is valid for $p/p(max) \leq 1/2$, and underestimates the cross section for lower values of this ratio). The neutrino event rates per interacting proton of table 1 have not accounted for meson absorption in the target. This has been studied in detail[12], and shows that a target thickness of one mean free path is optimum for energetic mesons. Fig. 9 shows how the thin target meson momentum spectrum is distorted by nucleon cascading and meson absorption in thick targets. Here, $q = (p=100\ GeV)/[T_o=0.305(400\ GeV)^{3/4}] = 3.65$, where, T_o is one of the parameters of the CKP formula. Consequently, the yields should be diminished by the factor 0.475.

B. Wide Band Beam

Kang, Walker, et al[14] have estimated that there will be about one event per picture when the 15-foot bubble chamber filled with hydrogen is exposed to the wide band neutrino beam produced by 400 GeV protons. This assumes a fiducial volume of 20 m^3, 3×10^{13} interacting protons per pulse, ideal focussing (100%) and a linearly rising neutrino total cross section. The calculation is based on the Hagedorn-Ranft model extrapolated to 400 GeV.

For 50,000 events we need about 50,000 pictures. The expected energy distribution of these 50,000 events is given in Table II. We see that while the bulk of events will be below 60 GeV a significant number of events at higher energies will be obtained.

An attempt has been made to estimate the (ν_e) production yield expected with

the broad band beam using the cross sections per nucleon computed by Wu and Yang[15] for a aluminum target and assuming they apply to hydrogen. This is given in Table III

TABLE II

Distribution of all events from 50,000 event exposure with 400 GeV broad-band beam, assuming

E (GeV)	Events
0-10	1,300
10-20	9,200
20-30	12,800
30-40	9,400
40-50	4,900
50-60	3,000
60-70	1,800
70-80	1,200
80-90	900
90-100	700
100-150	2,500
150-200	1,600
200-250	500

TABLE III

Expected production in broad band exposure with 50,000 total events using estimates of Wu and Yang[15].

Mass of IVB (GeV)	Events
3	28,000
5	3,500
8	350
10	100
15	5

IV. Analysis

A. Narrow Band Beam Events

With the EMI and a somewhat ambiguous knowledge* of the neutrino energy it will be possible to determine the momentum transfer squared Q^2, and the energy transfer, ν. With a large bubble chamber some of the final state hadrons will identify themselves by subsequent interaction in the hydrogen. In particular, we will do all we can in this regard to detect and identify the final nucleon. The EMI will be useful in identifying neutron stars by their lack of an outgoing muon.

B. Wide Band Beam Events

For high energy neutrino interactions we are beset with the problem of not being able to determine the neutrino energy. We shall adopt the following analysis procedure in order to obtain an approximation to the neutrino energy.

1) Measure the momenta of all charged tracks.
2) Identify the muon.
3) Identify as many other particles as possible.
4) Determine the transverse momentum of the missing neutral system.**
5) Set the energy of the neutral meson system equal to one half of the sum of the magnitude of the momenta of the charged mesons (but never less than the missing transverse momentum)
6) The approximate neutrino energy is the sum of the energies of all outgoing charged particles plus this assigned energy of the neutral system minus the proton rest mass.
7) Pray† and do some statistical type consistency tests.

---

* There are kaon and pion neutrinos in the beam.

** Those events that have no missing transverse momentum are candidates for "3c fit" class. For them E can be measured

† Replace 7) with a Phase I Quantameter as soon as possible (Proposal 9D to be submitted).

Actually, this procedure might work reasonably well for the average event. For example, suppose the muon receives 2/3 of the initial neutrino energy. Of the remaining 1/3 only 1/3 will be energy of neutral particles. Therefore, 1/9 of the energy would be missing. Results from the narrow band exposure will also help.

V. Experimental Equipment

The equipment required by this experiment may be summarized as follows:

1. external proton beam having an energy of around 400 GeV and an intensity of 2 or 3 x 10^{13} interacting protons per pulse,

2. neutrino beam facility consisting of a low Z target (1 mean free path thick), narrow-band and broad-band focusing systems, meson drift space, and muon shield,

3. neutrino beam monitors to determine the shape of the neutrino energy spectrum and to measure the neutrino flux during a given bubble chamber run,

4. NAL 30 m^3 bubble chamber with liquid hydrogen filling,*

5. EMI to distinguish muons from hadrons produced when neutrinos interact in the bubble chamber.

Each of the items listed represents a major developmental effort with the total far exceeding the capabilities of any one group. It is important to us, nevertheless, to have a working knowledge of each of these facilities, and for this reason members of our collaboration have participated and will continue to participate in each phase of the NAL 30 m^3 bubble chamber program.

Our main effort will, of course, be invested in the area of muon identification. The remainder of this section contains a brief description of the EMI and indicates how it will be used to improve our understanding of the physics of neutrino interactions. A more detailed description is given in NAL Proposal 9C.

A preliminary sketch of the complete EMI geometry is shown in Figure 10a and 10b. The complete EMI consists of: 1) a passive internal absorber filling the space between the magnet coils and matching the coil thickness in collision lengths (3.2 collision lengths stainless steel subtending approximately 180° horizontally and weighing 20 tons); 2) an active detector-absorber-detector

---

* Requests for deuterium and neon filling will be deferred until more is known about the bubble chamber operation.

sandwich (3 collision lengths stainless steel subtending 60° vertically and nearly 180° horizontally and weighing 111 tons. The "Phase I EMI"[3] will consist of the passive internal absorber and a single detector plane. The detector planes will be multi-wire proportional chambers with x, y, and diagonal position information in each plane.

The vertical distribution of muons at a radius of R = 3.2 meters measured from the center of the bubble chamber is shown in Fig. 11 for 10-GeV neutrinos incident. This distribution was obtained from Monte Carlo calculations and is similar for both the Parton and Pomeronchuk-Exchange models. Less than 10% of the muons are outside ± 2 meters. The EMI shown in Fig. 10 is centered at a radius of 3.5 meters and has a total height of 5 meters, assuring 90% efficiency at 10 GeV.

The horizontal distribution at R = 3.2 meters is strongly influenced by the magnetic field. This is apparent in Fig. 12 where the spread in horizontal coordinates is given for various incident neutrino energies. An acceptance of ± 90° will work well at 10 GeV and will be of some use down to 2 GeV. The geometric efficiency versus energy is plotted in Fig. 13 for an EMI with horizontal acceptance of ± 90° and a verticle acceptance of ± 30°, essentially the geometry shown in Fig. 10a, b. Fig. 3 has already shown in detail (i.e. in terms of x and y) how the muons from 20 GeV neutrinos are swept out by the bubble chamber magnetic field.

The geometric efficiency provides an indication primarily of what fraction of the muons are subject to particle identification. By extrapolating the individual tracks observed in the bubble chamber, it will be possible to determine which tracks may be identified.

Mesons and hadrons are distinguished in the EMI by requiring that all hadrons interact. No attempt is made to stop hadrons or to absorb the total hadron energy with good efficiency. Incident hadrons thus manifest themselves through track displacements indicating a large-angle scattering, through

hadronic cascades of multiplicity greater than unity, and through total absorption.

Experimental tests have been carried out at the Lawrence Berkeley Laboratory to determine the efficiency for rejecting pions in a muon identifier consisting of proportional chambers interspersed with iron absorber.[3] Some preliminary results from these tests are plotted in Fig. 14, which gives the fraction of the pions surviving (i.e., not yet distinguished from muons) versus the thickness of iron absorber.

A surviving pion is defined in these tests as an incident beam particle that passes through the absorber and produces a single track within the multiple-scattering envelope containing a given fraction of the incident muons. In the actual bubble-chamber experiment, particle trajectories will be determined by measuring individual tracks observed in the bubble chamber and by extrapolating these tracks out to the external detectors. The radius of the multiple-scattering envelope containing 96% of the muons is approximately 3 cm for 4 GeV particles at the first EMI detector plane, thus the accuracy required in the extrapolation is modest.

Fig. 14 implies that the Phase I EMI, consisting of internal passive absorber plus hydrogen plus vacuum walls (3.9 collision lengths = 30 cm iron equivalent), will reject (94 $\pm$ 1)% of the pions while accepting 96% of all muons. A more complete EMI, with an additional 3 collision lengths of stainless steel (6.9 collision lengths = 89 cm iron equivalent) will reject (98.5 $\pm$ 1)% of the pions while accepting 96% of all muons. For the complete EMI with two MWPC planes the pion rejection is estimated to be 99.5%.* As indicated previously, the Phase I EMI, with 94% pion rejection, is adequate for this proposal.

---

* Tests are continuing to verify this estimate.

For this present proposal, we plan tentatively to use the Phase I EMI. Clearly, if a more complete version of the EMI is available before the bubble chamber is operational, we would use this version. The EMI tests suggest that a single detector plane may be adequate for the complete EMI, in which case it may be relatively simple to go from a Phase I EMI to the complete model.

VI. Schedule and Participation

The time schedule for this experiment is related primarily to the date of successful operation of (a) the 15-foot bubble chamber filled with hydrogen and (b) the Phase I EMI. We assume target dates of January 1973 for both devices to be ready for experiments.

Prior to January 1973, the members of the UH-LBL collaboration will be heavily committed to the development and construction of the Phase I EMI (see Proposal 9C). This device will become an NAL facility for use with the bubble-chamber. At least one member of our collaboration is expected to be resident full-time during 1972 and until the EMI is fully working. Field tests of the prototype-EMI (by itself) and the Phase I-EMI (with the 15-foot bubble chamber) are essential to this program and will be conducted by this team at NAL. Thus, members of this collaboration should be quite familiar with the neutrino beam and bubble-chamber operation by January 1973.

Certain members of the UH-LBL collaboration are prepared to assist NAL, as needed, in the development of bubble-chamber track reconstruction computer programs. We are especially interested in the extrapolation of bubble-chamber tracks outward to the EMI detector-planes, since muon identification depends in part on the accuracy of the prediction of where the muon would hit the EMI.

Although others may be primarily responsible for development of a suitable narrow-band neutrino beam for bubble-chamber use (e.g., a narrow-band "horn", or a DC focusing device, e.g. quadrupoles), we wish to make use of such a facility and would be willing to assist in its development. We are particularly interested in focusing pions (and kaons) below 100 GeV, since the pion neutrino spectrum becomes too broad at higher energies. The narrow band pulsed horn, with predicted properties as described by Nezrick[6], appears to us to be promising for our application, although pulsed Quadrupoles of large aperature

($\theta < 4$ mr) are also a possibility.

In anticipation of doing experiments with the NAL 15-foot chamber, both the LBL and Hawaii groups have been preparing bubble-chamber track measuring devices suitable for low contrast (i.e., Scotchlite illuminated) film. In particular, the Hawaii group is acquiring a "SWEEPNIK" laser-beam measuring machine which successfully measures events from similar film.

The coordinated analysis of neutrino events occurring in the hydrogen bubble-chamber with muons detected externally in the EMI will be developed by our group (see Proposal 9C). Many EMI events per pulse are expected, so that matching to the bubble-chamber event is required. A computer program which inputs bubble-chamber data and matches to the EMI stored-data is needed.

These various projects are all related to this basic physics proposal for studying neutrino interactions in hydrogen. The authors of this proposal anticipate spending most of their available research time on EMI development and related projects up to the operation of the NAL 15-foot chamber and EMI in early 1973. We believe that the EMI (muon identification of most neutrino events) will greatly enhance the physics value of the bubble-chamber for neutrino physics. We are committed to establish the EMI as a working facility and test it with the bubble chamber by a short exposure aimed at instrumentation (Proposal 9C). This proposal (9B) is a "physics" proposal using the EMI.

We propose the following experimental runs:

50,000 wide band neutrino events (50,000 pictures)

5,000 narrow band neutrino events from a 100 ± 5 GeV meson beam (180,000 pictures)*

5,000 narrow band anti-neutrino events from a 100 ± 5 GeV meson beam (260,000 pictures)

---

*Calculated assuming 3×10^{13} 400 GeV protons incident on a one-mean-free path target followed by a Nezrick type Monohorn ($2 < \theta < 8$ mr), using the Risk Multiperipheral production model (See the boxed items of Table I)

It is probable that in order to test the mechanism that is causing breakdown in scaling we will run part of the NB exposure at different energies. The results of the counter neutrino experiments will determine the optimum energies. The order in which the narrow band or wide band exposures take place and the number of pictures required depend on factors that are unpredictable at the moment. We expect that our "instrumentation" analysis of the 10^4 events of proposal 9C will be well enough along by September 1973 that we would be ready at that time to begin the "Physics" exposures of the present proposal. Requests for exposure to deuterium and Neon will be deferred until more is known about the bubble chamber operation.

REFERENCES

1. University of Hawaii, Northwestern University, and University of California, Lawrence Radiation Laboratory, "Proposal for a High Energy Neutrino Experiment in the NAL 30 m^3 H_2, D_2 Bubble Chamber," NAL Proposal #9 (June 1970). (See also M.L. Stevenson "Neutrino Physics with Large H_2 Chambers", Proceedings of International Conference on Bubble Chamber Technology, pp. 56-122 (1970).)

2. A prototype quantameter has been successfully tested during the last year. Results of these tests will be published and are described in part in the following documents: "Delta Rays and the Proportional Quantometer," D. Yount, HEPG Report No. UH-511-92-71, February 8, 1971; "Multiwire Proportional Chambers with uniform Gain," S. Parker et al., submitted to Nucl.Instr. & Methods June 10, 1971.

3. The EMI and related tests are described in detail in NAL Proposal No. 9C "Proposal to Develop a Phase I External Muon Identifier (EMI) for use with the 30 m^3 Bubble Chamber," University of Hawaii and University of California Lawrence Radiation Laboratory (July 1971), and supporting documents.

4. The percentage of high energy neutrinos has been enhanced in the latest beam design due to the long meson drift space (400 m) and muon shield (1000 m). It is in the high energy region that the EMI is expected to be of greatest usefullness.

5. J.D. Bjorken and E.A. Paschos, SLAC-PUB 678 December 1969 (Lectures by Bjorken at 1969 Summer Study). See also the excellent reviews of A. Pais "Weak Interactions at High Energies" Conference of "Expectations for Particle Reactions at the New Accelerators," University of Wisconsin (1970) and C.H. Llewelyn Smith. "Neutrino Reactions at Accelerator Energies" SLAC.

6. Frank A. Nezrick, "A Monoenergetic Neutrino Beam Using Current-Sheet Focusing Elements" 1971 National Particle Accelerator Conference, Chicago 1-3 March 1971, IEEE Transactions on Nuclear Science.

7. D. Keefe, UCRL 16830 p. 311, 1966.
V.Z. Peterson UCRL 16830 p. 324, 1966.
F. Sciulli, B. Barish, W. Ford, T. Oddone, C. Peck, A Maschke, NAL Proposal No. 21, 1970.

8. R.W. Brown, R.H. Hobbs, and J. Smith (to be published). See also D. Cline, A.K. Mann, and C. Rubbia, Phys, Rev. Letters 25, 1309 (1971) and M.L. Stevenson, "High Energy Neutrino Physics (E>20 GeV) and the Constraints Placed on the Detectors," 1969 NAL Summer Study, Vol. 2, 121 (1969).

9. G. Cocconi, L.J. Koester, D.H. Perkins UCRL 10022 (1961) p. 167 (1961 High Energy Physics Study, Summer 1961).

10. Clifford Risk (private communication) and C. Risk and J.H. Friedman UCRL 20199 "Comparison of an inclusive Multipheral Model to Secondary Spectra in p-p Collisions."

11. Clifford Risk and M. Lynn Stevenson, Predicted Neutrino Fluxes for Ideal Narrow Band Systems. TM 318

12. M.L. Stevenson, "Targets for the Neutrino Beam: Concepts" Nal report TM-218.

13. A. Pais, Phys. Rev. Letters 9, 117 (1962); T.D. Lee, C.N. Yang, Phys. Rev. 126, 2239 (1962).

14. Y.W. Kang, J.K. Walker et al, NAL Report EM-265 (1970).

15. A.C.T. Wu, Yang, private communication.

16. L.G. Ratner, R.J. Ellis, G. Vannini, B.A. Babcock, A.D. Krisch, and J.B. Roberts, Phys. Rev. Letters 27, 68 (1971)

FIGURE CAPTIONS

1. Summary of the Kinematics of $\nu + N \rightarrow$ lepton + hadrons. Lepton Momentum Transfer Squared vs lepton Energy transfer. The parallel solid lines are loci of equal invariant hadron mass. On each line is given an estimate of the maximum pion multiplicity expected for such a mass. The dashed parabolic curves are loci of equal Lorentz contraction factors, γ_W, of the hadron system. The radial straight lines emerging from the point ($Q^2=0$, ν =20 GeV) are loci of equal lepton laboratory angle for an incident neutrino of 20 GeV.

2. Summary of 20 GeV neutrino event configuration for various values of $x(\equiv Q^2/2M\nu)$ and $y(\equiv E-E'/E)$. The arrow gives the muon momentum and the cones illustrate where the hadrons might go.

3. Summary of how the muons from 20 GeV neutrino interactions are bent by the bubble chamber magnetic field.

4. Distribution of 1000 events predicted by a "spin-1/2-parton" model where $\nu\beta$ is chosen to be a constant times $(1-x)$. $\sigma_R = \sigma_S = 0$.

5. Distribution of 1000 events predicted by the Pomeranchukon-exchange model where $\nu\beta$ is chosen to be a constant times $(1-x)$. $\sigma_L = \sigma_R$ and $\sigma_S = 0$.

6. Examples of how "scaling" might be broken by an intermediate vector boson of MASS 8 GeV for 20 and 50 GeV neutrinos

7. Summary of the probability of decay neutrinos from monoenergetic pions and kaons passing through the central 1 meter radius of the bubble chamber. The meson drift length is 400 meters. The muon shield is 1000 meters. Also shown is the fraction full width (at the base) of the neutrino energy spectrum.

figure captions 2

8. The number of narrow-band neutrino interactions within one meter of the beam axis per 10^{19} interacting protons as a function of the momentum of the meson beam ($\Delta p/p = 0.1$). The upper horizontal scales summarize the corresponding neutrino energies for pions and kaons.

9. These curves summarize how nucleon cascading and meson absorption in targets of various thicknesses distort the "primary" or "thin target" meson production spectrum. For a target of one-mean-free path thickness the yield of 100 GeV mesons produced by 400 GeV protons will be diminished by the factor 0.475.

10. The full external muon identifier (EMI). The Phase I EMI will consist of only one plane of multi-wire proportion chambers.

11. Vertical distribution of 10 GeV muons at the first detector plane.

12. Horizontal distribution of muons at the first detector plane.

13. Geometrical efficiency of the EMI as a function of neutrino energy.

14. Fraction of pions that survive as a function of absorber thickness.

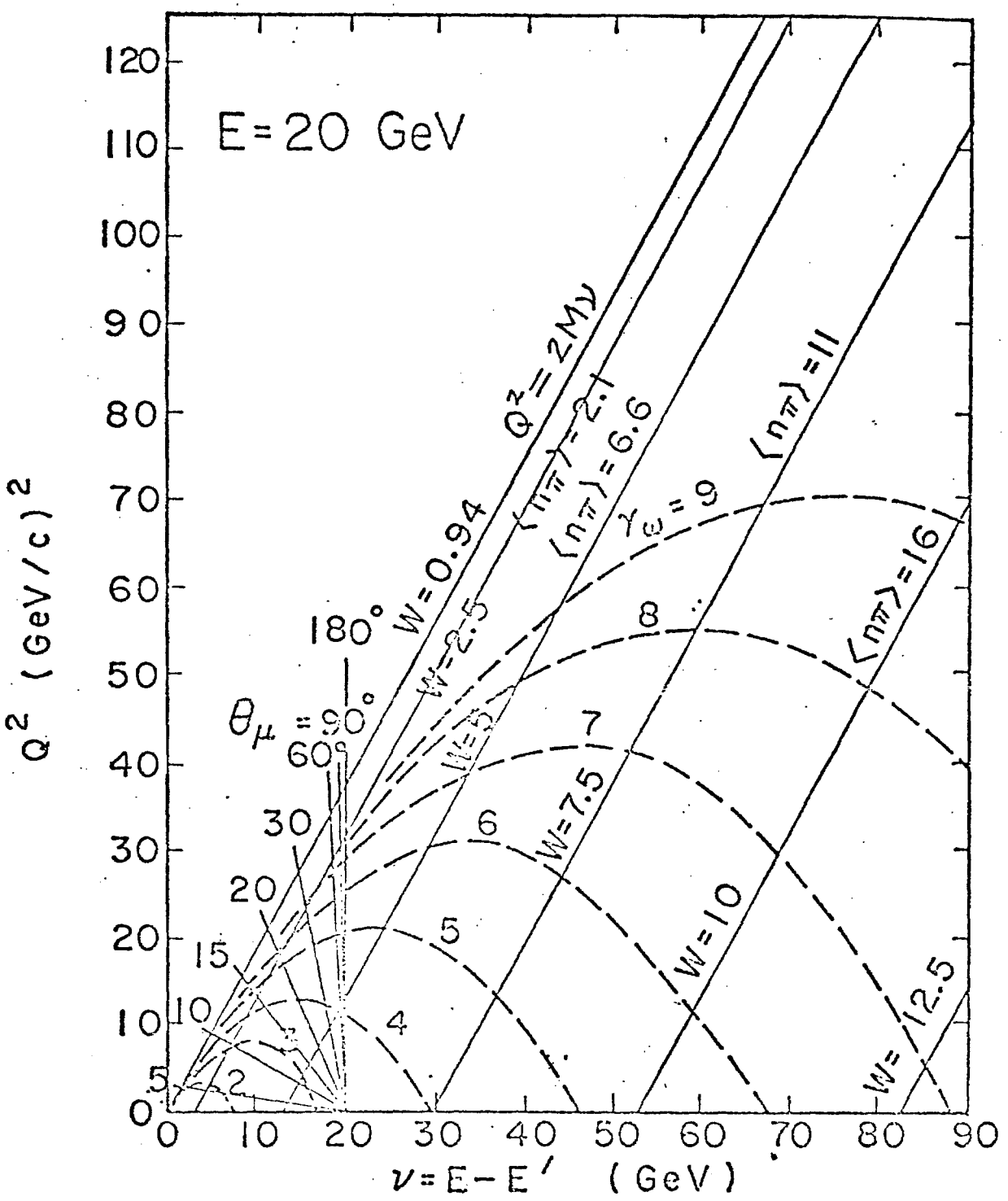

XBL709-3904

Fig. 1

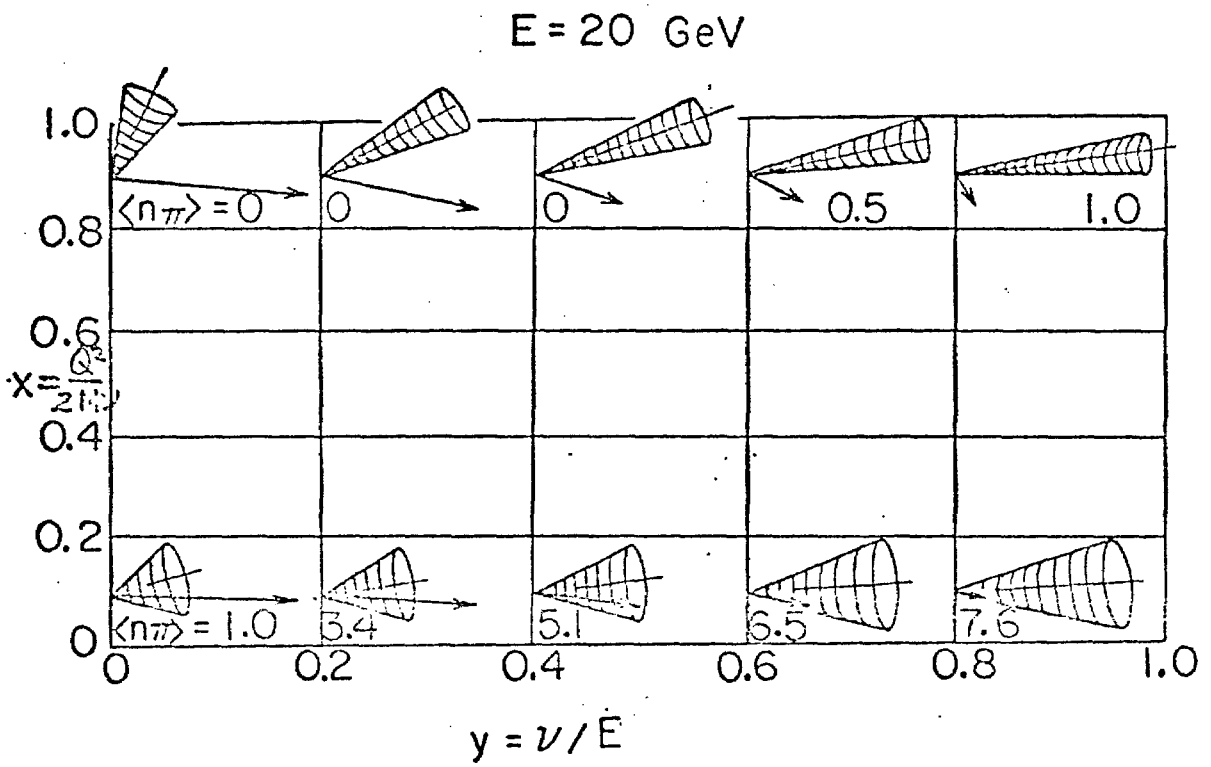

XBL709-3896

FIG. 2

Muon Trajectories

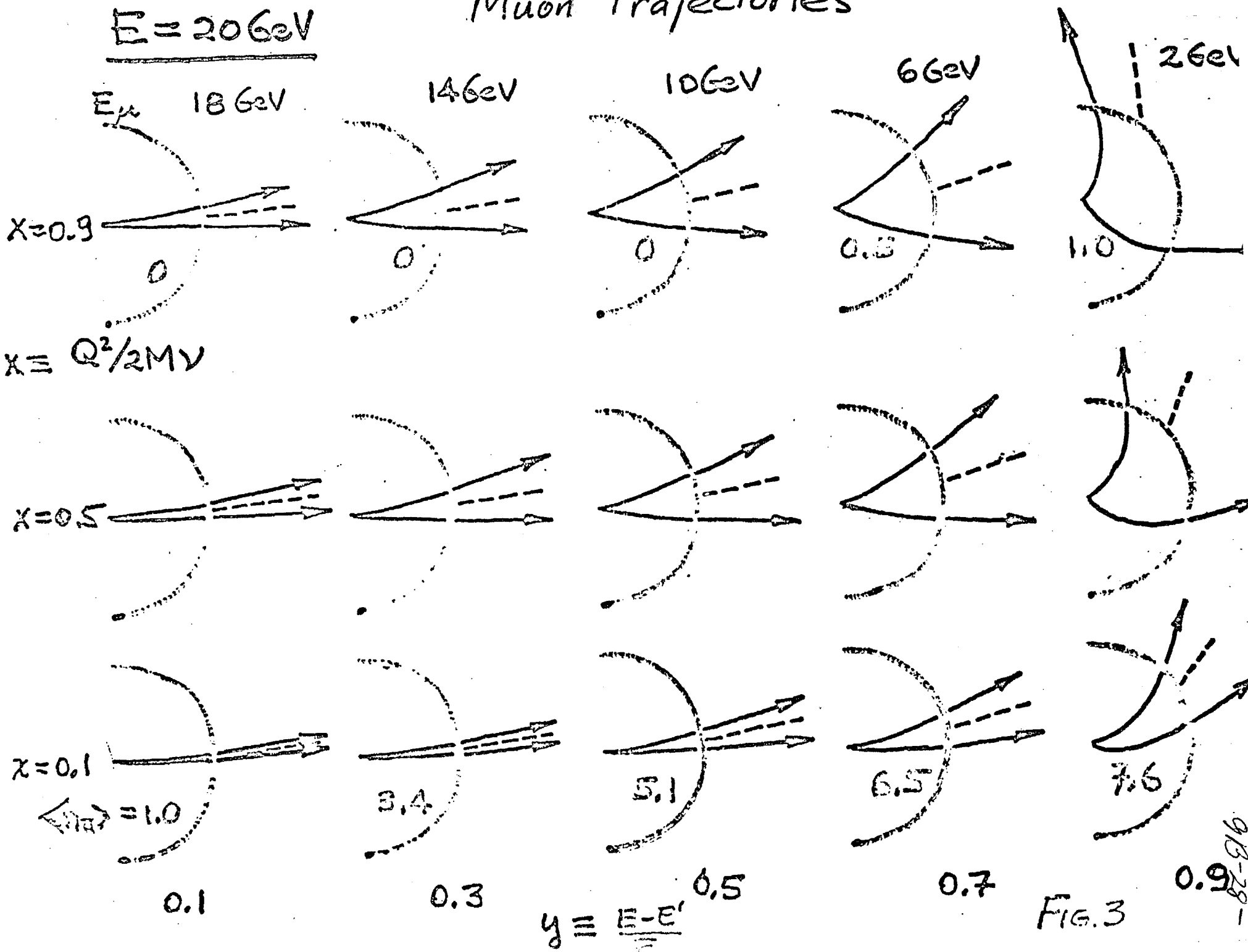

FIG. 3

9/13-28-1

Distribution of 1000 events

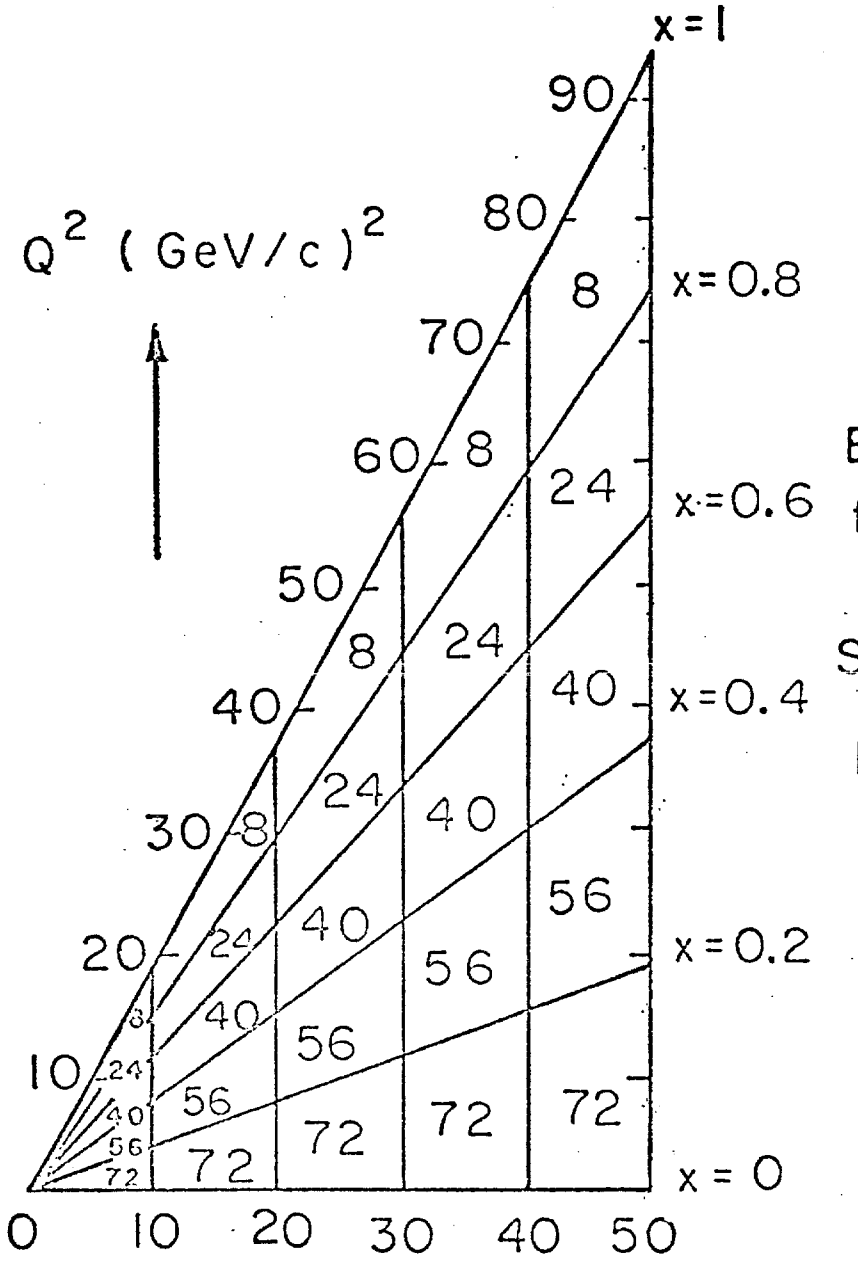

E=50 GeV
for $\nu\beta = K(1-x)$
$\sigma_R = \sigma_S = 0$
Spin $\frac{1}{2}$ Partons
$M_W = \infty$

XBL709-3893

FIG. 4

Distribution of 1000 events

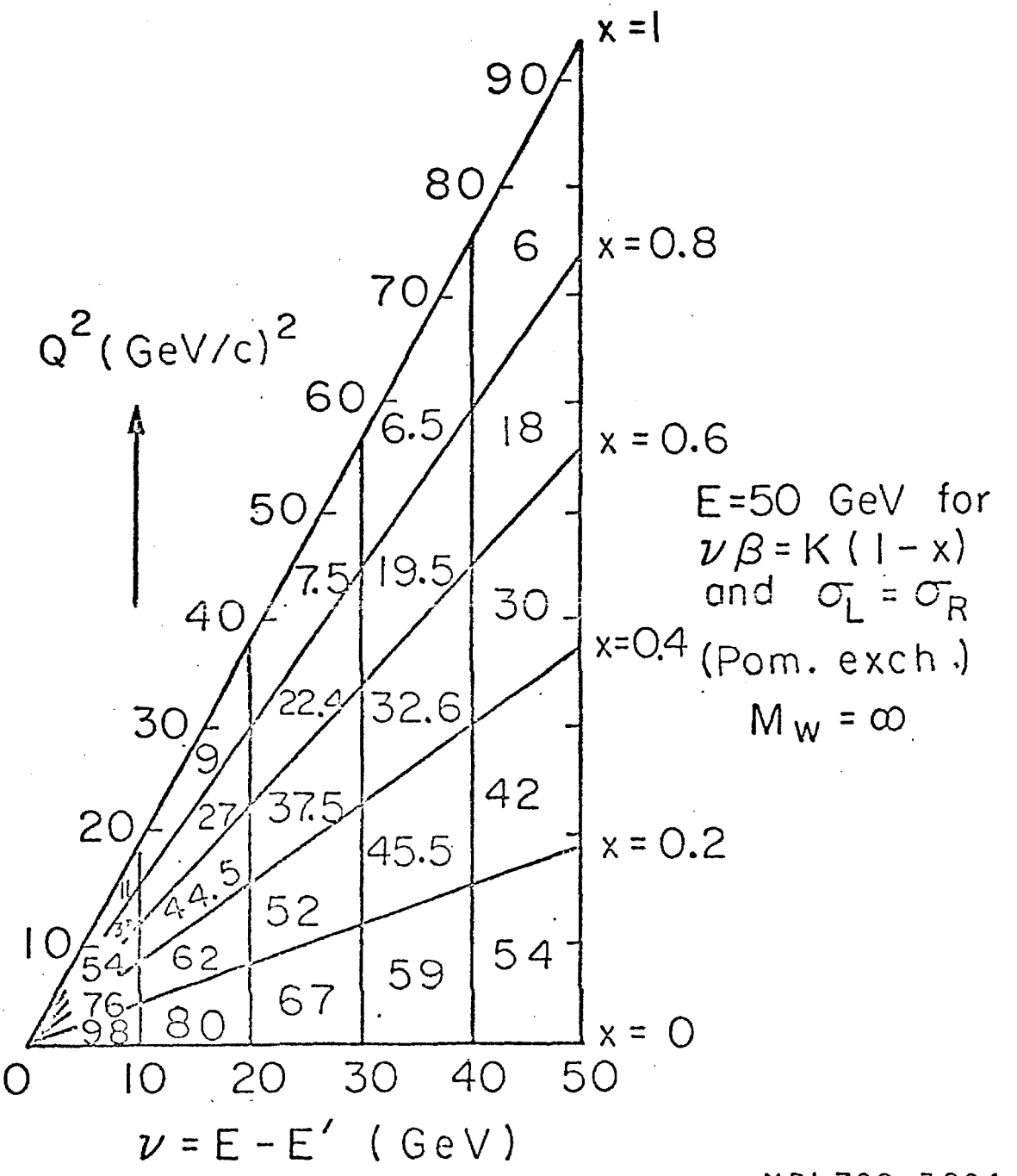

E=50 GeV for
$\nu\beta = K(1-x)$
and $\sigma_L = \sigma_R$
(Pom. exch.)
$M_W = \infty$

XBL709-3894

FIG. 5

Modification of Scaling with W Propagator

9B-31

for

$M_W = 8$ GeV

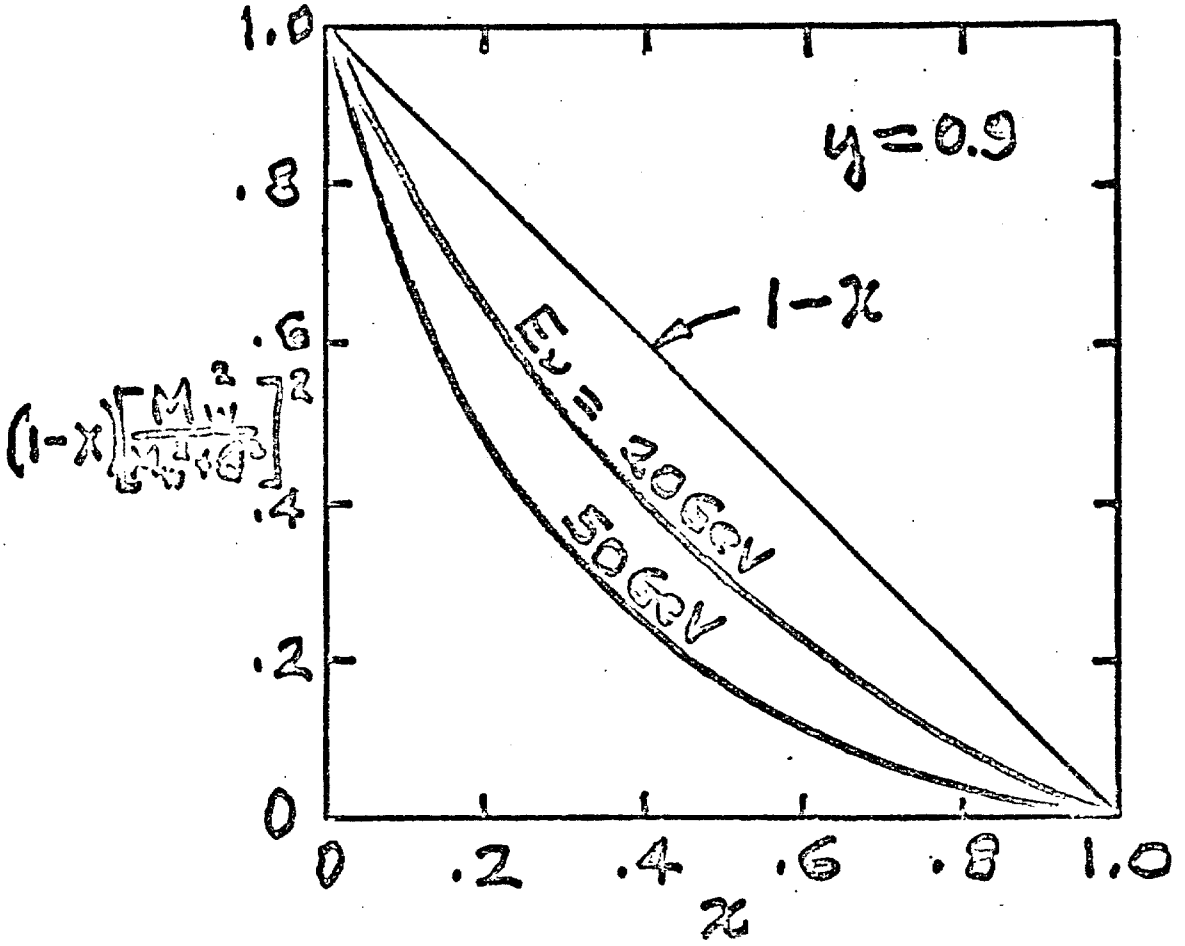

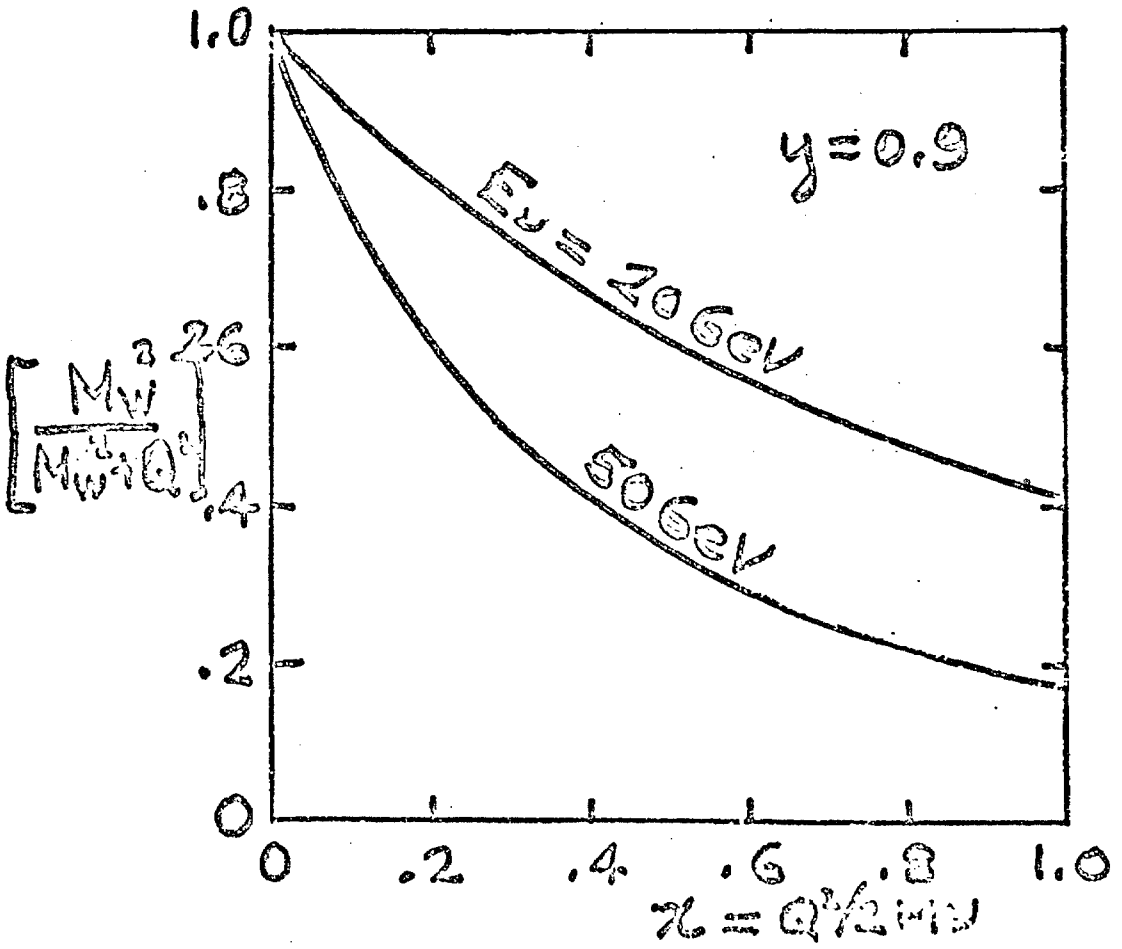

Fig. 6

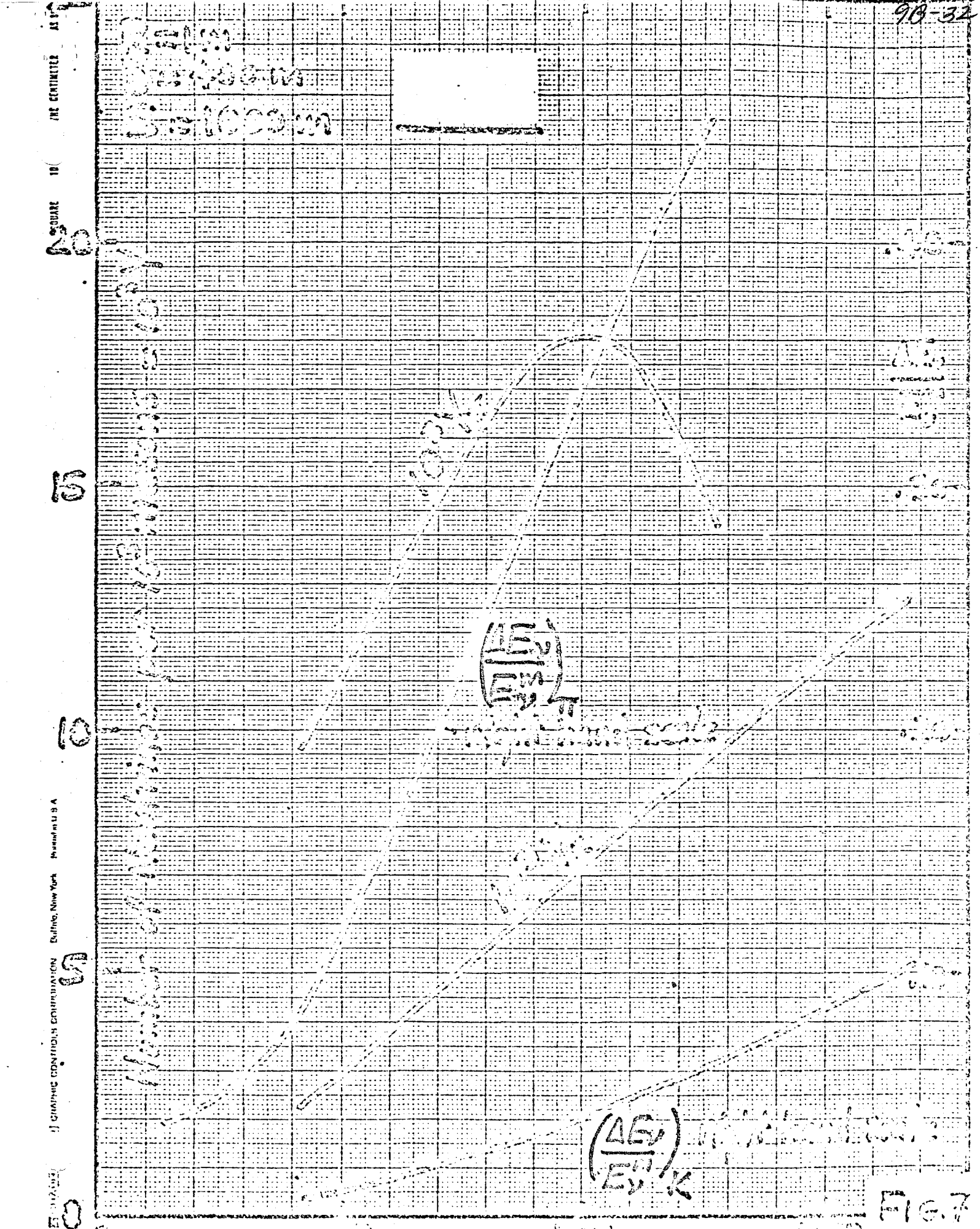

Fig. 7

Mass Absorption Coefficient

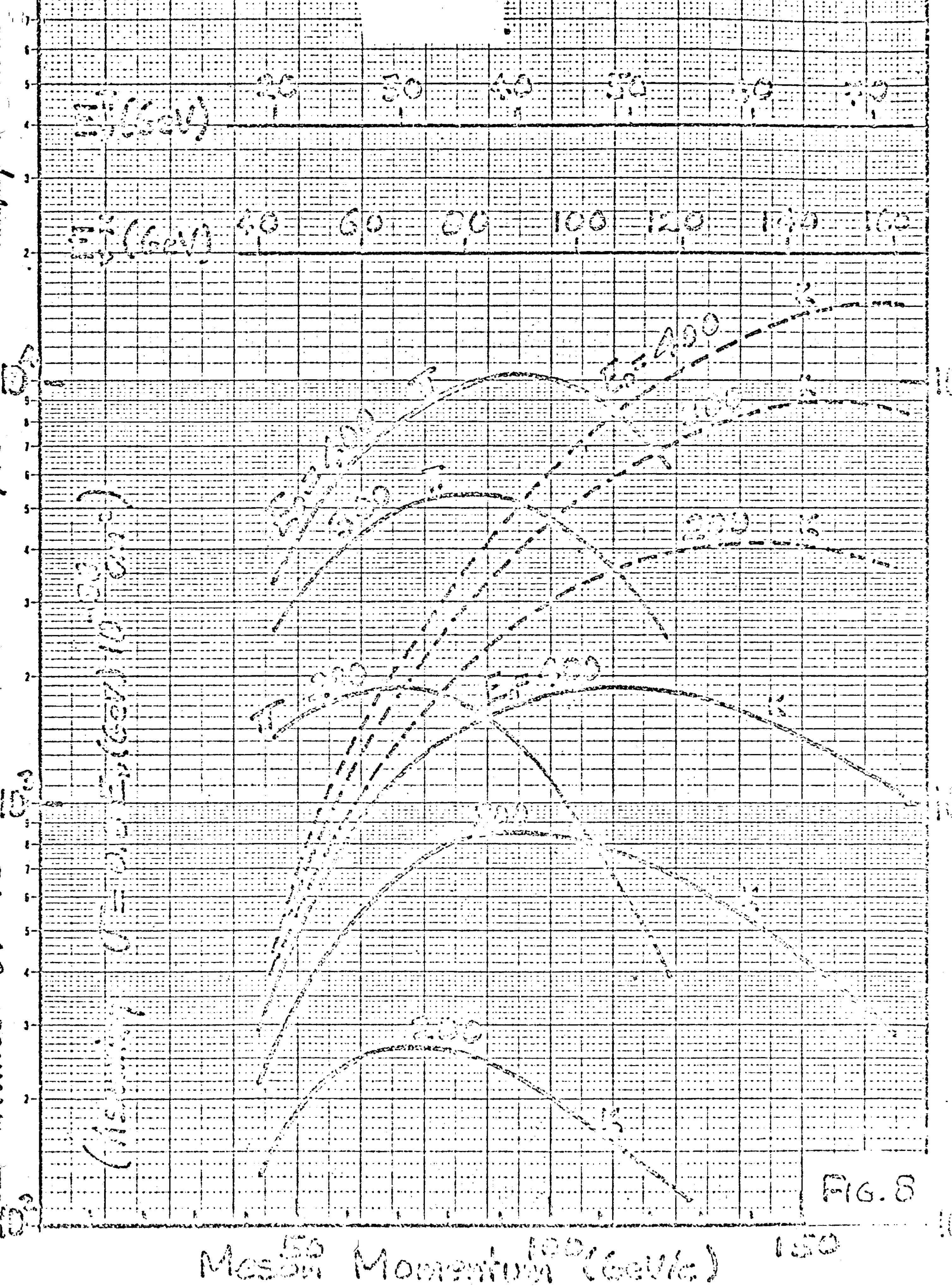

Number of Neutrino Interactions/10^{19} Interacting protons
E_π (GeV)
20 30 40 50 60 70
E_K (GeV)
40 60 80 100 120 140 160
10^3
10^2
Meson Momentum (GeV/c)
50 100 150
FIG. 8

$$\frac{dq}{d\left(\frac{dq}{dx}\right)_{\text{undistorted}}} = \frac{1}{\text{very thin target}}$$

$$b \equiv \frac{e^{-3Kq/4} - \beta\left(1 - \frac{\lambda}{\lambda_\pi}\right)}{\beta^2}$$

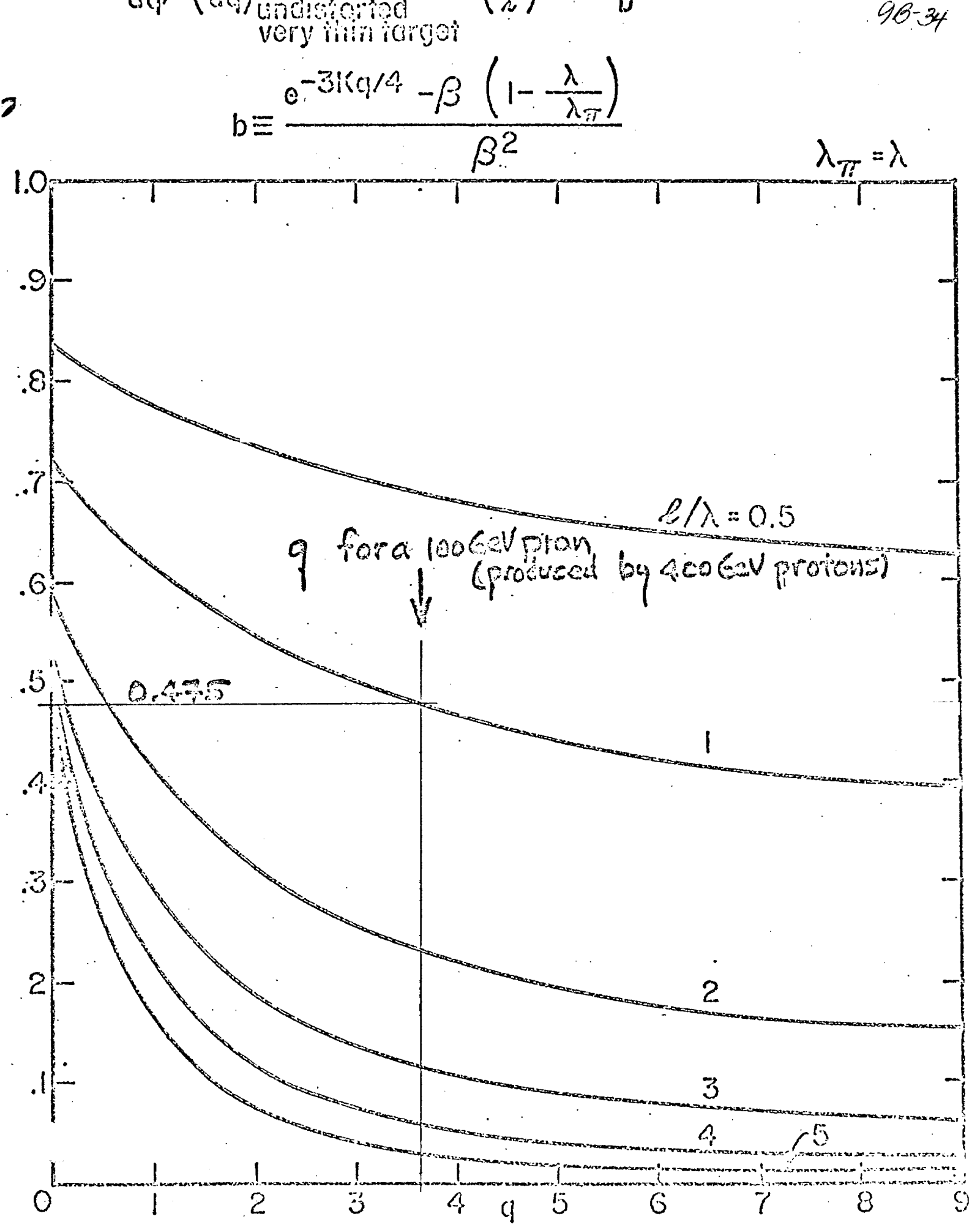

FIG. 9

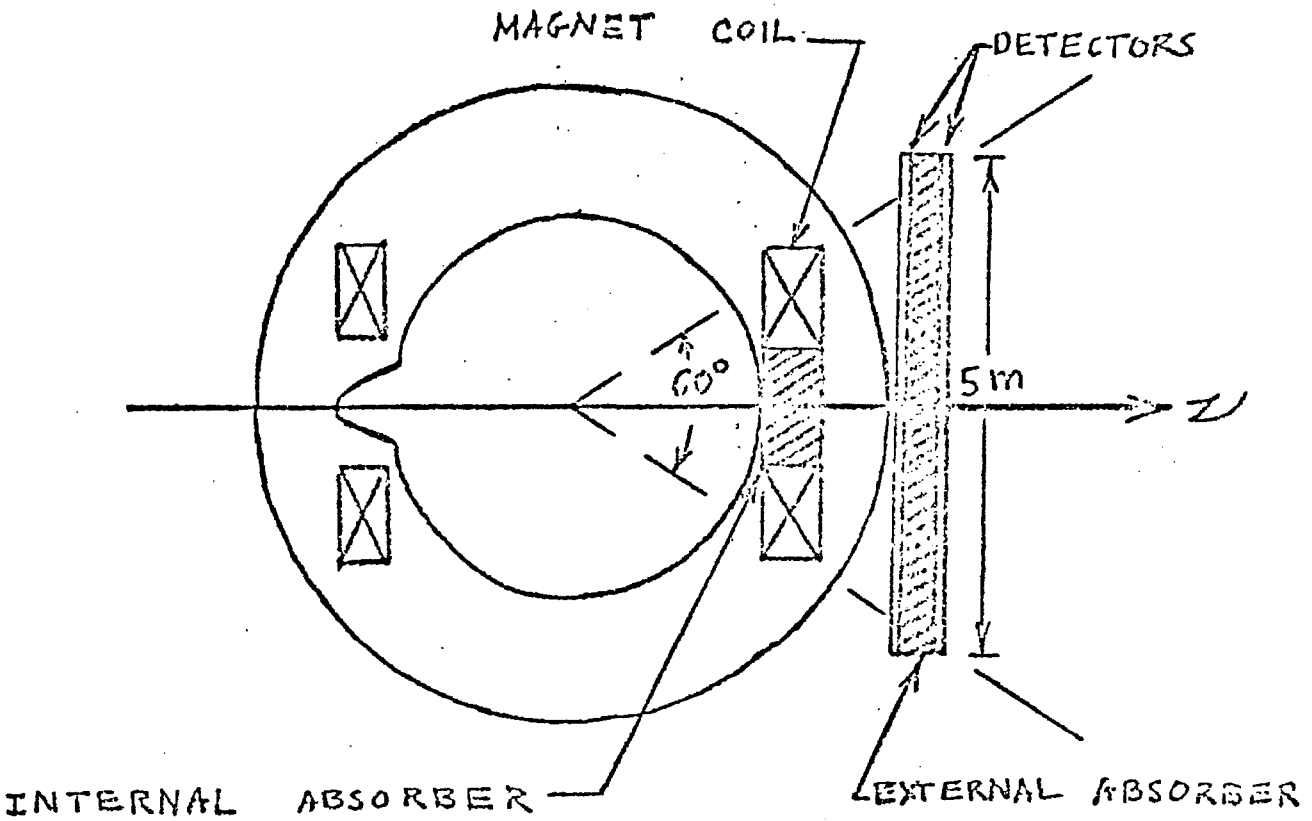

Fig. 10 a BUBBLE CHAMBER AND EMI, SIDE VIEW

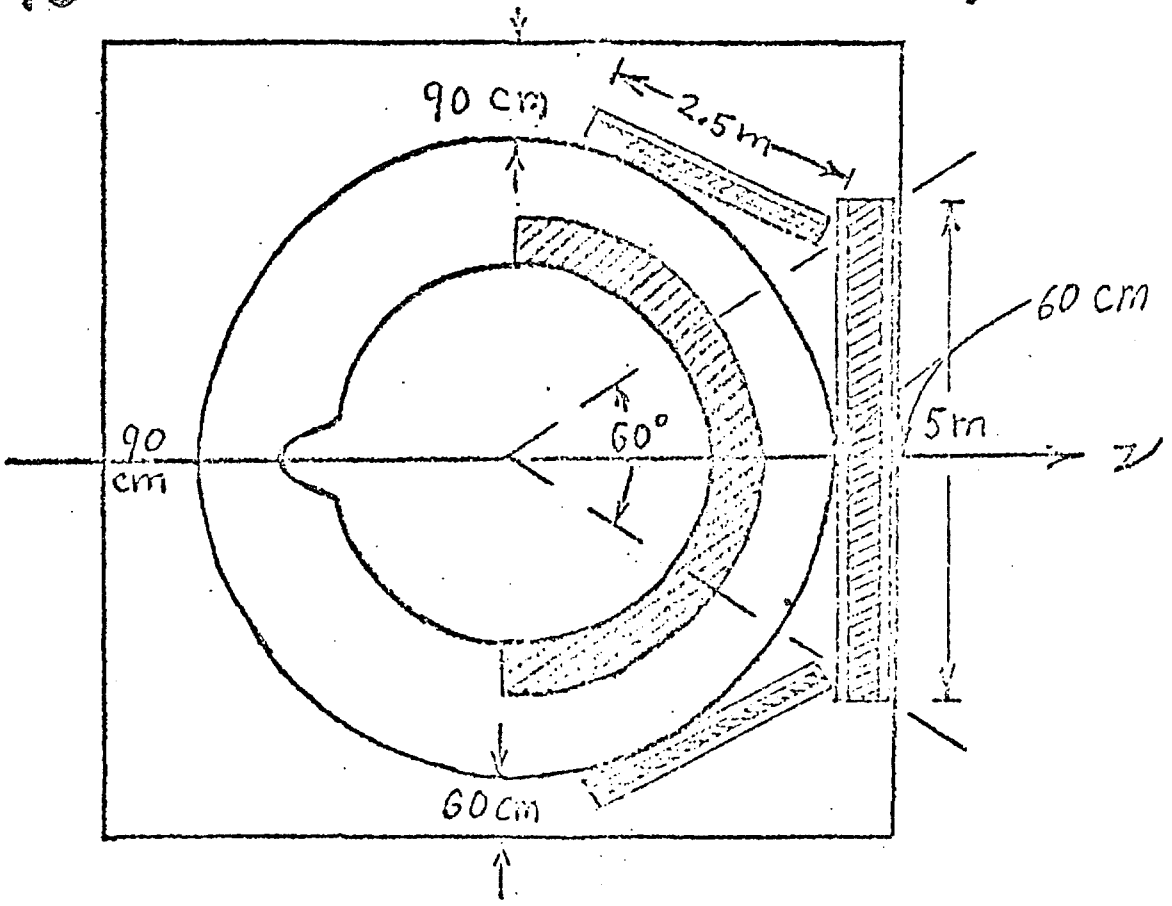

Fig. 10 b BUBBLE CHAMBER AND EMI, PLAN VIEW

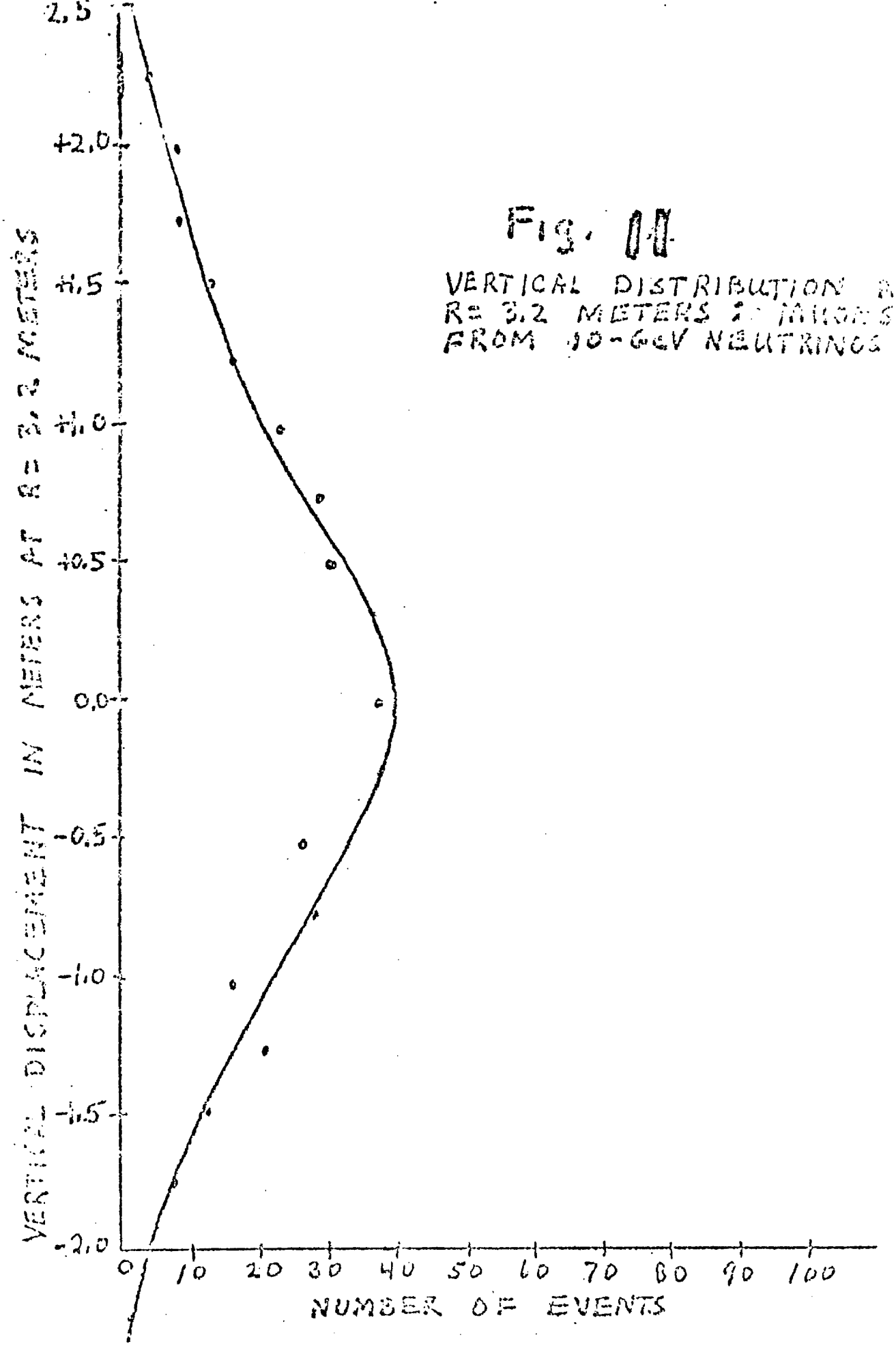

Fig. 11

VERTICAL DISTRIBUTION AT R = 3.2 METERS [illegible] MUONS FROM 30-GeV NEUTRINOS

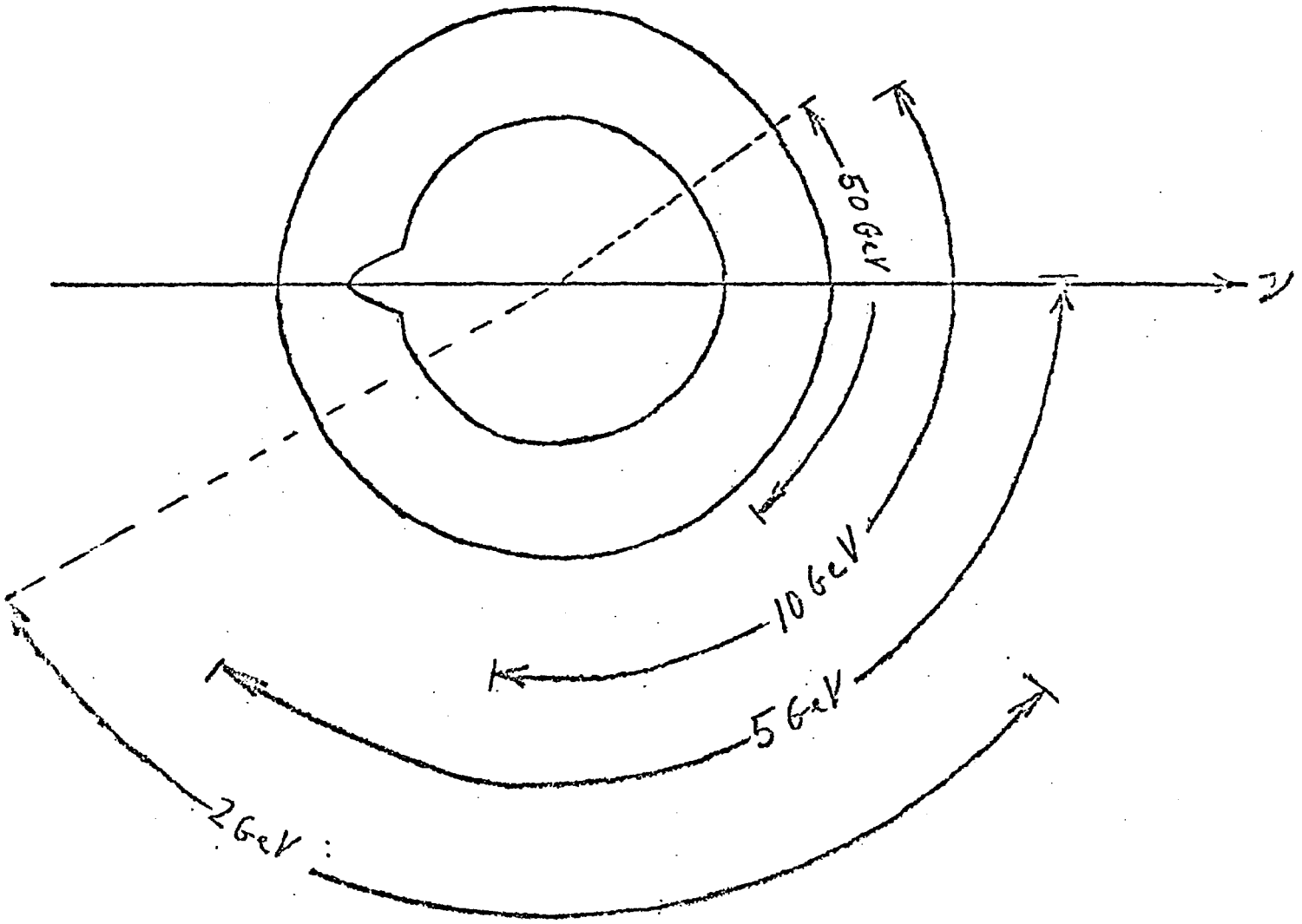

Fig. 12 HORIZONTAL DISTRIBUTION OF MUONS AT R = 3.2 METERS

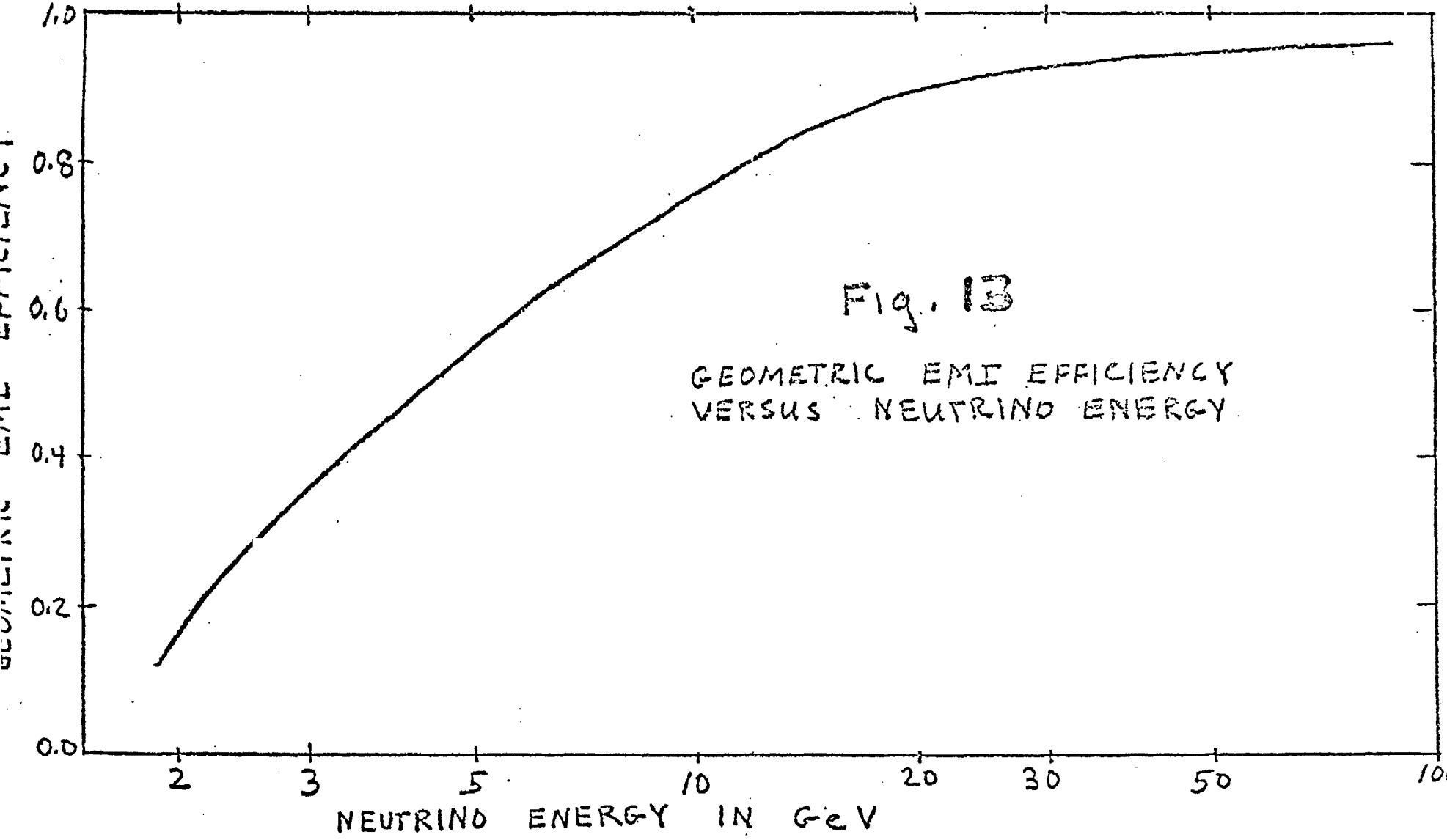

Fig. 13

GEOMETRIC EMI EFFICIENCY
VERSUS NEUTRINO ENERGY

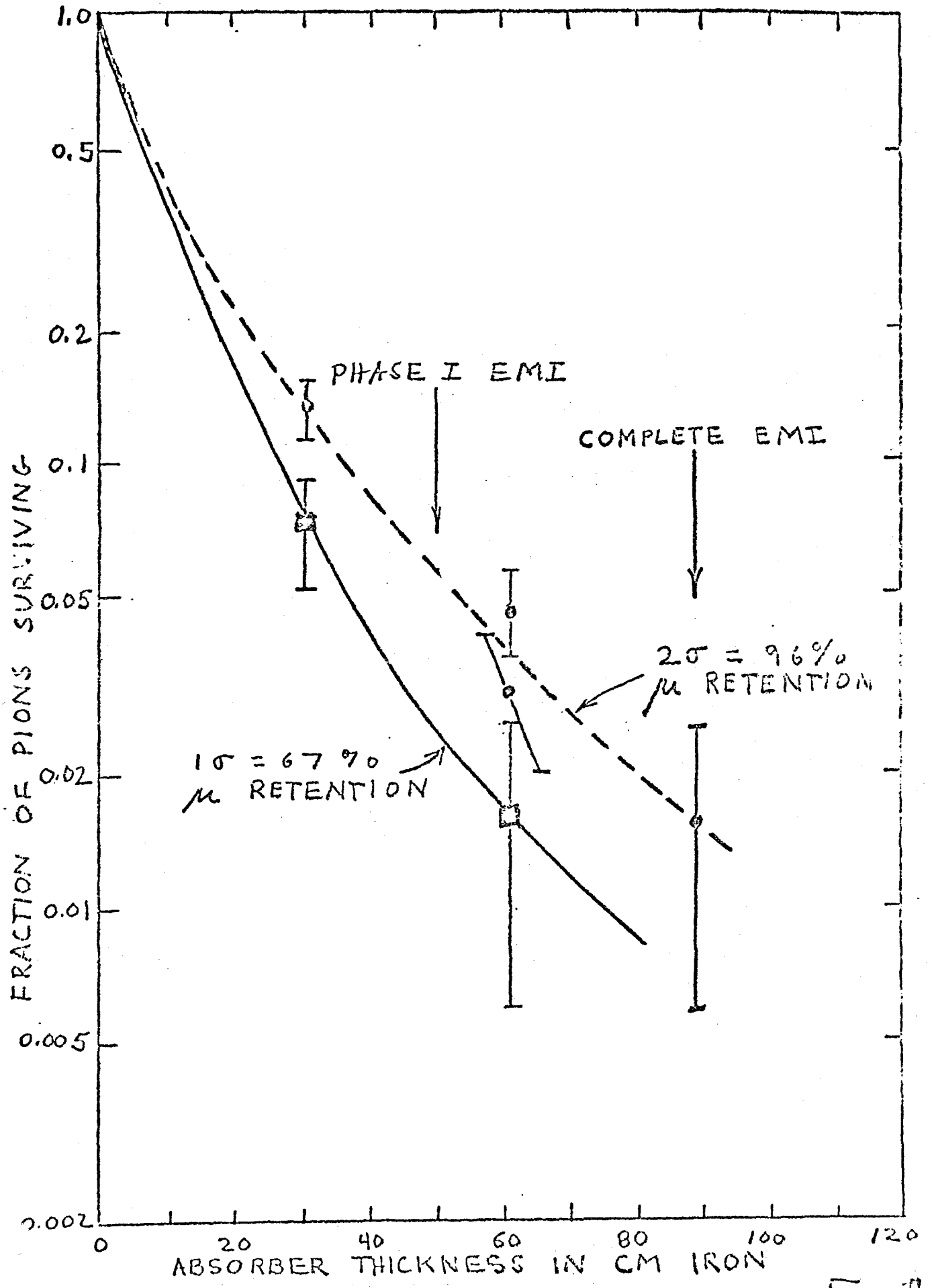
1.0
0.5
0.2
0.1
0.05
0.02
0.01
0.005
0.002
FRACTION OF PIONS SURVIVING
PHASE I EMI
COMPLETE EMI
2σ = 96% μ RETENTION
1σ = 67% μ RETENTION
0
20
40
60
80
100
120
ABSORBER THICKNESS IN CM IRON

Fig. 14

9C IN NOW LISTED AS 155

NAL PROPOSAL NO. 9B Rev.

Correspondent: M.L. Stevenson

University of California
Lawrence Berkeley Laboratory
Berkeley, California 94720
Telephone: FTS 18-415-843-2740 Ext. 6301

PROPOSAL TO STUDY ANTI NEUTRINO INTERACTIONS IN THE 30 m^3 NAL BUBBLE CHAMBER WITH THE PHASE I EXTERNAL MUON IDENTIFIER

R.J. Cence, F.A. Harris, S.I. Parker, M.W. Peters
V.Z. Peterson, V.J. Stenger
University of Hawaii

A. Barbarro-Galtieri, G.R. Lynch, J.P. Marriner,
F.T. Solmitz, M.L. Stevenson
University of California
Lawrence Berkeley Laboratory

October 3, 1974

SUMMARY

We will have analyzed approximately 2500 neutrino interactions by the time the 50,000 pictures test of the Phase I External Muon Identifier (EMI) is completed (E-155). We are now requesting 300,000 pictures of the 15 foot-hybrid*-bubble chamber, filled with hydrogen and exposed to a wide band anti neutrino beam, in order to obtain a comparable number of anti neutrino interactions. We request that at least 50,000 of these anti neutrino pictures be taken during the April-May 1975 run sequence. By that time we will have analyzed 200 neutrino interactions from the copied portion of Experiment 45A film and, hopefully, 500 additional events from the 10,000 picture portion of the above mentioned test sample that we are requesting from the October-November 1974 run sequence. In this way we will make an early comparison of the hadronic final states for neutrinos and anti neutrinos on hydrogen using the wide band beam. This was the original spirit of the deferred portion of our physics proposal 9B (9 July 71) which called for 50,000 wide band events.

Most of the physics arguments and how the kinematics of anti neutrino interactions place constraints on the detectors are contained in that proposal. The first three figures of that proposal are reproduced here. The first summarizes the kinematics, the second shows pictorial momentum vector diagrams to give some idea of what a 20 GeV neutrino interaction might look like. The Landau thermodynamic model[3] was used as a "worst-case" estimate of hadron multiplicity. The third figure summarizes how the muons are bent by the magnetic field and shows why we wanted to place the EMI proportional chambers at 90° azimuth to the neutrino direction.

* With External Muon Identifier. (See reference 2)

Physics Justification

The main purpose of the experiment is to supplement the information that has been obtained by the two counter neutrino experiments,[1] namely to provide detailed information about the hadronic state of anti neutrino interactions. Muon identification is crucial to a clear understanding. The geometrical efficiency of the EMI is greater for anti neutrinos because more of their muons go forward. (See Figs 1 & 3.) Furthermore, any neutrino contamination in the anti neutrino beam can be more readily dealt with if one employs the EMI.

A. Charged lepton current

1. Although, the neutrino energy is low ($\lesssim$50 GeV) we will search for jet-like structure of the "dressed up" recoiling parton and observe how the charge-momentum distribution compares with the corresponding neutrino induced state. It is very important in this analysis to know the direction of the momentum transfer vector. Unless the muon is identified and neutral current events removed from the sample, errors will be introduced into the analysis. (See Fig. 2)

2. The known $(1-y)^2$ dependence of the anti neutrino charged lepton current cross section makes anti neutrinos very useful for searching for the production of rare, massive hadronic states. From Fig. 1, which shows lines of constant hadron invariant mass W, one observes that thresholds for massive hadronic states occur at large y and small x ($\equiv Q^2/2M\nu$) where a paucity of events occurs. Fig. 4 shows, approximately, how the 2500 events will distribute themselves in the x, y space. Here, for simplicity, we have used $\nu W_2 \propto 1-x$. Charmed particles, if they exist, are expected to have leptonic decay modes. Here, again the EMI is useful for detecting its muonic decay mode.

3. Observation of the relative rates of $\Delta S = \Delta Q$ and $\Delta S = 0$ reactions à la Cabibbo, where the final state baryon systems may not be in the same SU(3) multiplet as the proton. For example,

$$\bar{\nu} + p \rightarrow \mu^+ + \left[\Sigma^{0*}_{(1385)} \rightarrow \begin{matrix}\Lambda\,\pi \\ \Sigma\,\pi\end{matrix}\right] \quad , \Delta S = \Delta Q$$

$$\bar{\nu} + p \rightarrow \mu^+ + \left[\Delta^0(1235) \rightarrow N\pi\right] \quad , \Delta S = 0$$

Here, there is a greater chance for misidentifying the muon than when the baryons are in the same multiplet as the proton. The EMI will eliminate the ambiguity.

4. Test of Adler's relation,

$$\lim_{E_\nu \rightarrow \infty} \frac{d\sigma(\bar{\nu}p)}{dQ^2} - \frac{d\sigma(\nu p)}{dQ^2} = \frac{G^2}{\pi}\left(\cos^2\theta_c + 2\sin^2\theta_c\right)$$

B. Neutral lepton current.

1. Although the neutral lepton current events can be identified in approximately 20 or 30% of the cases we have little chance of being able to determine x and y for them because of our inability to measure the energy-momentum of the neutral portion of the hadronic state. We will, however, try to extract the maximum amount of information from the charged portion. We are submitting a separate proposal to use the EMI with a light mixture of Ne in the hydrogen bubble chamber so as to be able to measure x and y.

2. Neutron background studies are crucial to an ultimate understanding of neutral current physics. We intend to search for anti neutrino interactions in the surrounding super conducting coils where the associated neutron interacts in the bubble chamber. From this we will be able to estimate the neutron background.

C. Possible Surprising Physics

With a detector system that maximizes particle identification, one is best able to detect unusual processes.

Apparatus Needed

A. 15' -- Hydrogen filled bubble chamber.

B. External Muon Identifier.

The twenty-five $1m^2$ - multiwire proportional chambers (MWPC) envelope the downstream portion of the 22' diameter vacuum tank. Fig. 5 summarizes the geometrical coverage of the 22 MWPC's used during the July-Aug 74 run of E45A. It shows the vertical and azimuthal coverage as viewed by an observer at the center of the bubble chamber. The plotted points are the predicted hit positions in the MWPC of incoming regenerated muons (from the berm and earth shield) that traverse the visible volume of the bubble chamber. Fig. 6 shows the deviation of the measured position in the EMI from the predicted one.[2] The RMS deviation is very nearly that expected from multiple scattering in the four interaction lengths absorber between the bubble chamber body and the MWPC's. More than 80 percent† of the observed hits fall within the "96% circle" centered at the predicted point. Less than two percent of these incoming tracks interact; consequently, they are mostly muons. Details of this earlier run (400 GeV triplet load) are given in TM513.[2]

C. Neutrino Beam Monitoring Equipment.

D. We would like to assist Experiment 31A (Derrick) in determining the effectiveness of the plug that is likely to be first installed for the April-May 75 run. We plan to operate the EMI during a reasonable fraction of E-31A's exposure in Oct-Nov 74.

E. Scan Projector suitable for monitoring the quality of the bubble chamber pictures from the test strips.

† Some of the beam spill was known to be out of time with the EMI gate during this early run.

Scope of the Experiment

1. 50,000 of 300,000 anti neutrino pictures to be taken during the April-May 1975 run sequence.
2. The remaining 250,000 pictures to be acquired as the schedule permits.
3. At this early stage of bubble chamber operation we shall assume that 30,000 pictures can be accumulated per week. The first 50,000 pictures will take about two weeks, and the remaining 250,000 another eight weeks.
4. Very little testing of equipment is required. We assume implicitly that all beams that are capable of producing neutron or charged background in the bubble chamber will have their spill times not during the bubble chamber sensitive time.

REFERENCES

1. NAL Experiment 21, California Institute of Technology - NAL Group. NAL Experiment 1A, Harvard-Pennsylvania-Wisconsin Group.

2. "Matching 'Muon' Tracks in The 15' Bubble Chamber To The EMI Proportional Chambers", University of Hawaii-LBL Group; Experiment 155, TM-513 (10 October 1974).

"Surveying The External Muon Identifier and The 15' Bubble Chamber With 250 GeV Mesons", TM-509 (16 July 1974), University of Hawaii-LBL Group.

Complete details of the construction and electronics of the MWPC's and an early test of muon identification are found in the following references:

a) NAL Proposal 155, "Development and Test of an External Muon Identifier for the 30 m^3 Bubble Chamber", R.J.Cence, F.A.Harris, S.I.Parker, M.W.Peters, V.Z.Peterson, V.J.Stenger, D.E.Yount; (UH) A.Barbarro-Galtieri, J.P.Marriner, F.T.Solmitz, M.L.Stevenson; (LBL) V.Z.Peterson, Proceedings of 1973 International Conference on Instrumentation for High Energy Physics at Frascati, Italy; "Hybrid Bubble Chamber Detection of Neutrino Events - The External Muon Identifier".

b) "Muon Identification Using Multiwire Proportional Chamber", F.A.Harris, S.I.Parker, V.Z.Peterson, D.E.Yount, M.L.Stevenson; Nuclear Instruments and Methods 103, 345 (1972).

c) "EMI Development - Half Meter Proportional Chamber Test Results", S.I.Parker and R.Jones, NAL TM-359, LBL 797, UH-511-122-72.

d) "Digitizing Electronics for the EMI Multiwire Proportional Chambers", E.Binnall, F.Kirsten, K.Lee and C.Nunnally, NAL TM-360, LBL 798.

3) For a recent discussion of this model see J.D.Bjorken and B.L.Ioffe "Annihilation of e^+e^- into Hadrons" SLAC-PUB-1467 (T/E) August 1974. (To be published in Izv. Acad. Nauk, SSSR, Ser. Fiz.)

FIGURE CAPTIONS

Figure 1. The kinematics of inelastic lepton scattering are summarized here. The solid lines radiating from $Q^2=0$, $\nu(=\nu_{max}=E)$ are loci of equal final lepton scattering angle. The parallel solid lines are loci of equal invariant final state hadron mass. They also show "worst case" predictions of hadron multiplicity. The radial line originating at $Q^2=0$, $\nu=0$ are loci of constant $x(=Q^2/2M\nu)$. The dashed curves are loci of constant Lorentz factors, γ_W of the hadron system.

Figure 2. Typical momentum vector diagrams for various regions in the x, y space are shown. The opening angles of the cones are typical of those expected of the Landau Thermodynamical model. A jet-like model would predict opening angles and multiplicities much smaller than these.

Figure 3. Typical Muon Trajectories in the 30 kG field of the 15' chamber are shown. The two solid curves for each (x,y) are the extremes for muons produced in the equatorial plane. The dashed curve is that for a muon emitted with its extreme dip value.

Figure 4. This figure shows approximately how the 2500 anti neutrino events will populate the x,y space.

Figure 5. The azimuthal and vertical coverage of the EMI, as viewed by an observer at the center of the bubble

chamber, is summarized here. It also shows where regenerated muons (from the rear portion of the 1000 meter earth shield) are predicted by the bubble chamber measurements to strike the EMI.

Figure 6. Summary of the deviation of the measured position of muons in the EMI from the predicted position using the bubble chamber picture. x is horizontal and y is vertical.

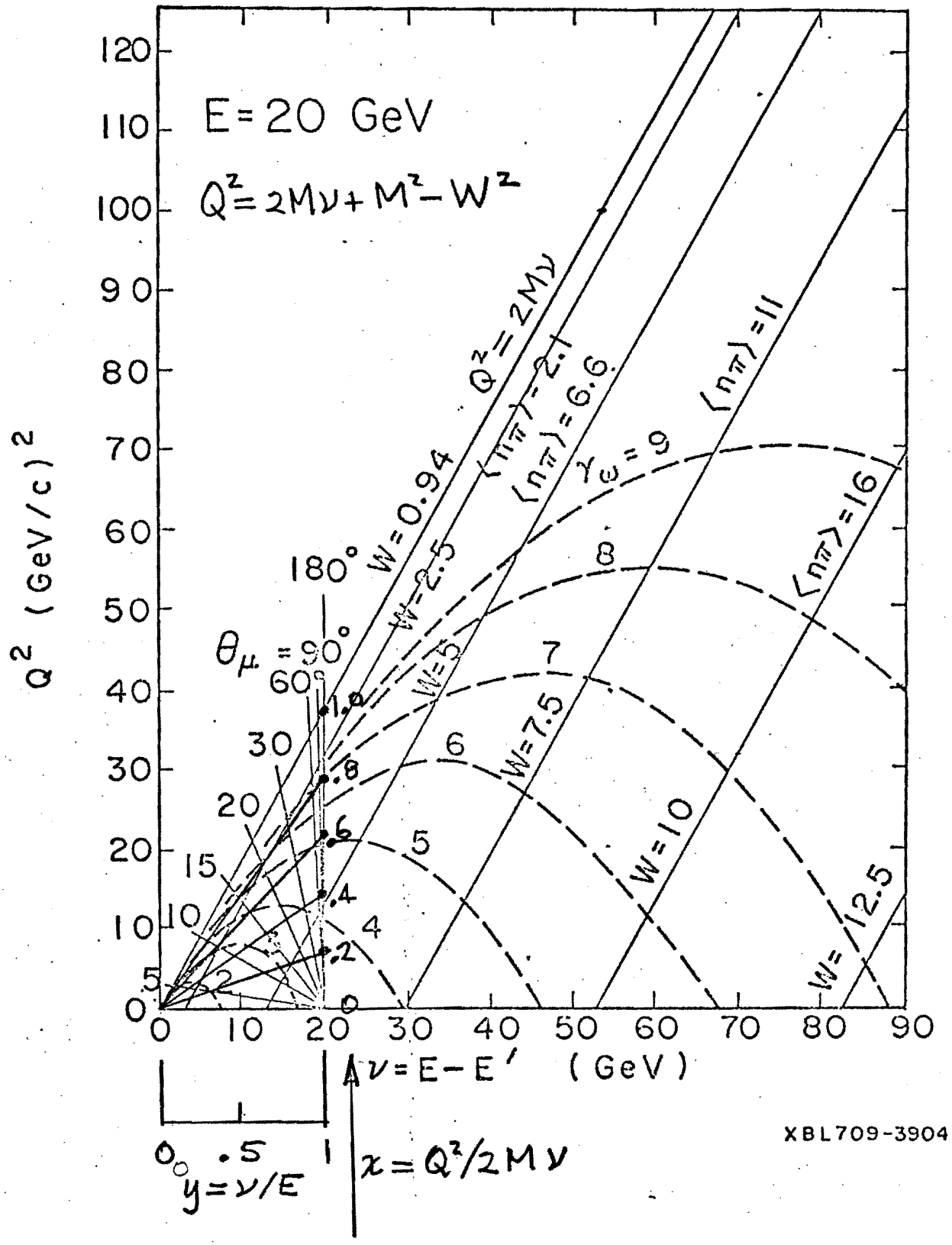
E = 20 GeV
$Q^2 = 2M\nu + M^2 - W^2$
Q^2 (GeV/c)^2
$\nu = E - E'$ (GeV)
$x = Q^2/2M\nu$
$y = \nu/E$
$Q^2 = 2M\nu$
W = 0.94
W = 2.5
W = 5
W = 7.5
W = 10
W = 12.5
$\langle n\pi \rangle$ = 2.1
$\langle n\pi \rangle$ = 6.6
$\langle n\pi \rangle$ = 11
$\langle n\pi \rangle$ = 16
γ_ω = 9
θ_μ = 90°
180°
XBL709-3904

FIG. 1

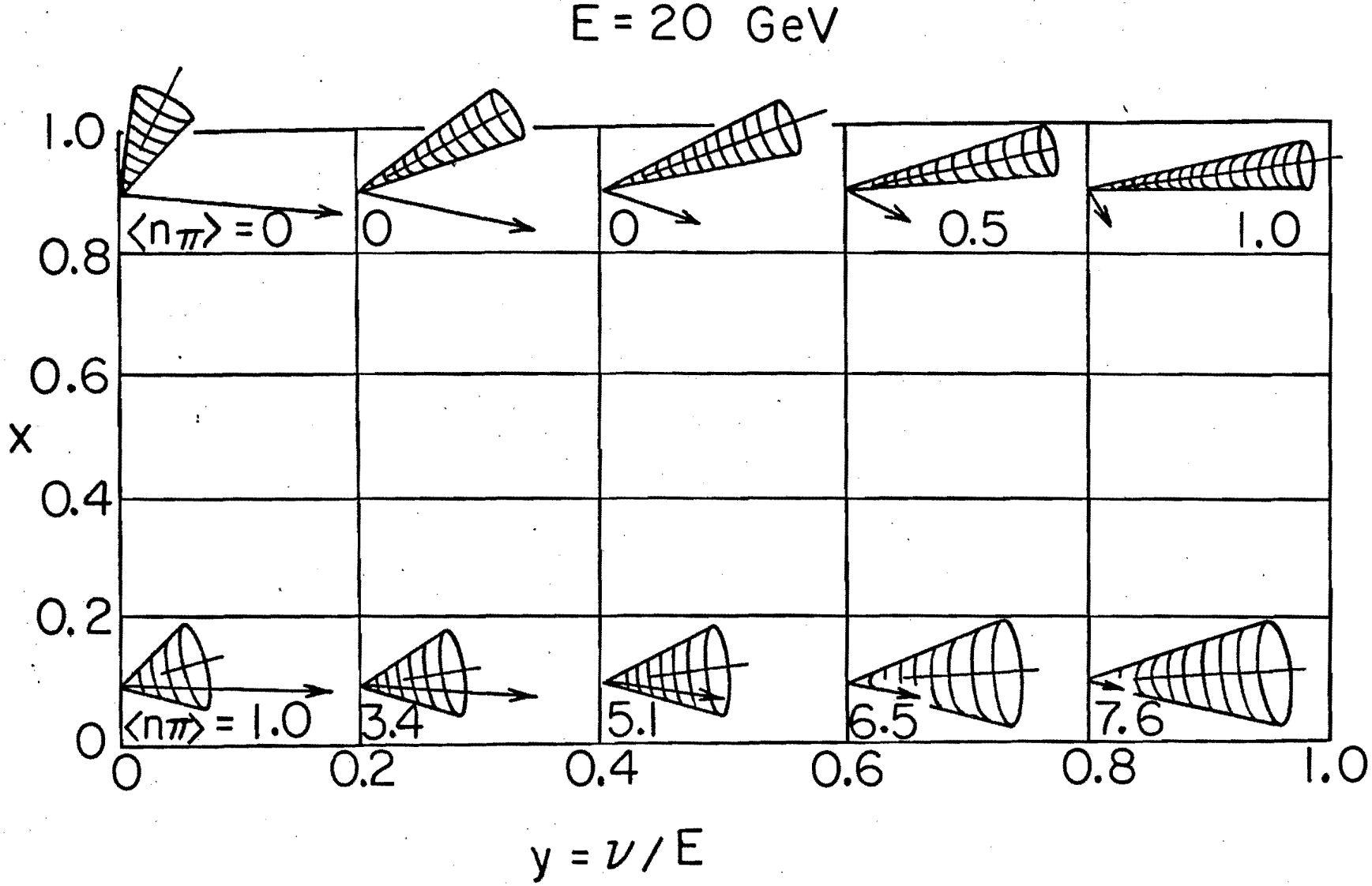

XBL709-3896

FIG. 2

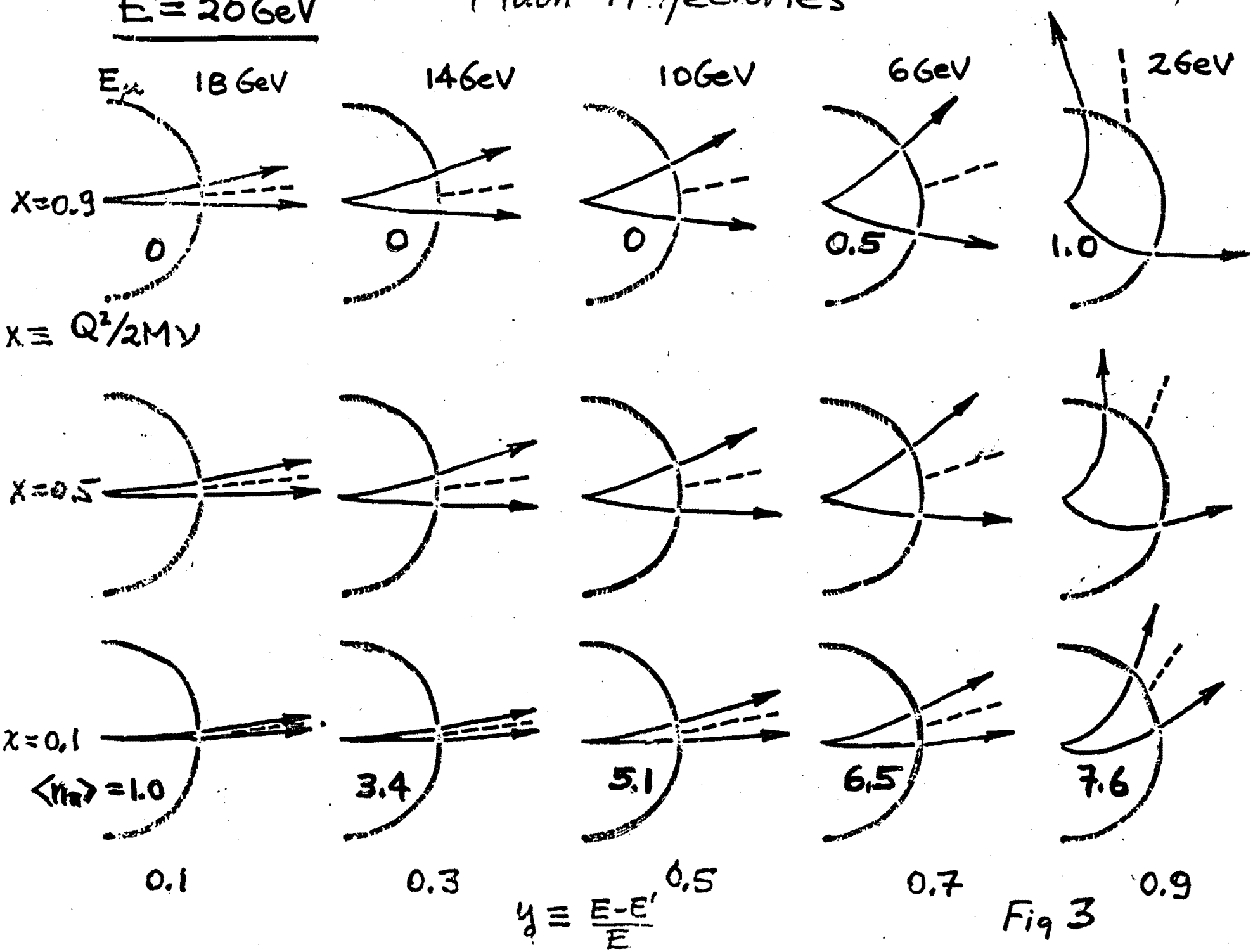
E' = 20 GeV
Muon Trajectories
E_μ 18 GeV
14 GeV
10 GeV
6 GeV
2 GeV
X=0.9
X=0.5
X=0.1
0
0
0
0.5
1.0
$\langle n_{ch} \rangle$ = 1.0
3.4
5.1
6.5
7.6
$X \equiv Q^2/2M\nu$
0.1
0.3
0.5
0.7
0.9
$y \equiv \frac{E-E'}{E}$

Fig 3

Distribution of 2500 events

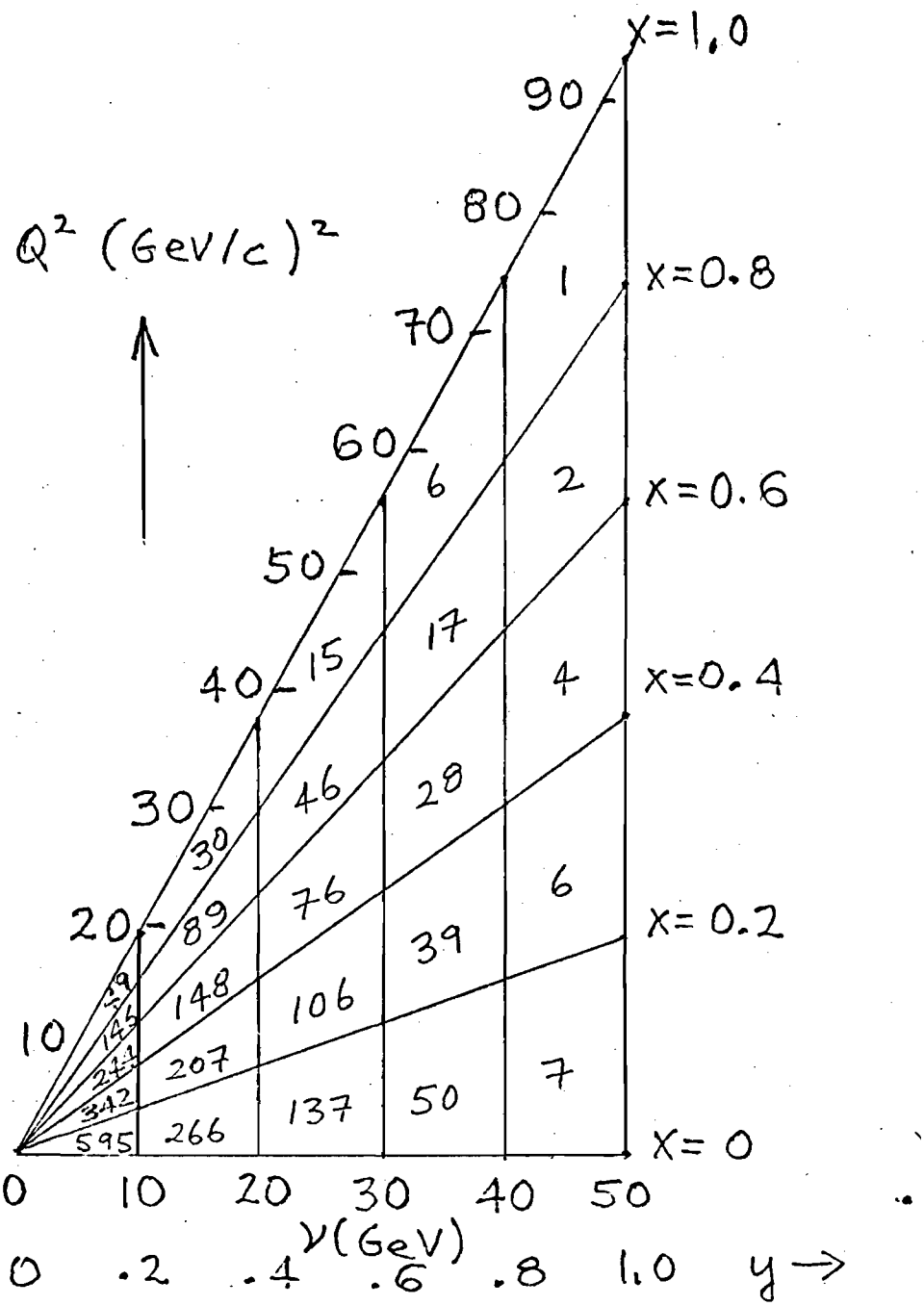

$$\frac{d^2\sigma}{dx\,dy} \approx \frac{G^2 ME}{\pi}\,\frac{Q^2}{2\pi}\,(1-x)\left\{\sigma_L + (1-y)\,\sigma_S + (1-y)^2\sigma_R\right\}$$

with $\sigma_L = \sigma_S = 0$. $\sigma_{L,S,R}$ ARE HELICITY CROSS SECTIONS

Fig 4

CHAMBER NUMBERS

0	25	20	9	17	21	19	18	0
16	14	4	22	2	15	3	23	0
0	11	8	5	10	7	13	12	0

NUMBER OF HITS

0	0	10	26	46	20	0	0	0
0	4	31	48	68	47	11	0	0
0	2	22	61	49	41	9	1	0

$|p| > 5$ GeV/c

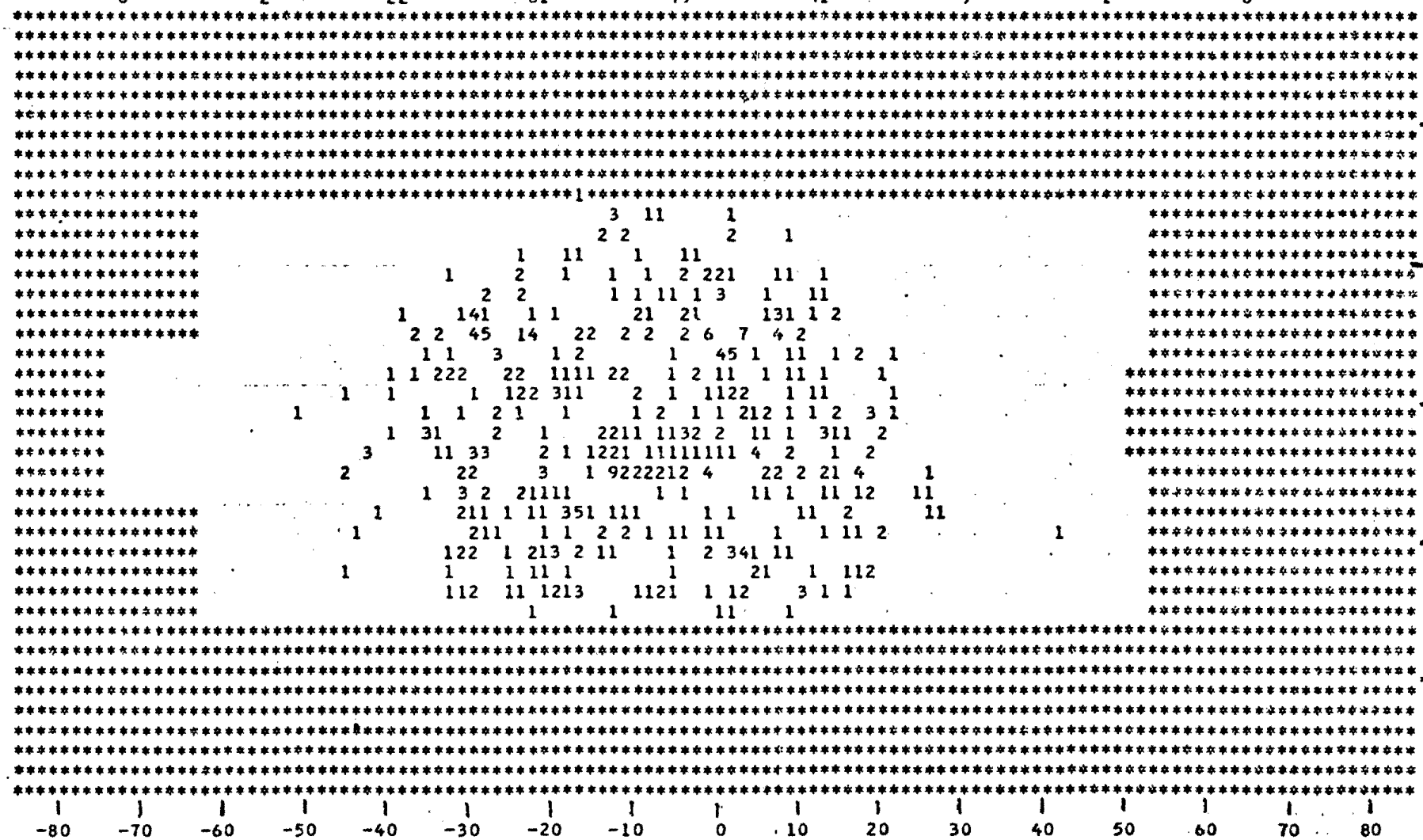

AT END OF INPUT TAPE READING, ELAPSED CP TIME IS 84.463 SEC.

Fig 5

END OF DATA INPUT PHASE. KIOWA HAS PROCESSED A TOTAL OF 492 EVENTS FROM GETUM.1

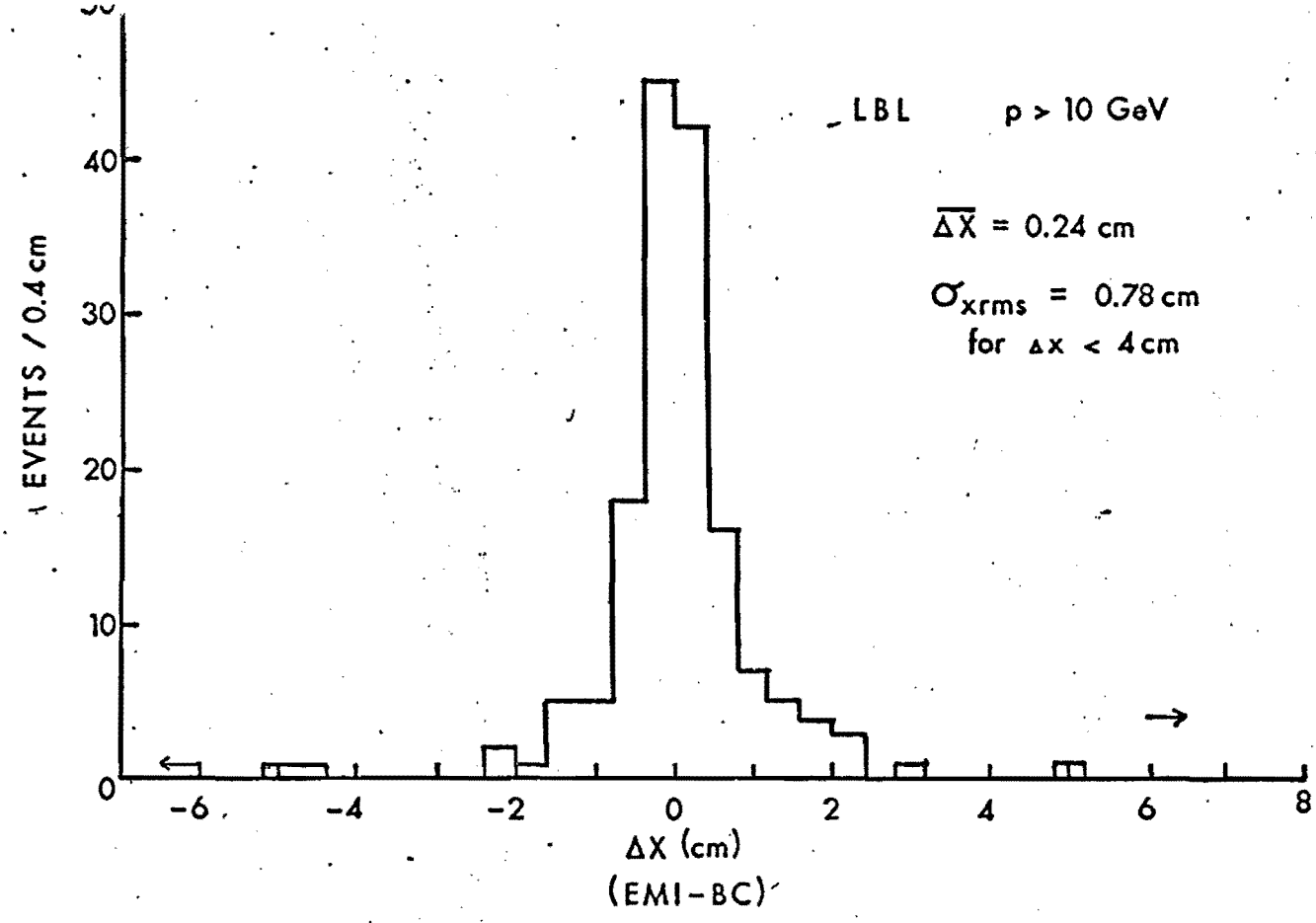

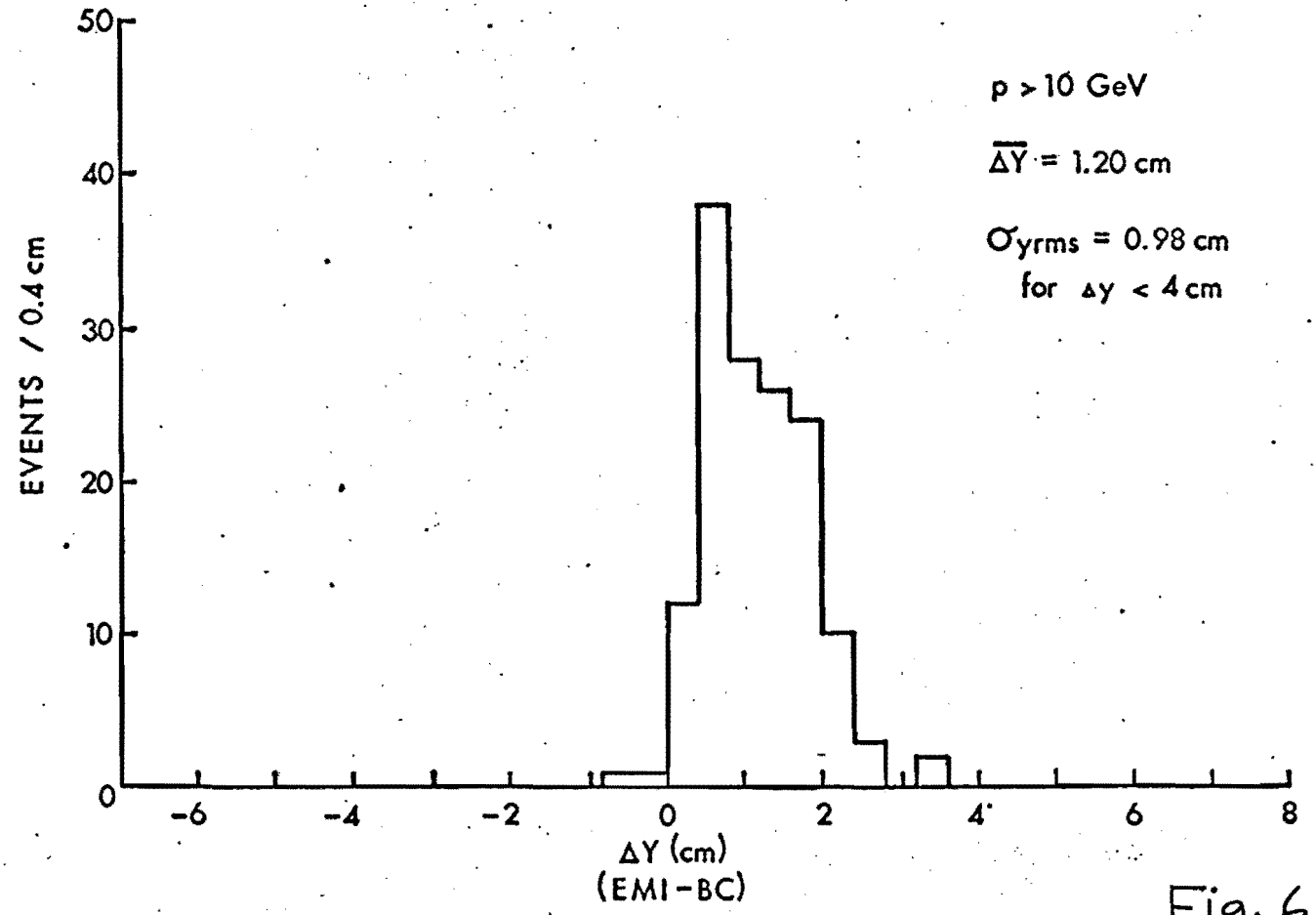

Fig. 6

~~Figure 3a~~